ABSTRACT

CHUKWUMA, CHINAZAM EMMANUEL. The Fate of Siderophores: Biotic Degradation of Siderophores (Under the direction of Dr. Owen Duckworth and Dr. Reza Ghiladi).

Siderophores are low-molecular weight biomolecules with a high affinity for ferric iron (Fe^{III}) that are critical to iron (Fe) acquisition in both plants and microbes, particularly in iron-limited environments. Although their biosynthesis and biology have been extensively studied, little is known about the environmental fate of siderophores, including their potential reactions with common degradative enzymes and interactions with plant-associated microbes, which may influence or hinder the ability to promote the uptake of Fe for plants and microbes.

To address these knowledge gaps, the goals of this dissertation were to: (i) assess the potential of extracellular soil enzymes (including phenol oxidase, peroxidase, and protease) to degrade siderophores and investigate their antagonistic effects; (ii) investigate the biotic degradation of siderophores by microbial symbionts and their role in influencing siderophore stability and facilitating Fe uptake systems; and (iii) conduct a detailed examination of the biochemical mechanisms underlying siderophore degradation, evaluate the significance of siderophores in facilitating Fe acquisition in fungi, and analyze the role of fungal species in producing and utilizing siderophores for efficient Fe uptake. A suite of analytical techniques, including reaction kinetics, liquid chromatography-mass spectrometry (LC-MS), high-resolution mass spectrometry, UV-Visible spectrophotometry, and nuclear magnetic resonance (NMR) spectroscopy, was employed to examine reactivities and structural modifications of siderophores under environmentally relevant conditions. The findings revealed that siderophore degradation by extracellular oxidative enzymes was highly dependent on structure, Fe^{III} complexation, and pH. Notably, free (apo-) siderophores exhibited significantly higher degradation rates (90%) than their Fe-bound counterparts. Hydrogen peroxide (H_2O_2) was found to promote degradation even in the absence of enzymatic catalysis, particularly affecting catecholate-type siderophores such as protochelin. These degradation kinetics suggest that microbial extracellular enzymes in soil microbiomes may contribute to the turnover of plant- or microbe-derived siderophores, thereby modulating Fe availability in competitive ecosystems.

Additionally, the root-associated fungus *Pyrenophora biseptata* was shown to degrade the hydroxamate siderophore desferrioxamine B (DFOB) under iron-limiting, mildly acidic to neutral conditions. Tandem MS/MS and spectral analyses demonstrated the loss of structural hydroxamate groups not only from DFOB but also from the fungus's own tris-hydroxamate siderophores (e.g., Neocoprogen I/II, Coprogen, Dimerum acid). The observed degradation results were linked to the fungus's reductive Fe uptake pathway, wherein the formation of transient Fe^{II} species reduces hydroxamate moieties, forming amides without Fe chelating abilities. This siderophore-inactivating behavior was found to be common among diverse fungi possessing genes for the reductive Fe uptake system, suggesting a self-regulatory or competitive mechanism that influences Fe bioavailability within plant-fungal symbioses and surrounding microbiomes.

The Fate of Siderophores: Biotic Degradation of Siderophores

by
Chinazam Emmanuel Chukwuma

A dissertation submitted to the Graduate Faculty of
North Carolina State University
in partial fulfillment of the
requirements for the degree of
Doctor of Philosophy

Chemistry

Raleigh, North Carolina
2025

APPROVED BY:

Dr. Owen Duckworth Committee Chair	Dr. Reza Ghiladi Co-Chair
Dr. Wei Shi	Dr. Thomas Makris

BIOGRAPHY

Emmanuel was born in Nigeria and raised in the town of Owerri, located in the eastern region of the country. He spent much of his childhood in rural areas, where he developed a deep appreciation for nature through farming, fishing, playing soccer, and exploring the outdoors. As a teenager, he developed a strong interest in agricultural chemistry and fish farming, interests that ultimately inspired him to pursue a B.S in industrial chemistry at Madonna University, Nigeria. During his undergraduate studies, he discovered a passion for analytical chemistry, particularly in environmental applications. He was especially drawn to courses focused on analytical methodologies in environmental chemistry, where he was first introduced to the study of nutrient mobility and transport in soil systems. These early experiences sparked a desire to explore how chemical processes influence environmental and agricultural sustainability. After graduating in 2016, he briefly worked in the chemical industry before pursuing an M.S. in analytical chemistry at the University of Aberdeen (UoA) in Scotland, UK, under the supervision of Dr. Jörg Feldmann. There, he expanded his research experience by focusing on the use of advanced analytical instrumentation to isolate and characterize secondary metabolites from microbial and plant sources. His thesis, titled "An Automated Traceability Approach for RIPPs (Cyanobactins: Patellamide & Trunkamide) for Environmental Implications," explored the environmental significance of these bioactive compounds. In 2021, he began his Ph.D. in chemistry at North Carolina State University (NCSU), working under the mentorship of Dr. Owen Duckworth and Dr. Oliver Baars. His doctoral research focused on elucidating the environmental fate and functional roles of siderophores, specialized iron-chelating compounds, in microbial and plant iron acquisition, nutrient competition, and transport processes. Following the completion of his Ph.D. in 2025, Emmanuel plans to transition into an industry role, where he aims to apply his expertise in analytical and environmental chemistry to solve real-world challenges in agriculture, sustainability, and environmental health.

ACKNOWLEDGMENTS

Over the past four years, I have been incredibly fortunate to receive support and inspiration from many people who have shaped my personal and scientific journey. I am deeply grateful to everyone who contributed, but several individuals deserve special recognition. To Owen Duckworth, thank you for being an exceptional advisor. Your mentorship, support, and the many learning opportunities you provided have been instrumental in my growth as a scientist. I am truly grateful and look forward to continuing our collaboration. To Oliver Baars, your guidance and insight profoundly shaped my scientific thinking. Thank you for your steadfast support throughout this journey. To Reza Ghiladi, thank you for your unwavering support and for randomly paying for lunch at Coco Bongo. To Marc Cubeta, I deeply appreciated our engaging conversations, your knowledge, and encouragement that helped steer my research in important ways. To my committee members, thank you for your time, thoughtful feedback, and belief in my work. Your support has been invaluable.

To my parents and family, thank you for your love, prayers, and unshakable belief in me. Your strength has carried me through every challenge. To my wife and best friend, Emmanuella, thank you for your love, patience, and enduring endless siderophore talk. I could not have done this without you. To my lab mates, Juliet, Tim, and Anna, thank you for the camaraderie, laughter, and support. You made the lab a better place every day.

This work is the result of many hands and hearts. Thank you all.

TABLE OF CONTENTS

LIST OF TABLES

Chapter 2

Chapter 4

Appendix A (Supplementary Information for Chapter 2)

Appendix B (Supplementary Information for Chapter 3)

LIST OF FIGURES

Chapter 1

Chapter 2

Chapter 3

Chapter 4

Appendix A (Supplementary Information for Chapter 2)

Appendix B (Supplementary Information for Chapter 3)

Appendix C (Supplementary Information for Chapter 4)

Chapter 1
Introduction

1.1 Iron in the environment

Essential trace metals, including copper (Cu), iron (Fe), magnesium (Mg), manganese (Mn), molybdenum (Mo), and zinc (Zn), are vital to the proper functioning of both organisms and ecosystems. They play critical roles as cofactors in enzymes that drive crucial biochemical processes [1]. Unfortunately, the low bioavailability of these trace metals to plants and microbes represents a significant barrier that can impede biochemical functions, threatening both food production and the integrity of biogeochemical cycles [2, 3]. Research data has also indicated a troubling decline in nutrient content in crops over the years, specifically with diminished levels of Fe observed since 1950 [4], which impacts overall crop yield and human nutrition.

Iron is essential throughout all kingdoms of life, but is poorly bioavailable in soil. Iron is not just a micronutrient; it is a cornerstone element vital for essential biological processes, including electron transfer during respiration and photosynthesis, the synthesis of nucleic acids and chlorophyll, nitrate reduction, nitrogen fixation, and the detoxification of harmful oxygen radicals [5]. Its unique electronic structure enables Fe to undergo reversible changes in oxidation states across a broad spectrum of redox potentials [2]. Furthermore, it serves as a cofactor and catalyst in countless cellular and enzymatic processes within plants, making it essential for both food security and human health [6, 7]. The growing global population and the impacts of climate change have further exacerbated the issue of Fe bioavailability [8]. Although acidic soil can be Fe deficient, the more pervasive problem lies in calcareous soils, which comprise about 30% of the world's farmland. Here, the low solubility of Fe^{III} (oxyhydr)oxide minerals can lead to nutrient stress and plant disease, such as “lime-induced chlorosis”. Factors that impact Fe availability include soil pH, redox conditions, and the binding of Fe to soil minerals or organic matter. Additionally, high concentrations of potentially toxic metal(-loid)s, such as cadmium (Cd), arsenic (As), as well as abnormally high Cu and Zn, can hinder the uptake and translocation of Fe within plants, exacerbating nutrient deficiencies [9].

The implications of Fe bioavailability extend beyond plants to microbiomes. Specifically, Fe competition directly influences microbial activity, disease suppression, and host-pathogen dynamics [3, 10]. For example, when Fe is readily accessible, it can heighten plant susceptibility to pathogenic fungal diseases. In contrast, Fe bound by high-affinity ligands, such as those secreted by beneficial microbes into the rhizosphere, may help reduce disease susceptibility [10-14]. By understanding the intricate soil processes that disrupt nutrient uptake, we can identify key

environmental conditions that lead to nutrient stress in our crops and beneficial microbes, as well as strategies to suppress harmful fungal diseases. Hence, to study ways to both improve or constrain the bioavailability of Fe, it is essential to thoroughly examine past approaches to promote Fe nutrition and sustainable agricultural practices, from which we can gain valuable insights that pave the way for groundbreaking solutions to enhance soil health and crop productivity.

1.2 Historical approaches to increasing Fe Bioavailability

As mentioned earlier, Fe availability is critical for successful agricultural practices, and Fe complexing agents can play a vital role in enhancing Fe bioavailability. Agronomists have explored a variety of techniques to cultivate Fe-sensitive plants in calcareous soils. These methods include replacing local soil with acidic alternatives through excavation [15] and foliar applications of inorganic Fe salts like ferrous sulfate ($FeSO_4$) [16, 17]. However, the effectiveness of ferrous sulfate may cause stomatal opening during spraying, potentially causing Fe toxicity, thereby limiting its benefits [17]. Although foliar applications can provide quick relief, the effects are often temporary, as symptoms may reemerge as new foliage appears, necessitating frequent reapplications [18]. Moreover, inorganic Fe salts, especially Fe^{II} salts, are prone to rapid oxidation when exposed to air, significantly undermining their effectiveness [19]. These applications of Fe salts may also negatively impact the uptake of other essential nutrients, such as Zn, due to their antagonistic relationship [20].

In the early 1950s, Fe-EDTA (ethylenediamine-tetraacetic acid) emerged as a source of Fe for citrus plants grown in sandy soils [21, 22]. By the late 1950s and early 1960s, Fe-EDDHA (ethylenediamine di-o-hydroxyphenylacetic acid) gained recognition as one of the most effective complexing agents for addressing lime-induced chlorosis [23, 24]. The adoption of synthetic complexing agents revolutionized agricultural practices aimed at improving plant Fe nutrition. However, relying on synthetic Fe complexing agents for addressing Fe deficiencies is often not cost-effective for the majority of field crops. Additionally, these molecules are poorly biodegradable and can persist in our environment, raising sustainability concerns [25]. In response to these issues, researchers are actively investigating novel and efficient strategies to enhance Fe bioavailability, which is essential for promoting overall plant health and optimizing agricultural output. This research leverages a different approach to ensure a sustainable and productive agrarian future by studying intrinsic mechanisms of Fe transport and uptake in soil.

1.3 Plant Fe Availability

Although farmers continuously explore innovative methods to enhance Fe availability in soil, it is crucial to recognize that plants themselves have evolved strategies to tackle Fe deficiency. Despite being abundant in the soil, Fe bioavailability is restricted in oxygenated soil environments above pH > 6. This is largely due to the formation of stable and insoluble Fe^{III} oxyhydroxides, along with sorption to organic matter or minerals that render Fe inaccessible. Within the rhizosphere, Fe occurs in two distinct oxidation states: reduced, as ferrous ion (Fe^{II}), and oxidized, as ferric ion (Fe^{III}). In aerobic soils, Fe is readily oxidized to its ferric state, leading to the formation of highly insoluble ferric oxyhydroxide minerals, such as goethite and hematite. The general reaction for hydroxide precipitation can be described by the equation [26]:

$$Fe^{3+} + 3(OH)^{-} = Fe(OH)_3 \text{ (solid)} \qquad \textbf{(Eq. 1)}$$

Due to the Fe-limiting conditions, plants employ two strategies to acquire Fe from the soil solution. The first strategy (Strategy I), predominantly used by all dicotyledonous and nongraminaceous plants, involves rhizosphere acidification, enhanced activity of membrane-bound reductases, and facilitating Fe uptake through a specialized ferrous transporter [26, 27]. Through the activation of a specific plasma membrane H^{+}-ATPase in root epidermal cells, Strategy I plants lower the pH of their surroundings [28], a response that aims to increase Fe solubility in soils. However, in many high-pH soils, which often contain carbonates (i.e., $CaCO_3$), overcoming the soil's buffering capacity is essential for this mechanism to be effective [2, 26]. Though rhizosphere acidification is limited to a narrow area surrounding the roots, it represents a vital, localized response. Also, the activation of reductase genes further enhances the kinetic lability of Fe, potentially improving its availability [29]. Yet, due to the rapid reoxidation of Fe^{II} in circumneutral pH and the high redox potential in oxic soils, this strategy tends to operate effectively only on a molecular scale.

The second strategy (Strategy II) used by graminaceous plants and microorganisms is to exude specialized agents like organic acids, extracellular enzymes, and, importantly, siderophores to facilitate the solubilization and uptake of essential nutrients from the soil. Siderophores are low molecular weight metal-chelating metabolites (ranging from 200–2000 Da) secreted by bacteria, fungi, and graminaceous plants in response to low Fe availability [30, 31]. Notably, research has shown that the secretion of phytosiderophores (PS) is effective at Fe binding and promoting transport, enabling Strategy II plants to absorb Fe^{III}-PS complexes through a specialized yellow

stripe-like (YSL) transporter of the oligopeptide transporter (OPT) family [32]. This transporter (YSL) was elucidated through studies on the yellow stripe 1 (ys1) mutant of maize, which struggles to respond effectively to Fe deficiency due to a defect in its ability to take up Fe^{III}-phytosiderophore complexes. However, this issue can be remedied by exogenous application of mugineic acids, a phytosiderophore [27, 33].

Furthermore, the function of exudates is crucial for enhancing plant nutrition, preserving soil health, and suppressing pathogenic microorganisms [3, 13, 34]. A compelling illustration that strategy II has an edge over strategy I is in the capacity of grasses to thrive in calcareous soils, which generally do not support the growth of dicots. This adaptability underscores the significance of understanding and harnessing these natural strategies to improve plant growth and soil health, particularly in the context of Fe deficiency.

1.4 Fe Uptake by Microbes

Microorganisms exude a structurally diverse suite of siderophores (Figure 1) to bind and take up Fe from otherwise biologically unavailable sources [2, 35-38]. Different microorganisms employ various siderophore-mediated Fe transport systems. Fungi, in particular, utilize four different mechanisms for siderophore-mediated Fe transport systems [39]. (i) In the shuttle mechanism, used for transporting ferrichrome in *Ustilago maydis*, the Fe^{III}–siderophore complex is transported across the cell membrane, and Fe^{III} is released from the ligand and reduced by the reductive enzymes, leaving the free siderophore to be recycled [40]. (ii) In the taxicab mechanism, there is a ligand exchange of the Fe^{III} from the extracellular siderophore across the cell membrane to intracellular ligands, which is used by *Rhodotorula* species [41]. (iii) For the hydrolytic mechanism, the whole Fe^{III}–siderophore complex is transported into the cell and is subjected to several reductive and degradative processes to release the Fe^{III}, after being reduced to Fe^{II} inside the cell, and the siderophore is excreted again, as seen in the uptake of Fe^{III}–triacetylfusarinine complexes by *Mycelia sterilia* [42]. (iv) Finally, in the reductive uptake mechanism, the Fe^{III}–siderophore complex is not transported across the cell membrane, but the reduction of Fe^{III} to Fe^{II} occurs at the cell membrane and is taken up by the cell, and the siderophore may be degraded, as observed in *Saccharomyces cerevisiae* [43-47].

For bacterial siderophores, the Fe transport systems vary between gram-positive and gram-negative bacteria. Gram-negative bacteria, such as *Escherichia sp*., possess outer membrane

receptors that recognize and bind the Fe^{III}–siderophore complexes at the cell surface [48]. This binding is the first step in a process that relies on an energy-dependent transport system, which includes the utilization of membrane receptor proteins, periplasmic binding proteins, and inner membrane transport proteins [49]. Following successful transport, Fe^{III}–siderophore complexes are released into the periplasmic space before entering the cytoplasm [50], where they undergo reduction by specialized reductases to ultimately yield bioavailable Fe^{II}.

In contrast, the gram-positive bacteria (e.g., *Bacillus sp*.) lack outer membrane receptors and thus utilize a different strategy. Here, Fe^{III}–siderophore complexes are bound by periplasmic siderophore binding proteins anchored to the cell membrane, a mechanism necessitated by the absence of a periplasmic space [51]. These Fe^{III}–siderophore complexes are then further transported by ATP-dependent transporters to the cytoplasm, similar to the transport mechanisms in gram-negative bacteria [52]. Moreover, another distinction between Gram-positive and Gram-negative bacteria pertains not only to the cell wall structure, Gram-positive bacteria retain crystal violet stain, appearing purple/blue under a microscope [53], whereas Gram-negative bacteria do not retain the crystal violet stain [54, 55].

1.5 Siderophores

As described above, a diverse array of siderophores produced by plants and microbes (>500 structurally distinct siderophores have been identified [56, 57]) are typically present in soils at low concentrations (typically in the μM range) but can be found at up to mM concentrations in bulk soil [31, 58-60]. Siderophores enhance Fe bioavailability by binding, solubilizing, and transporting biologically unavailable Fe^{III}, such as Fe-bound in Fe minerals or humic matter, by using negatively charged oxygen as donor atoms because of their high affinity for Fe^{III}; thus, the higher the partial charge on the oxygen, the tighter the interaction [56]. The three major binding groups incorporated into siderophore structures based on the oxygen ligands for Fe^{III} coordination are catecholate, hydroxamate, and carboxylate (α-hydroxycarboxylate) (Figure 1), with each having a high selectivity for Fe^{III} [61]. Each binding moiety possesses a high affinity for Fe^{III} based on its denticity, charge density (pK_a values), and number of donor atoms [56]. Based on thermodynamic considerations, the stability of Fe^{III}–siderophore complexes for catecholates is $\log K_f$ (Fe^{III}) within the 49.0–52.0 range, and is approximately logKf (Fe^{III}) 30.5 for hydroxamates and 17.1 for carboxylates [56, 62].

The most common siderophore geometry is octahedral, thereby allowing six ligands to be arranged around the Fe center with a minimum amount of ligand repulsion as in the case of catecholate siderophores, mostly produced by certain bacteria (e.g., enterobactin (enterochelin) produced by *Escherichia coli*, *Salmonella typhimurium*, and *Klebsiella pneumoniae* [63], where each catechol group contributes two oxygen atoms for chelation with Fe to form a hexadentate octahedral complex. The octahedral field favors the formation of the thermodynamically stable high-spin Fe^{III} species. Few other bacteria like *Bacillus cereus* produce a mixture of catecholate siderophores, petrobactin, and bacillibactin [64], or a siderophore (pyoverdine) with mixed chelating moieties where catecholate is one of the members, secreted by *Pseudomonads* [62, 65-67]. The function of these mixed or multiple siderophores is, however, not clear, but their synthesis appears to be under independent control. Under different environmental conditions, the secretion of one or other of the siderophores appears to predominate. With some pairs, one will be a more potent scavenger for polymeric inorganic Fe and will exchange Fe before cellular uptake [68]. Some siderophores are also used as storage molecules for Fe and do not rapidly donate Fe once they gain entry to the cell [56]. Some secondary siderophores may even facilitate the absorption of other metals in either the presence or absence of Fe [31, 69-71].

Hydroxamate siderophores, the most common group of siderophores found in nature, are produced both by bacteria and fungi, and are the dominant class of siderophores produced by fungi [31, 36, 72, 73]. For example, ferribactin, desferrioxamine B (DFOB), and desferrioxamine E (DFOE) are secreted by *Pseudomonas fluorescens* and *Streptomyces coelicolor* [74, 75]. Additionally, *Trichoderma spp.* and *Fusarium spp*. produce coprogens [76] and fusigen [77-79], respectively. Hydroxamate siderophores can be categorized into three structural families: fusarinines, coprogens, and ferrichromes [36, 80]. Fusarinines can take various forms, including monomers, linear dimers, and cyclic trimers [36]. Comparatively, coprogens are characterized as linear dihydroxamate and trihydroxamate ligands, while ferrichromes primarily exist as cyclic hexapeptides [36]. The principal structural unit of the hydroxamate moiety is derived from L-ornithine [39, 80, 81], which consists of C (=O) N-(OH) R, where R is either an amino acid or a derivative of it. Two of the oxygen atoms from each hydroxamate group form a bidentate ligand with Fe, resulting in a hexadentate conformation containing three bidentate binding groups, as observed in most fungal hydroxamate siderophores [36, 39]. The hexadentate siderophores predominate in nature [82], forming 1:1 complexes with Fe^{III} [36]. These complexes are thermodynamically stable and exhibit high spin

[83, 84], which contributes to the specificity of siderophores for the Fe^{III} ions. The interaction between Fe^{III} and the donor atoms is largely electrostatic, resulting in the siderophore forming a distorted octahedron of O atoms around the metal [82]. Previous reports indicate that the strong binding between Fe^{III} and hydroxamate siderophores protects the complexes from hydrolysis and enzymatic degradation in the environment [47, 62]. Hydroxamate siderophores, especially desferrioxamine (DFO), have been recognized for their medical applications, particularly in treating Fe overload conditions such as β-thalassemia and aluminum toxicity [85, 86]. However, the use of DFO has been associated with various problems and side effects [87-89].

Carboxylate siderophores are produced mostly by plants, such as mugineic acid (phytosiderophore) [31]; however, bacteria like *Rhizobium* and *Staphylococcus spp*., and fungi like *Mucorales* also excrete carboxylate and α-hydroxycarboxylate type siderophores [62]. Carboxylate siderophores bind to Fe through carboxyl and hydroxyl groups [90], and the carboxylates can be species-specific, as seen with staphyloferrin A, produced by *Staphylococcus hyicus* DSM 20459 under reduced Fe conditions [91]. This siderophore transports Fe not only to the producer strain but also to other *Staphylococci* species [62, 91]. The best-characterized carboxylate siderophore, rhizobactin, produced by *Rhizobium meliloti* strain DM4, has an amino polycarboxylic acid consisting of ethylene diamine dicarboxyl and hydroxyl-carboxyl moieties that act as Fe chelating groups [92].

To represent the wide variety of siderophore structures and chemistries in this research, three siderophore models were used in this dissertation, and each characteristic of one of the three most common chelating moieties found in siderophore structures was represented (Figure 2). Protochelin is a bacterial tris-aminocatecholate siderophore, desferrioxamine B (DFOB) represents a bacterial tris-hydroxamate siderophore, and proline-2′-deoxymugineic acid (PDMA) is a carboxylate phytosiderophore analog. PDMA has been recently introduced as a synthetic phytosiderophore analog with high stability regarding abiotic degradation when compared to the natural phytosiderophore 2′-deoxymugineic acid (DMA) [93].

1.5.1 Importance of siderophores

As Fe is a cofactor required for several cellular and physiological activities in plants [94, 95], Fe starvation significantly reduces the quantity and quality of crop production. Siderophore secretion has been reported to enhance plant growth via Fe nutrition [96-98], can also inhibit Fe uptake by plants

[99], and can also protect against pathogens [13, 100]. For instance, *Azadirachta indica* was reported to produce ferrioxamines that contribute to plant Fe nutrition, as well as promote root and shoot growth [101, 102]. The role of microbial activity in Fe uptake by plants has been illustrated with *Escherichia coli* from the sugarcane (*Saccharum sp*.) [103] and *Streptomyces sp.*[104], *Aspergillus niger*, *Penicillium citrinum,* and *Trichoderma harzianum,* which were correlated to siderophore production and enhanced plant growth, elevated root and shoot biomass and lengths [105-107]. Sometimes, plants can also modify the structure of the root-soil microbial community to favor the growth of more siderophore-secreting microbes by secreting phenolic exudates from their roots [108]. Besides utilizing microbial siderophores, plants can also synthesize phytosiderophores, which can bind Fe directly and promote solubilization from unavailable sources in soil [109, 110]. Thus, the siderophores originated either from microbes or plants, and are recognized as the potential source of Fe for their survival and growth.

Siderophores can also act as biological control agents, as demonstrated in the inhibition of *Erwinia carotovora* and *Gaeumannomyces graminis* by several plant-growth-promoting *Pseudomonas fluorescens* strains [111], and pyoverdine siderophores produced by pseudomonads control the wilt diseases caused by *Fusarium oxysporum* [112, 113]. The biocontrol mechanism depends on the role of siderophores as competitors for Fe to reduce Fe availability for phytopathogens [31, 62, 114]. Other applications of siderophores include for bioremediation of heavy metals in contaminated soils [115, 116] by binding to and precipitating out a wide array of toxic metals, e.g., Cr^{3+}, Al^{3+}, Cu^{2+}, Eu^{3+}, and Pb^{2+}, that generate oxidative stress, which can cause damage to plant DNA [117-120].

The wide applications of siderophores reveal that it is promising for new technologies and management strategies for diverse applications, including ecology [62, 121-123], agriculture [31, 124], bioremediation [125, 126], biosensors [127, 128], and medicine [129-132]. Therefore, there is a need to learn and characterize more siderophores, unveil their new functions, and understand their mechanism of operation in different habitats for the benefit of plants and microbes alike.

1.5.2 Fate of Siderophores

The general process of Fe acquisition with siderophores may involve the following steps: (1) siderophore biosynthesis and secretion [3, 133]; (2) diffusion of the free siderophore in the extracellular medium [134, 135], (3) chelation of Fe^{III} from environmental sources [136]; (4) diffusion of

the Fe^{III}-siderophore complex back to the cell surface [82], and (5) Fe uptake from the Fe^{III}-siderophore complex for example via ferric siderophore transporters or reductive Fe uptake [137-139]. For siderophores to function as listed above, transport from and to the organism cell or root to an Fe source is critical (Figure 3). However, soils are complex systems, where a wide range of antagonistic chemical and physical processes, such as enzymatic activities and siderophore degradation by facilitated Fe uptake systems, may disrupt this nutrient uptake process [137, 139, 140].

Enzymes may play a crucial role in the degradation of siderophores. Importantly, siderophores are thought to be stable against degradation due to chemical modifications that protect them from enzymatic activity [142]. The chelation of Fe can also further impede the action of hydrolytic enzymes [143]. Nevertheless, extracellular oxidative enzymes, for example, phenol oxidases, peroxidases, and proteases, involved in organic matter decomposition and nutrient cycling [139, 144-148] could potentially react with siderophores in the extracellular environment, based on their activities [144, 149]. A few previously reported examples of enzymatic siderophore degradation, with microbes able to grow on siderophores not just for Fe acquisition but also as their carbon source. This involved the hydrolysis of the amide bonds in the hydroxamate-type siderophores, such as desferrioxamine B [143, 147, 148] and Ferrichrome A [150-152]. Research studies have also documented that the hydrolytic degradation of DFOB leads to the production of dihydroxamic and monohydroxamic acids [148]. Moreover, the degradations of catecholate siderophores and some phytosiderophores, including DMA, are believed to be initiated by intracellular oxidative enzymes [145].

Phenol oxidase and peroxidase both contain Fe in their heme complexes [153, 154]. By binding to apoenzymes, heme can control these enzyme activities [155]. Thus, siderophores could sequester Fe from enzymes, which could consequently lead to the deactivation of these key soil enzyme functions. However, the extent to which extracellular enzymes contribute to the degradation of siderophores in soil remains to be fully ascertained. These extracellular enzymes could potentially act as antagonistic bioagents, either impeding or facilitating the siderophore chelating function. Hence, while the enzymatic degradation of siderophores is evidently a critical aspect of microbial metabolism and nutrient cycling, further research is needed to elucidate the roles and mechanisms of extracellular enzymes in this complex process.

Additionally, bacteria often utilize enzymes to degrade siderophores within their cells to remove Fe from the siderophore complexes. For instance, *Escherichia coli* (E. coli) bacterium hydrolyses the enterobactin trilactone scaffold using the enzyme esterase Fes to exchange Fe from the ferric-enterobactin chelate [56, 156, 157]. Most studies have focused on siderophore degradation occurring inside microbial cells. However, it is noteworthy that these intracellular enzymes can be released into the extracellular environment following microbial lysis [146]. Once outside, these enzymes may retain their functionality, particularly in soil solutions, where they might interact physically and chemically with humus and clay minerals. Thus, to acquire energy, carbon, and other nutrients for growth and metabolism, soil microbes also frequently exude extracellular enzymes for degrading organic compounds.

Aside from enzyme activities, the exploration of Fe uptake in various organisms, particularly in the context of microbial interactions, has unveiled a web of competition and cooperation that shapes ecological dynamics. As researchers delved deeper into these interactions, they discovered the intriguing phenomenon of "piracy," where certain bacteria exploit exogenous siderophores produced by other organisms as an Fe source for their own benefit, thereby compromising the effectiveness of siderophores for the original producing organism [140]. This phenomenon was notably documented in specific *Campylobacter* species [158], which, despite lacking the ability to produce their siderophores, effectively appropriated compounds like enterobactin and ferrichrome. Such behavior not only undermines the original producers' ability to obtain Fe but also subtly alters the competitive landscape of microbial communities, allowing those that possess siderophore receptors to thrive [159].

Building on these findings, subsequent studies expanded the understanding of bacterial Fe competition by demonstrating that some bacteria, capable of degrading plant-derived siderophores, including hydroxymugineic acid (HMA), to access their Fe content, can also successfully utilize the trishydroxamate siderophores like desferrioxamine B (DFOB) for Fe acquisition [160]. This ability provides them with a competitive advantage over plants such as maize and oats, which cannot access DFOB for Fe acquisition.

As the narrative of Fe uptake unfolded, researchers turned their attention to fungi, recognizing their crucial role in the ecosystem. Fungi from a wide range of ecologies employ techniques for Fe uptake and decomposition of complex organic matter, including being prolific producers of extracellular enzymes that facilitate these processes [161]. However, studies revealed

that not all fungal species possess equal capabilities in degrading organic matter through enzyme activities; as individual species, they may specialize in degrading specific substrates [162]. For instance, *Saccharomyces cerevisiae*, although it does not secrete siderophores, cleverly acquires Fe from siderophores through alternative pathways, including both non-reductive and reductive uptake pathways [43, 44, 136]. This discovery highlighted yet another alternative strategy for Fe acquisition, where the generated Fe^{II} could, in turn, reduce hydroxamates to amides [45], facilitating broader access to necessary nutrients.

Additionally, the tension between competing microbial species and their surrounding environments became even clearer with investigations into the dynamic interplay between the soil pathogenic *actinomycete Amycolatopsis* and the *streptomycete S. coelicolor*. Here, the *Amycolatopsis* produced the siderophore amychelin, which effectively inhibited Fe uptake by the *S. coelicolor* [103, 163]. Yet, in a twist of fate, *Amycolatopsis* could utilize desferrioxamine E produced by the *streptomycete* [163], illustrating the complex interdependence and rivalry within microbial communities. Despite these explorations, many questions remain unanswered regarding the intricate interactions that disrupt siderophore function and affect Fe uptake among various organisms. Research into these dynamics would not only deepen our understanding of microbial competition but also emphasize the biochemical mechanisms that could redefine prevailing notions of host-pathogen relationships. This dissertation intends to unravel these complexities, inching closer to a comprehensive understanding of how Fe acquisition and uptake strategies inform the larger narrative of ecological interactions and nutrient cycling in diverse environments.

Taken together, these observations are evidence of the chemical ‘‘tug of war’ in the soil environment that revolves around the uptake of a limited supply of nutrient metals. The snatching of Fe from plant and animal hosts is viewed as an important virulent factor, mediated by the structure of the siderophores they produce [164, 165]. For example, siderophore synthesis was reported to make endophytic bacteria of rice competitive in the colonization of plant tissue and exclude other microorganisms from the same ecological niche [140, 166]. Thus, understanding the potential biotic degradation of siderophores could answer the following questions: (1) what happens after siderophores are secreted into the soil environment? And (2) what biochemical mechanisms of Fe uptake in microbes impact siderophore cycling? This research aims to provide knowledge about the mechanism of competition in microbial and plant community interactions, either by rendering siderophores ineffective for Fe chelation or increasing Fe availability to competing organisms.

1.6 Summary

This research aims to understand the antagonistic interactions, particularly how degradation could affect the siderophore cycling and Fe uptake mechanisms in plants, fungi, and bacteria. Even though various organisms have evolved techniques to scavenge Fe, particularly in competitive environments where siderophore-producing organisms vie against other microbes [44, 140, 163] or compete for resources with plant-microbe symbionts [31, 166]. At present, there is poor knowledge of the extent to which degradation influences siderophore availability, function, and efficacy for organismal Fe uptake. Therefore, understanding these dynamics is crucial for clarifying misconceptions about crop Fe nutrition and enhancing our knowledge of plant-microbe interactions in the soil.

To achieve this overarching goal, the research will focus on three specific objectives:

1. Assess the potential of extracellular soil enzymes (such as phenol oxidase, peroxidase, and protease) to degrade siderophores and investigate their antagonistic effects.
2. Investigate the biotic degradation of siderophores by microbial symbionts and their role in influencing siderophore stability and facilitating Fe uptake systems.
3. Conduct a detailed examination of the biochemical mechanisms underlying siderophore degradation, evaluate the significance of siderophores in facilitating Fe acquisition in fungi, and analyze the role of fungal species in producing and utilizing siderophores for efficient Fe uptake.

The research will incorporate a series of laboratory-based biological and chemical experiments designed to trace degradation patterns of various classes of microbial and plant siderophores (as illustrated in Figure 2). Key approaches include: (1) quantifying the effects of isolated extracellular enzymes on siderophore stability; (2) verifying these effects through studies with microbial symbionts known to produce enzymes that either degrade siderophores or entrain siderophores from other sources for Fe competition and uptake; and (3) surveying mechanisms of Fe uptake based on the degradation of siderophores observed in these interactions and their relevance in fungi biology. Quantifying siderophores and their degradation products, which are present in micromolar concentrations, poses an analytical challenge. However, we leverage a highly sensitive and selective high-resolution liquid chromatography-mass spectrometry (HR-LC-MS) method to measure these metal-complexing agents [167, 168]. This technique allows for the identification of specific unknown siderophores and degradation products through the stable isotope distribution of

chelated metals as a fingerprint. Chemical structure characterization is achieved by analyzing MS spectra of molecular fragments (MS^n [168, 169]) and ancillary measurements (particularly NMR [170]) as necessary. These advancements enhance our ability to track both siderophores and their potential degradation products. Thereafter, results from these experiments will give insights into the fate of siderophores in terms of the dynamic mechanisms for Fe acquisition and competition between organisms.

Given the structural diversity among siderophores produced by different organisms, it is anticipated that significant differences will emerge in their degradation dynamics and overall capacity to deliver Fe to organisms. Building on previous research regarding intracellular enzymes and siderophore structures [37, 143, 148], the following hypotheses will be tested using tris-aminocatecholate siderophore protochelin, tris-hydroxamate siderophore DFOB, and the carboxylate phytosiderophore analog PDMA.:

1. Proteases (hydrolytic enzymes) will degrade all three siderophores due to the presence of amide linkages in their structures (Figure 2).
2. Protochelin, which contains catechol groups, will degrade through oxidative enzymes (phenol oxidase and peroxidase), whereas DFOB and PDMA will be resistant to degradation by these same oxidative enzymes due to the absence of phenol groups in their structure.

Furthermore, this research will also investigate Fe uptake mechanisms that could contribute to siderophore degradation, as suggested by prior studies on fungi [42, 45]. It is expected that the selected fungi symbionts will demonstrate varied capabilities in degrading specific siderophores.

Ultimately, this research aims to illuminate the relationships between siderophore structure, degradation patterns, and Fe acquisition processes. By understanding these principles, we may develop strategies to manipulate soil properties in a manner that enhances Fe uptake, thereby improving plant Fe nutrition and crop resilience. This structured approach is intended to provide new insights into the fate of siderophores in soil ecosystems, promoting better strategies for enhancing agricultural productivity and sustainability.

1.7 Structure of Dissertation

This dissertation is organized as follows: Chapter 1 (this chapter) is an overview of the literature and highlights the motivation for this work. Chapter 2 provides an in-depth investigation of siderophore degradation by model extracellular enzymes and their mechanism. Chapter 3

reports on the inactivation of siderophore iron-chelating moieties by the fungal wheat root symbiont *Pyrenophora biseptata*. Chapter 4 discusses the link between hydroxamate degradation by *Pyrenophora biseptata* and reductive Fe uptake mechanisms in the fungus and investigates the extent to which this dynamic Fe assimilation process involving reoxidation of Fe^{II} impacts the fate of siderophores in fungal biology. Chapter 5 provides alternative experimental approaches, conclusions of this dissertation, and suggests future research directions.

Appendices A–C contain the supplementary information for Chapters 2–4, respectively.

REFERENCES

1. J. B. Glass and V. J. Orphan, 'Trace metal requirements for microbial enzymes involved in the production and consumption of methane and nitrous oxide', *Frontiers in microbiology*, 3 (2012): 61.

2. P. Lemanceau, P. Bauer, S. Kraemer and J.-F. Briat, Iron dynamics in the rhizosphere as a case study for analyzing interactions between soils, plants and microbes, (2009).

3. A. Robin, G. Vansuyt, P. Hinsinger, J. M. Meyer, J.-F. Briat and P. Lemanceau, 'Iron dynamics in the rhizosphere: consequences for plant health and nutrition', *Advances in agronomy*, 99 (2008): 183-225.

4. D. R. Davis, M. D. Epp and H. D. Riordan, 'Changes in USDA food composition data for 43 garden crops, 1950 to 1999', *Journal of the American College of Nutrition*, 23 (2004): 669-682.

5. S. B. Kuzyk, E. Hughes and V. Yurkov, 'Discovery of siderophore and metallophore production in the aerobic anoxygenic phototrophs', *Microorganisms*, 9 (2021): 959.

6. G. Conway and G. Toenniessen, 'Feeding the world in the twenty-first century', *Nature*, 402 (1999): C55-C58.

7. R. M. Welch and R. D. Graham, 'A new paradigm for world agriculture: meeting human needs: productive, sustainable, nutritious', *Field Crops Research*, 60 (1999): 1-10.

8. T. A. Long, H. Tsukagoshi, W. Busch, B. Lahner, D. E. Salt and P. N. Benfey, 'The bHLH transcription factor POPEYE regulates response to iron deficiency in Arabidopsis roots', *The Plant Cell*, 22 (2010): 2219-2236.

9. A. Wallace, 'Historical landmarks in progress relating to iron chlorosis in plants', *Journal of Plant Nutrition*, 5 (1982): 277-288.

10. A. Khan, P. Singh and A. Srivastava, 'Synthesis, nature and utility of universal iron chelator–Siderophore: A review', *Microbiological research*, 212 (2018): 103-111.

11. M. Schrettl, O. Ibrahim-Granet, S. Droin, M. Huerre, J.-P. Latgé and H. Haas, 'The crucial role of the Aspergillus fumigatus siderophore system in interaction with alveolar macrophages', *Microbes and infection*, 12 (2010): 1035-1041.

12. J. D. Fetherston, O. Kirillina, A. G. Bobrov, J. T. Paulley and R. D. Perry, 'The yersiniabactin transport system is critical for the pathogenesis of bubonic and pneumonic plague', *Infection and immunity*, 78 (2010): 2045-2052.

13. J. W. Kloepper, J. Leong, M. Teintze and M. N. Schroth, 'Enhanced plant growth by siderophores produced by plant growth-promoting rhizobacteria', *Nature*, 286 (1980): 885-886.

14. P. Lemanceau, Role of competition for carbon and iron in mechanisms of soil suppressiveness to Fusarium wilts, *Vascular wilt diseases of plants,* (1989): 385-396.

15. R. Jackson, *Gardening on chalk and lime soil*, (2020).

16. J. L. Eddings and A. Brown, 'Absorption and translocation of foliar-applied iron', *Plant Physiology*, 42 (1967): 15-19.

17. E. Wallihan, T. Embleton and R. Sharpless, Response of chlorotic citrus leaves to iron sprays in relation to surfactants and stomatal apertures, *Proc. Amer. Soc. Hort. Sci,* (1964): 210-217.

18. R. Koenig and M. R. Kuhns, 'Control of iron chlorosis in ornamental and crop plants', *AG-SO*, 1 (2002): 1.

19. S. Sharma, S. Chandra, A. Kumar, P. Bindraban, A. K. Saxena, V. Pande and R. Pandey, 'Foliar application of iron fortified bacteriosiderophore improves growth and grain Fe concentration in wheat and soybean', *Indian Journal of microbiology*, 59 (2019): 344-350.

20. S. Ram, V. K. Malik, V. Gupta, S. Narwal, M. Sirohi, Ankush, V. Pandey, O. P. Gupta, A. K. Misra and G. Singh, 'Impact of foliar application of iron and zinc fertilizers on grain iron, zinc, and protein contents in bread wheat (Triticum aestivum L.)', *Frontiers in Nutrition*, 11 (2024): 1378937.

21. I. Stewart and C. Leonard, 'Chelates as sources of iron for plants growing in the field', *Science*, 116 (1952): 564-566.

22. Leonard. CD, An available source of iron for plants, *Am. Soc. Hortic. Sci. Proc.,* (1953): 103-110.

23. Y. Chen and P. Barak, 'Iron nutrition of plants in calcareous soils', *Advances in agronomy*, 35 (1982): 217-240.

24. H. Kroll, 'The ferric chelate of ethylenediamine di (o-hydroxy-phenylacetic acid) for treatment of lime-induced chlorosis', *Soil Science*, 84 (1957): 51-54.

25. A. Wallace and G. Wallace, 'Some of the problems concerning iron nutrition of plants after four decades of synthetic chelating agents', *Journal of Plant Nutrition*, 15 (1992): 1487-1508.

26. M. Shenker and Y. Chen, 'Increasing iron availability to crops: fertilizers, organo-fertilizers, and biological approaches', *Soil Science & Plant Nutrition*, 51 (2005): 1-17.

27. C. Curie and J.-F. Briat, 'Iron transport and signaling in plants', *Annual Review of Plant Biology*, 54 (2003): 183-206.

28. T. C. Fox and M. L. Guerinot, 'Molecular biology of cation transport in plants', *Annual review of plant biology*, 49 (1998): 669-696.

29. H. Marschner and V. Römheld, 'Strategies of plants for acquisition of iron', *Plant and Soil*, 165 (1994): 261-274.

30. B. Schwyn and J. Neilands, 'Universal chemical assay for the detection and determination of siderophores', *Analytical Biochemistry*, 160 (1987): 47-56.

31. E. Ahmed and S. J. Holmström, 'Siderophores in environmental research: roles and applications', *Microbial biotechnology*, 7 (2014): 196-208.

32. M. N. Hindt and M. L. Guerinot, 'Getting a sense for signals: regulation of the plant iron deficiency response', *Biochimica et Biophysica Acta (BBA)-Molecular Cell Research*, 1823 (2012): 1521-1530.

33. T. Brumbarova and P. Bauer, 'Iron uptake and transport in plants', *Plant membrane and vacuolar transporters*, (2008): 149-172.

34. P. Lemanceau, P. Bauer, S. Kraemer and J.-F. Briat, 'Iron dynamics in the rhizosphere as a case study for analyzing interactions between soils, plants and microbes', *Plant and Soil*, 321 (2009): 513-535.

35. J. Neilands, 'Iron absorption and transport in microorganisms', *Annual review of nutrition*, 1 (1981): 27-46.

36. J. C. Renshaw, G. D. Robson, A. P. Trinci, M. G. Wiebe, F. R. Livens, D. Collison and R. J. Taylor, 'Fungal siderophores: structures, functions and applications', *Mycological Research*, 106 (2002): 1123-1142.

37. G. Winkelmann, 'Microbial siderophore-mediated transport', *Biochemical Society Transactions*, 30 (2002): 691-696.

38. C. Wandersman and P. Delepelaire, 'Bacterial iron sources: from siderophores to hemophores', *Annual review of microbiology*, 58 (2004): 611.

39. D. van der Helm and G. Winkelmann, 'Hydroxamates and polycarboxylates as iron transport agents (siderophores) in fungi', *Metal ions in fungi*, 11 (1994): 39-98.

40. O. Ardon, R. Nudelman, C. Caris, J. Libman, A. Shanzer, Y. Chen and Y. Hadar, 'Iron uptake in Ustilago maydis: tracking the iron path', *Journal of Bacteriology*, 180 (1998): 2021-2026.

41. G. Winkelmann, 'Molecular recognition and transport of siderophores in fungi', *Iron transport in microbes, plants and animals*, (1987): 317-336.

42. J. P. Adjimani and T. Emery, 'Stereochemical aspects of iron transport in Mycelia sterilia EP-76', *Journal of Bacteriology*, 170 (1988): 1377-1379.

43. C. C. Philpott, 'Iron uptake in fungi: a system for every source', *Biochimica et Biophysica Acta (bba)-molecular cell research*, 1763 (2006): 636-645.

44. C. W. Yun, T. Ferea, J. Rashford, O. Ardon, P. O. Brown, D. Botstein, J. Kaplan and C. C. Philpott, 'Desferrioxamine-mediated iron uptake in Saccharomyces cerevisiae: evidence for two pathways of iron uptake', *Journal of Biological Chemistry*, 275 (2000): 10709-10715.

45. C. W. Yun, M. Bauler, R. E. Moore, P. E. Klebba and C. C. Philpott, 'The role of the FRE family of plasma membrane reductases in the uptake of siderophore-iron in Saccharomyces cerevisiae', *Journal of Biological Chemistry*, 276 (2001): 10218-10223.

46. E. Lesuisse, P.-L. Blaiseau, A. Dancis and J.-M. Camadro, 'Siderophore uptake and use by the yeast Saccharomyces cerevisiae', *Microbiology*, 147 (2001): 289-298.

47. G. Winkelmann, 'Ecology of siderophores with special reference to the fungi', *Biometals*, 20 (2007): 379-392.

48. K. D. Krewulak and H. J. Vogel, 'Structural biology of bacterial iron uptake', *Biochimica et Biophysica Acta (BBA)-Biomembranes*, 1778 (2008): 1781-1804.

49. B. F. Matzanke, *Structures, coordination chemistry and functions of microbial iron chelates*, (1991).

50. N. Noinaj, M. Guillier, T. J. Barnard and S. K. Buchanan, 'TonB-dependent transporters: regulation, structure, and function', *Annual review of microbiology*, 64 (2010): 43-60.

51. T. Fukushima, B. E. Allred, A. K. Sia, R. Nichiporuk, U. N. Andersen and K. N. Raymond, 'Gram-positive siderophore-shuttle with iron-exchange from Fe-siderophore to apo-siderophore by Bacillus cereus YxeB', *Proceedings of the National Academy of Sciences*, 110 (2013): 13821-13826.

52. V. Braun and K. Hantke, 'Recent insights into iron import by bacteria', *Current opinion in chemical biology*, 15 (2011): 328-334.

53. O. Sizar, S. W. Leslie and C. G. Unakal, 'Gram-positive bacteria', (2017).

54. K. Taskar and S. Gupta, 'A Review: Exploring Basic Methods of Gram Positive and Gram Negative Bacteria', (2021).

55. T. J. Silhavy, D. Kahne and S. Walker, 'The bacterial cell envelope', *Cold Spring Harbor perspectives in biology*, 2 (2010): a000414.

56. R. C. Hider and X. Kong, 'Chemistry and biology of siderophores', *Natural product reports*, 27 (2010): 637-657.

57. S. M. Kraemer, A. Butler, P. Borer and J. Cervini-Silva, 'Siderophores and the dissolution of iron-bearing minerals in marine systems', *Reviews in Mineralogy and Geochemistry*, 59 (2005): 53-84.

58. P. Powell, G. Cline, C. Reid and P. Szaniszlo, 'Occurrence of hydroxamate siderophore iron chelators in soils', *Nature*, 287 (1980): 833-834.

59. V. Rai, N. Fisher, O. W. Duckworth and O. Baars, 'Extraction and detection of structurally diverse siderophores in soil', *Frontiers in Microbiology*, 11 (2020): 581508.

60. E. Ahmed and S. J. Holmström, 'The effect of soil horizon and mineral type on the distribution of siderophores in soil', *Geochimica et Cosmochimica Acta*, 131 (2014): 184-195.

61. G. Xiao, D. Van Der Helm, F. Goerlitz, R. Hider and P. Dobbin, 'Structures of 3-hydroxy-1-(2-methoxyethyl)-2-methyl-4-pyridinone, its hydrochloride and 1-ethyl-3-hydroxy-2-methyl-4-pyridinone hydrochloride hydrate', *Acta Crystallographica Section C: Crystal Structure Communications*, 49 (1993): 1646-1649.

62. M. Saha, S. Sarkar, B. Sarkar, B. K. Sharma, S. Bhattacharjee and P. Tribedi, 'Microbial siderophores and their potential applications: a review', *Environmental Science and Pollution Research*, 23 (2016): 3984-3999.

63. B. Dave, K. Anshuman and P. Hajela, 'Siderophores of halophilic archaea and their chemical characterization', (2006).

64. M. K. Wilson, R. J. Abergel, K. N. Raymond, J. E. Arceneaux and B. R. Byers, 'Siderophores of Bacillus anthracis, Bacillus cereus, and Bacillus thuringiensis', *Biochemical and biophysical research communications*, 348 (2006): 320-325.

65. S. A. Leong and J. Neilands, 'Siderophore production by phytopathogenic microbial species', *Archives of biochemistry and biophysics*, 218 (1982): 351-359.

66. P. Cornelis, 'Iron uptake and metabolism in pseudomonads', *Applied microbiology and biotechnology*, 86 (2010): 1637-1645.

67. M. E. Peek, A. Bhatnagar, N. A. McCarty and S. M. Zughaier, 'Pyoverdine, the major siderophore in Pseudomonas aeruginosa, evades NGAL recognition', *Interdisciplinary perspectives on infectious diseases*, 2012 (2012).

68. G. Ghssein and Z. Ezzeddine, 'A review of Pseudomonas aeruginosa metallophores: Pyoverdine, pyochelin and pseudopaline', *Biology*, 11 (2022): 1711.

69. A. M. Timofeeva, M. R. Galyamova and S. E. Sedykh, 'Bacterial siderophores: classification, biosynthesis, perspectives of use in agriculture', *Plants*, 11 (2022): 3065.

70. J. Kramer, Ö. Özkaya and R. Kümmerli, 'Bacterial siderophores in community and host interactions', *Nature Reviews Microbiology*, 18 (2020): 152-163.

71. I. J. Schalk, M. Hannauer and A. Braud, 'New roles for bacterial siderophores in metal transport and tolerance', *Environmental microbiology*, 13 (2011): 2844-2854.

72. M. Höfte, 'Classes of microbial siderophores', *Iron chelation in plants and soil microorganisms*, (1993): 3-26.

73. G. Winkelmann and H. Drechsel, 'Microbial siderophores', *Biotechnology*, 7 (1997): 199-246.

74. B. Maurer, A. Müller, W. Keller-Schierlein and H. Zähner, 'Ferribactin, a Siderochrome from Pseudomonas fluorescens Migula: 61. Mitteilung Ferribactin, ein Siderochrom aus Pseudomonas fluorescens Migula', *Archiv für Mikrobiologie*, 60 (1968): 326-339.

75. B. Saharan and V. Nehra, 'Plant growth promoting rhizobacteria: a critical review', *Life Sci Med Res*, 21 (2011): 30.

76. H. Zähner, W. Keller-Schierlein, R. Hütter, K. Hess-Leisinger and A. Deer, 'Stoffwechselprodukte von Mikroorganismen: 40. Mitteilung Sideramine aus Aspergillaceen', *Archiv für Mikrobiologie*, 45 (1963): 119-135.

77. H. Diekmann and H. Zähner, 'Konstitution von Fusigen und dessen Abbau zu Δ2-Anhydromevalonsäurelacton', *European Journal of Biochemistry*, 3 (1967): 213-218.

78. J. M. Sayer and T. F. Emery, 'Structures of the naturally occurring hydroxamic acids, fusarinines A and B', *Biochemistry*, 7 (1968): 184-190.

79. J. Neilands, 'Microbial iron transport compounds (sidero-chromes)', *Inorganic biochemistry*, 1 (1973): 167-202.

80. G. Winkelmann, 'Structures and functions of fungal siderophores containing hydroxamate and complexone type iron binding ligands', *Mycological Research*, 96 (1992): 529-534.

81. G. Winkelmann, 'Importance of siderophores in fungal growth, sporulation and spore germination', *Frontiers in mycology*, (1991): 49-65.

82. A. Albrecht-Gary and A. Crumbliss, 'Coordination chemistry of siderophores: thermodynamics and kinetics of iron chelation and release', *Metal ions in biological systems*, 35 (1998): 239-327.

83. J. Neilands, 'Siderophores', *Archives of biochemistry and biophysics*, 302 (1993): 1-3.

84. J. Neilands, 'Siderophores: structure and function of microbial iron transport compounds', *Journal of Biological Chemistry*, 270 (1995): 26723-26726.

85. J. P. Day and P. Ackrill, 'The chemistry of desferrioxamine chelation for aluminum overload in renal dialysis patients', *Therapeutic drug monitoring*, 15 (1993): 598-601.

86. G. Faa and G. Crisponi, 'Iron chelating agents in clinical practice', *Coordination Chemistry Reviews*, 184 (1999): 291-310.

87. D. T. Dexter, R. J. Ward, A. Florence, P. Jenner and R. R. Crichton, 'Effects of desferrithiocin and its derivatives on peripheral iron and striatal dopamine and 5-hydroxytryptamine metabolism in the ferrocene-loaded rat', *Biochemical pharmacology*, 58 (1999): 151-155.

88. G. J. Kontoghiorghes, 'Comparative efficacy and toxicity of desferrioxamine, deferiprone and other iron and aluminium chelating drugs', *Toxicology letters*, 80 (1995): 1-18.

89. A. E. Martell, R. Motekaitis, Y. Sun, R. Ma, M. Welch and T. Pajeau, 'New chelating agents suitable for the treatment of iron overload', *Inorganica chimica acta*, 291 (1999): 238-246.

90. B. Dave and H. Dube, 'Chemical characterization of fungal siderophores', (2000).

91. J. Meiwes, H.-P. Fiedler, H. Haag, H. Zähner, S. Konetschny-Rapp and G. Jung, 'Isolation and characterization of staphyloferrin A, a compound with siderophore activity from Staphylococcus hyicus DSM 20459', *FEMS microbiology letters*, 67 (1990): 201-205.

92. M. Smith and J. Neilands, 'Rhizobactin, a siderophore from Rhizobium meliloti', *Journal of Plant Nutrition*, 7 (1984): 449-458.

93. M. Suzuki, A. Urabe, S. Sasaki, R. Tsugawa, S. Nishio, H. Mukaiyama, Y. Murata, H. Masuda, M. S. Aung and A. Mera, 'Development of a mugineic acid family phytosiderophore analog as an iron fertilizer', *Nature communications*, 12 (2021): 1-13.

94. J. F. Briat, I. Fobis-Loisy, N. Grignon, S. Lobréaux, N. Pascal, G. Savino, S. Thoiron, N. Von Wirén and O. Van Wuytswinkel, 'Cellular and molecular aspects of iron metabolism in plants', *Biology of the Cell*, 84 (1995): 69-81.

95. T. Kobayashi and N. K. Nishizawa, 'Iron uptake, translocation, and regulation in higher plants', *Annual review of plant biology*, 63 (2012): 131-152.

96. D. E. Crowley, Microbial siderophores in the plant rhizosphere, *Iron nutrition in plants and rhizospheric microorganisms,* (2006): 169-198.

97. E. Gamalero and B. R. Glick, 'Mechanisms used by plant growth-promoting bacteria', *Bacteria in agrobiology: plant nutrient management*, (2011): 17-46.

98. M. Omidvari, R. A. Sharifi, M. Ahmadzadeh and P. A. Dahaji, 'Role of fluorescent pseudomonads siderophore to increase bean growth factors', *Journal of Agricultural Science*, 2 (2010): 242.

99. S. Dey, P. Regon, S. Kar and S. K. Panda, 'Chelators of iron and their role in plants' iron management', *Physiology and Molecular Biology of Plants*, 26 (2020): 1541-1549.

100. E. Gamalero and B. R. Glick, Bacterial ACC deaminase and IAA: interactions and consequences for plant growth in polluted environments, *Handbook of phytoremediation,* (2011): 763-773.

101. H. Siebner-Freibach, Y. Hadar and Y. Chen, 'Siderophores sorbed on Ca-montmorillonite as an iron source for plants', *Plant and Soil*, 251 (2003): 115-124.

102. V. Verma, S. Singh and S. Prakash, 'Bio-control and plant growth promotion potential of siderophore producing endophytic Streptomyces from Azadirachta indica A. Juss', *Journal of basic microbiology*, 51 (2011): 550-556.

103. S. Rungin, C. Indananda, P. Suttiviriya, W. Kruasuwan, R. Jaemsaeng and A. Thamchaipenet, 'Plant growth enhancing effects by a siderophore-producing endophytic streptomycete isolated from a Thai jasmine rice plant (Oryza sativa L. cv. KDML105)', *Antonie Van Leeuwenhoek*, 102 (2012): 463-472.

104. M. Gangwar and G. Kaur, 'Isolation and characterization of endophytic bacteria from endorhizosphere of sugarcane and ryegrass', *Internet J Microbiol*, 7 (2009): 139-144.

105. S. Yadav, R. Kaushik, A. K. Saxena and D. K. Arora, 'Diversity and phylogeny of plant growth-promoting bacilli from moderately acidic soil', *Journal of Basic Microbiology*, 51 (2011): 98-106.

106. W. Qi and L. Zhao, 'Study of the siderophore-producing Trichoderma asperellum Q1 on cucumber growth promotion under salt stress', *Journal of basic microbiology*, 53 (2013): 355-364.

107. L. van Schöll, T. W. Kuyper, M. M. Smits, R. Landeweert, E. Hoffland and N. v. Breemen, 'Rock-eating mycorrhizas: their role in plant nutrition and biogeochemical cycles', *Plant and Soil*, 303 (2008): 35-47.

108. C. W. Jin, G. X. Li, X. H. Yu and S. J. Zheng, 'Plant Fe status affects the composition of siderophore-secreting microbes in the rhizosphere', *Annals of botany*, 105 (2010): 835-841.

109. J. Masalha, H. Kosegarten, Ö. Elmaci and K. Mengel, 'The central role of microbial activity for iron acquisition in maize and sunflower', *Biology and Fertility of Soils*, 30 (2000): 433-439.

110. H. Marschner, V. Römheld and M. Kissel, 'Different strategies in higher plants in mobilization and uptake of iron', *Journal of plant nutrition*, 9 (1986): 695-713.

111. C. Voisard, C. Keel, D. Haas and G. Dèfago, 'Cyanide production by Pseudomonas fluorescens helps suppress black root rot of tobacco under gnotobiotic conditions', *The EMBO Journal*, 8 (1989): 351-358.

112. B. Schippers, A. W. Bakker and P. A. Bakker, 'Interactions of deleterious and beneficial rhizosphere microorganisms and the effect of cropping practices', *Annual Review of Phytopathology*, 25 (1987): 339-358.

113. K. Pal, K. Tilak, A. Saxcna, R. Dey and C. Singh, 'Suppression of maize root diseases caused by Macrophomina phaseolina, Fusarium moniliforme and Fusarium graminearum by plant growth promoting rhizobacteria', *Microbiological research*, 156 (2001): 209-223.

114. A. Beneduzi, A. Ambrosini and L. M. Passaglia, 'Plant growth-promoting rhizobacteria (PGPR): their potential as antagonists and biocontrol agents', *Genetics and molecular biology*, 35 (2012): 1044-1051.

115. M.-K. Zhang, Z.-Y. Liu and H. Wang, 'Use of single extraction methods to predict bioavailability of heavy metals in polluted soils to rice', *Communications in soil science and plant analysis*, 41 (2010): 820-831.

116. R. A. Wuana and F. E. Okieimen, 'Heavy metals in contaminated soils: a review of sources, chemistry, risks and best available strategies for remediation', *International Scholarly Research Notices*, 2011 (2011).

117. L. M. Gaetke and C. K. Chow, 'Copper toxicity, oxidative stress, and antioxidant nutrients', *Toxicology*, 189 (2003): 147-163.

118. A. Nair, A. A. Juwarkar and S. K. Singh, 'Production and characterization of siderophores and its application in arsenic removal from contaminated soil', *Water, Air, and Soil Pollution*, 180 (2007): 199-212.

119. M. Rajkumar, N. Ae, M. N. V. Prasad and H. Freitas, 'Potential of siderophore-producing bacteria for improving heavy metal phytoextraction', *Trends in biotechnology*, 28 (2010): 142-149.

120. S. O'Brien, D. J. Hodgson and A. Buckling, 'Social evolution of toxic metal bioremediation in Pseudomonas aeruginosa', *Proceedings of the Royal Society B: Biological Sciences*, 281 (2014): 20140858.

121. A. Magdalena, M. Mathilde and J. Edith, 'Chapter five-siderophores: from natural roles to potential applications', *J Adv Appl Microbiol*, 106 (2019): 193-225.

122. S. Rapti, S. C. Boyatzis, S. Rivers and A. Pournou, 'Siderophores and their applications in wood, textile, and paper conservation', *Microorganisms in the deterioration and preservation of cultural heritage*, (2021): 301-339.

123. B. Xie, X. Wei, C. Wan, W. Zhao, R. Song, S. Xin and K. Song, 'Exploring the biological pathways of siderophores and their multidisciplinary applications: A comprehensive review', *Molecules*, 29 (2024): 2318.

124. S. K. Ghosh, T. Bera and A. M. Chakrabarty, 'Microbial siderophore–A boon to agricultural sciences', *Biological Control*, 144 (2020): 104214.

125. Z. Roskova, R. Skarohlid and L. McGachy, 'Siderophores: an alternative bioremediation strategy?', *Science of the Total Environment*, 819 (2022): 153144.

126. M. Majewska, A. Słomka and A. Hanaka, 'Siderophore-producing bacteria from Spitsbergen soils—novel agents assisted in bioremediation of the metal-polluted soils', *Environmental Science and Pollution Research*, 31 (2024): 32371-32381.

127. B. Khasheii, P. Mahmoodi and A. Mohammadzadeh, 'Siderophores: Importance in bacterial pathogenesis and applications in medicine and industry', *Microbiological Research*, 250 (2021): 126790.

128. S. B. Mayegowda and M. N. Gadilingappa, 'Microbial Siderophores: A New Insight on Healthcare Applications', *BME frontiers*, 6 (2025): 0112.

129. B. Nagoba and D. V. Vedpathak, 'Medical applications of siderophores–a review', *European Journal of General Medicine*, 8 (2011): 230-233.

130. G. Tonziello, E. Caraffa, B. Pinchera, G. Granata and N. Petrosillo, 'Present and future of siderophore-based therapeutic and diagnostic approaches in infectious diseases', *Infectious disease reports*, 11 (2019): 8208.

131. D. Fan and Q. Fang, 'Siderophores for medical applications: imaging, sensors, and therapeutics', *International Journal of Pharmaceutics*, 597 (2021): 120306.

132. A. K. Passari, B. Ruiz-Villafán, R. Cruz-Bautista, V. Díaz-Domínguez, R. Rodríguez-Sanoja and S. Sanchez, 'Opportunities and challenges of microbial siderophores in the medical field', *Applied Microbiology and Biotechnology*, 107 (2023): 6751-6759.

133. H. Boukhalfa and A. L. Crumbliss, 'Chemical aspects of siderophore-mediated iron transport', *Biometals*, 15 (2002): 325-339.

134. J. I. Wirgau, I. Spasojević, H. Boukhalfa, I. Batinić-Haberle and A. L. Crumbliss, 'Thermodynamics, kinetics, and mechanism of the stepwise dissociation and formation of Tris (L-lysinehydroxamato) iron (III) in aqueous acid', *Inorganic chemistry*, 41 (2002): 1464-1473.

135. C. Ratledge, 'Iron metabolism and infection', *Food and nutrition bulletin*, 28 (2007): S515-S523.

136. S. Dhungana and A. L. Crumbliss, 'Coordination chemistry and redox processes in siderophore-mediated iron transport', *Geomicrobiology Journal*, 22 (2005): 87-98.

137. W. Schenkeveld, E. Oburger, B. Gruber, Y. Schindlegger, S. Hann, M. Puschenreiter and S. Kraemer, 'Metal mobilization from soils by phytosiderophores–experiment and equilibrium modeling', *Plant and Soil*, 383 (2014): 59-71.

138. W. Schenkeveld, Y. Schindlegger, E. Oburger, M. Puschenreiter, S. Hann and S. Kraemer, 'Geochemical processes constraining iron uptake in strategy II Fe acquisition', *Environmental science & technology*, 48 (2014): 12662-12670.

139. O. W. Duckworth, J. R. Bargar and G. Sposito, 'Coupled biogeochemical cycling of iron and manganese as mediated by microbial siderophores', *Biometals*, 22 (2009): 605-613.

140. J. M. Harrington, O. W. Duckworth and K. Haselwandter, 'The fate of siderophores: antagonistic environmental interactions in exudate-mediated micronutrient uptake', *Biometals*, 28 (2015): 461-472.

141. S. M. Kraemer, O. W. Duckworth, J. M. Harrington and W. D. Schenkeveld, 'Metallophores and trace metal biogeochemistry', *Aquatic Geochemistry*, 21 (2015): 159-195.

142. D. A. Brown, L. P. Cuffe, N. J. Fitzpatrick and Á. T. Ryan, 'A DFT study of model complexes of zinc hydrolases and their inhibition by hydroxamic acids', *Inorganic Chemistry*, 43 (2004): 297-302.

143. G. Winkelmann, B. Busch, A. Hartmann, G. Kirchhof, R. Süßmuth and G. Jung, 'Degradation of desferrioxamines by Azospirillum irakense: Assignment of metabolites by HPLC/electrospray mass spectrometry', *Biometals*, 12 (1999): 255-264.

144. R. L. Sinsabaugh, 'Phenol oxidase, peroxidase and organic matter dynamics of soil', *Soil Biology and Biochemistry*, 42 (2010): 391-404.

145. C. Kim, W. W. Lorenz, J. T. Hoopes and J. F. Dean, 'Oxidation of phenolate siderophores by the multicopper oxidase encoded by the Escherichia coli yacK gene', *Journal of bacteriology*, 183 (2001): 4866-4875.

146. L. Tian, E. Dell and W. Shi, 'Chemical composition of dissolved organic matter in agroecosystems: correlations with soil enzyme activity and carbon and nitrogen mineralization', *Applied Soil Ecology*, 46 (2010): 426-435.

147. N. Zaya, A. Roginsky, J. Williams and D. Castignetti, 'Evidence that a deferrioxamine B degrading enzyme is a serine protease', *Canadian Journal of Microbiology*, 44 (1998): 521-527.

148. A. Pierwola, T. Krupinski, P. Zalupski, M. Chiarelli and D. Castignetti, 'Degradation pathway and generation of monohydroxamic acids from the trihydroxamate siderophore deferrioxamine B', *Applied and environmental microbiology*, 70 (2004): 831-836.

149. H. Toberman, C. D. Evans, C. Freeman, N. Fenner, M. White, B. A. Emmett and R. R. Artz, 'Summer drought effects upon soil and litter extracellular phenol oxidase activity and soluble carbon release in an upland Calluna heathland', *Soil Biology and Biochemistry*, 40 (2008): 1519-1532.

150. M. Villavicencio and J. Neilands, 'An inducible ferrichrome A-degrading peptidase from *Pseudomonas* FC-1', *Biochemistry*, 4 (1965): 1092-1097.

151. R. Warren and J. Neilands, 'Microbial degradation of the ferrichrome compounds', *Microbiology*, 35 (1964): 459-470.

152. R. Warren and J. Neilands, 'Mechanism of microbial catabolism of ferrichrome A', *Journal of Biological Chemistry*, 240 (1965): 2055-2058.

153. A. Enoki, S. Itakura and H. Tanaka, 'The involvement of extracelluar substances for reducing molecular oxygen to hydroxyl radical and ferric iron to ferrous iron in wood degradation by wood decay fungi', *Journal of biotechnology*, 53 (1997): 265-272.

154. H. Tanaka, S. Itakura and A. Enoki, 'Hydroxyl radical generation by an extracellular low-molecular-weight substance and phenol oxidase activity during wood degradation by the white-rot basidiomycete Trametes versicolor', *Journal of Biotechnology*, 75 (1999): 57-70.

155. S. Adak and R. K. Banerjee, 'Haem propionates control oxidative and reductive activities of horseradish peroxidase by maintaining the correct orientation of the haem', *Biochemical Journal*, 334 (1998): 51-56.

156. M. Miethke and M. A. Marahiel, 'Siderophore-based iron acquisition and pathogen control', *Microbiology and molecular biology reviews*, 71 (2007): 413-451.

157. M. A. Fischbach, H. Lin, D. R. Liu and C. T. Walsh, 'How pathogenic bacteria evade mammalian sabotage in the battle for iron', *Nature Chemical Biology*, 2 (2006): 132-138.

158. B. H. Baig, I. Wachsmuth and G. Morris, 'Utilization of exogenous siderophores by Campylobacter species', *Journal of clinical microbiology*, 23 (1986): 431-433.

159. F. Harrison, J. Paul, R. C. Massey and A. Buckling, 'Interspecific competition and siderophore-mediated cooperation in Pseudomonas aeruginosa', *The ISME journal*, 2 (2008): 49-55.

160. E. Bar-Ness, Y. Hadar, Y. Chen, V. Romheld and H. Marschner, 'Short-term effects of rhizosphere microorganisms on Fe uptake from microbial siderophores by maize and oat', *Plant physiology*, 100 (1992): 451-456.

161. H. El-Gendi, A. K. Saleh, R. Badierah, E. M. Redwan, Y. A. El-Maradny and E. M. El-Fakharany, 'A comprehensive insight into fungal enzymes: Structure, classification, and their role in mankind's challenges', *Journal of Fungi*, 8 (2021): 23.

162. M. Frąc, S. E. Hannula, M. Bełka and M. Jędryczka, 'Fungal biodiversity and their role in soil health', *Frontiers in microbiology*, 9 (2018): 707.

163. M. F. Traxler, M. R. Seyedsayamdost, J. Clardy and R. Kolter, 'Interspecies modulation of bacterial development through iron competition and siderophore piracy', *Molecular microbiology*, 86 (2012): 628-644.

164. J. Franke, K. Ishida and C. Hertweck, 'Evolution of siderophore pathways in human pathogenic bacteria', *Journal of the American Chemical Society*, 136 (2014): 5599-5602.

165. C. Ratledge and L. G. Dover, 'Iron metabolism in pathogenic bacteria', *Annual reviews in microbiology*, 54 (2000): 881-941.

166. I. Loaces, L. Ferrando and A. Fernández Scavino, 'Dynamics, diversity and function of endophytic siderophore-producing bacteria in rice', *Microbial ecology*, 61 (2011): 606-618.

167. O. Baars, F. o. M. Morel and D. H. Perlman, 'ChelomEx: Isotope-assisted discovery of metal chelates in complex media using high-resolution LC-MS', *Analytical Chemistry*, 86 (2014): 11298-11305.

168. O. Baars and D. H. Perlman, Small molecule LC-MS/MS fragmentation data analysis and application to siderophore identification, *Applications from Engineering with MATLAB Concepts,* (2016): 189.

169. O. Baars, X. Zhang, F. M. Morel and M. R. Seyedsayamdost, 'The siderophore metabolome of Azotobacter vinelandii', *Applied and Environmental Microbiology*, 82 (2016): 27-39.

170. O. Baars, F. M. Morel and X. Zhang, 'The purple non-sulfur bacterium Rhodopseudomonas palustris produces novel petrobactin-related siderophores under aerobic and anaerobic conditions', *Environmental microbiology*, 20 (2018): 1667-1676.

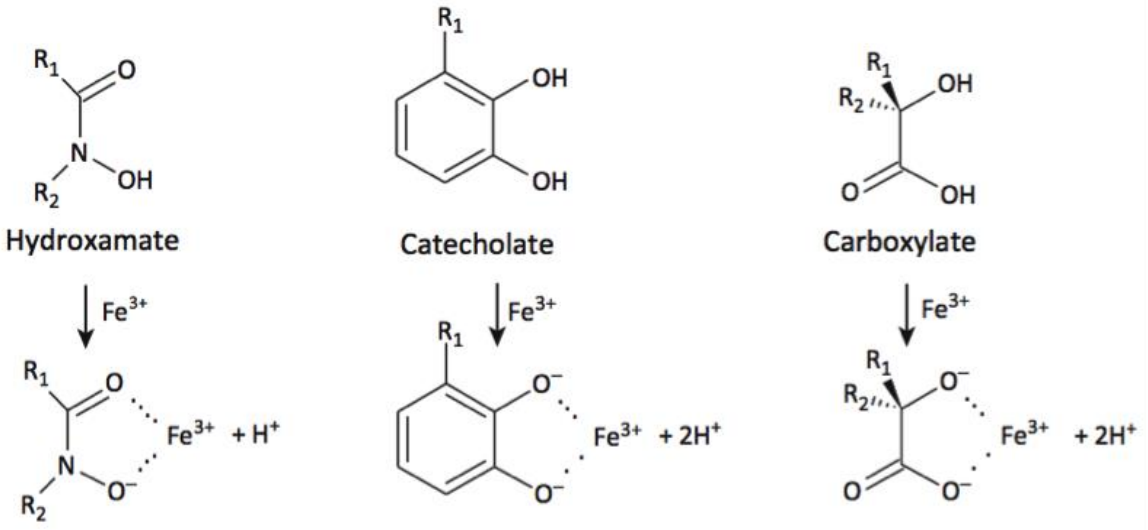

Figure 1. Structure of the three chelating moieties incorporated in siderophore structures.

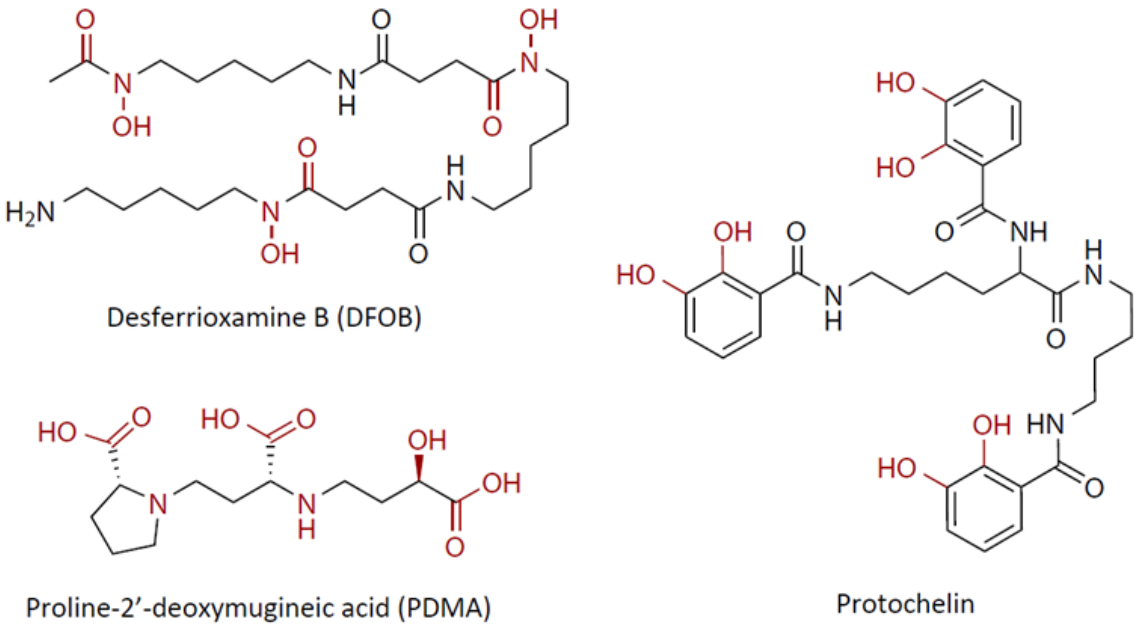

Figure 2. Structure of the three siderophore structures in this study. The different moieties involved in Fe complexation are indicated in red.

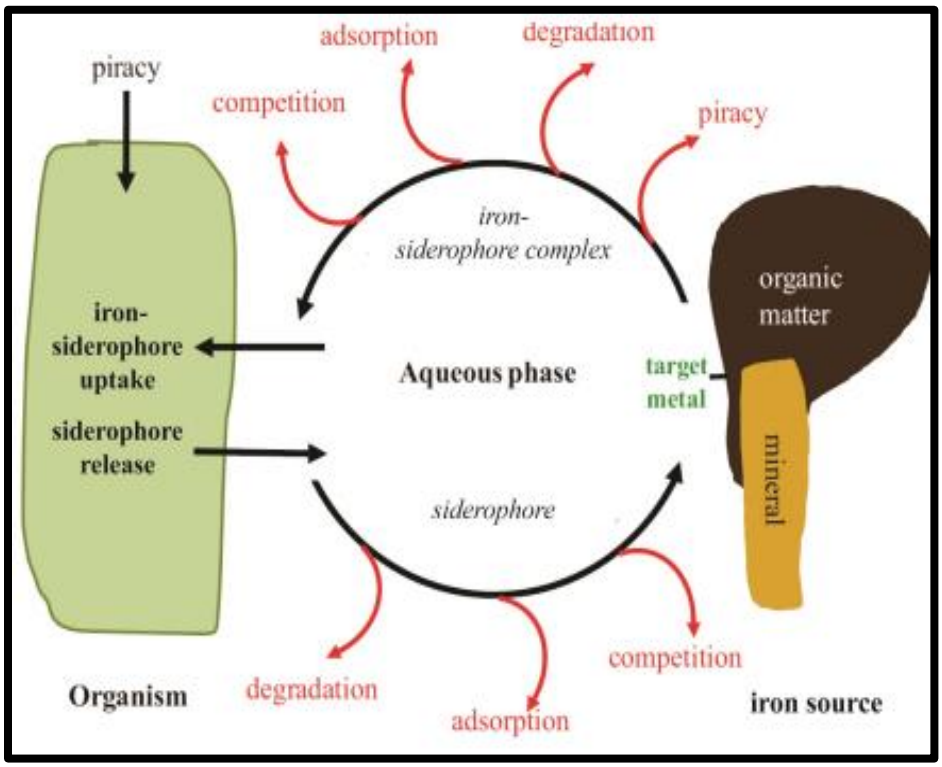

Figure 3. Schematics show antagonistic interactions between siderophores, Fe(III)-siderophore complexes, and reactive soil components. Red arrows represent disruptive interactions that form the basis of the research work. Adapted from Kraemer et al. (2015)[141].

Chapter 2

Degradation of catecholate, hydroxamate, and carboxylate model siderophores by extracellular enzymes

2.1 Introduction

Iron (Fe) is an essential nutrient for plant growth and crop production. Competition for Fe impacts microbial activity and host-pathogen interactions [1, 2]. At circumneutral pH and in oxygenated environments, Fe bioavailability is restricted by the formation of low solubility Fe^{III} oxide and hydroxide minerals. Bacteria [3, 4], fungi [5], and graminaceous plants [2, 6-8] exude siderophores, a structurally diverse class of small molecules, to solubilize, complex, and promote the uptake of Fe from otherwise biologically unavailable sources. Iron acquisition with siderophores is typically conceptualized to occur via the following steps: (1) siderophore biosynthesis and secretion [2, 9]; (2) diffusion of the free siderophore in the extracellular medium [10-12]; (3) complexation of Fe^{III} from environmental sources [13-15]; (4) diffusion of the Fe^{III}-siderophore complex back to the cell surface [16, 17]; and (5) Fe uptake from the Fe^{III}-siderophore complex via processes such as ferric siderophore transporters or reductive Fe uptake [18, 19].

Through the transport and solubilization processes, there may be numerous sinks for siderophores that disrupt Fe uptake [20-22]. Among the possible siderophore sinks are reactions with environmentally common extracellular enzymes [6, 13, 23]. Extracellular enzymes may have high activities at circumneutral pH, as plants and microbes secrete them to promote the degradation of organic matter, lignin, and phenolic compounds [24], and the cycling of nutrients [25, 26].

At present, we have a poor understanding of how common degradative extracellular enzymes may react with siderophores. Previously reported examples of enzymatic siderophore degradation have focused on intracellular processes that allow microbes to utilize siderophores as a carbon substrate. The reported degradation reactions involved the hydrolysis of the amide bonds in the siderophores desferrioxamine B [27, 28], and ferrichrome A [29-31]. In addition to siderophore degradation for carbon acquisition, some bacteria may utilize enzymes to release Fe^{III} from high-affinity triscatecholate siderophores. For example, *Escherichia coli* expresses ferric enterobactin esterase to hydrolyze the enterobactin trilactone scaffold, promoting bioavailability of the bound Fe [12, 32, 33]. More recently, a reduction of hydroxamate groups in trishydroxamate siderophores was reported in cultures of the root wheat symbiont *Pyrenophora biseptata* [34].

In this study, we specifically investigated whether selected model extracellular enzymes were able to react with and possibly degrade apo-siderophores and Fe^{III}-siderophore complexes. The three chosen model enzymes included phenol oxidase (a tyrosinase) from the cultivated mushroom *Agaricus bisporus*, peroxidase from horseradish, and proteases from the bacterium

Streptomyces griseus, all of which are known to be involved in organic matter decomposition and nutrient cycling [15, 24, 25, 27, 35-38]. It is worth noting that there are three phenol oxidase subtypes: catechol oxidases (catalyze the oxidation of o-diphenols), aurone synthases (oxidize chalcones to aurones, yellow pigment), and tyrosinases (hydroxylate monophenols and oxidize o-diphenols), the last of which we used in this study [39]. To represent the wide variety of siderophore structures and chemistries, we used three model siderophores: protochelin, a bacterial triscatecholamide siderophore; desferrioxamine B (DFOB), a bacterial trishydroxamate siderophore; and proline-2′-deoxymugineic acid (PDMA), a synthetic carboxylate phytosiderophore analog, developed as a novel effective iron fertilizer [40, 41]. To reduce the cost of synthesis and increase the stability of PDMA over its natural counterpart, deoxymugineic acid, the azetidine-2-carboxylic acid group in DMA has been substituted with L-proline. Each of the three siderophores was reacted as the apo-siderophore and as the Fe^{III} complex with each of the three enzymes. The degradation was monitored over time by UV-visible spectrophotometry and liquid chromatography-mass spectrometry (LC-MS). The observed siderophore degradation depended not only on the siderophore structure but also on the binding state: the ferric complexes were less reactive than the apo siderophores. Reaction kinetics for the protochelin degradation reactions were rapid and suggested the potential for catechol siderophore degradation via extracellular enzymes in microbiomes; however, further studies are required to elucidate the impact of side reactions in different ecosystem matrices.

2.2 Materials and methods

2.2.1 Siderophores.

Protochelin was synthetically prepared by the Small Molecule Synthesis Facility (SMSF) at Duke University, as previously reported [21]. PDMA was provided as PDMA·2HCl by Aichi Steel Corporation, Japan [40]. DFOB was purchased as deferoxamine mesylate salt from Sigma-Aldrich and used as received (Fig 1). Stock solutions of 10 mM were prepared in 10 mL of methanol for protochelin or 10 mL of deionized water (MQ) for DFOB and PDMA. Working solutions were prepared by diluting the stock solution to 100 μM with MQ water. To prepare the Fe^{III}-siderophore complex, 100 μM $FeCl_3$ was added to 100 μM of siderophore in MQ water. The mixture was left to stand for 1 hour in the dark with occasional shaking and then centrifuged at ca. 22000 × *g* for 3 minutes. Formation of Fe^{III}-siderophore complexes was confirmed by spectrophotometric and

liquid chromatography-mass spectrometry (LC-MS) analyses. Siderophore stocks were immediately used or stored for up to two weeks at −20 ºC.

2.2.2 Enzymes and enzyme activity.

The following three enzymes were used: (1) phenol oxidase isolated from the mushroom *Agaricus bisporus* (MilliporeSigma T3824, lyophilized powder; ≥ 1000 units/mg solid); (2) peroxidase from horseradish (Type II, MilliporeSigma P8250, 150-250 units/mg solid); and (3) protease from *Streptomyces griseus* (MilliporeSigma P5147, ≥ 3.5 units/mg). Protease from *Streptomyces griseus* consists of at least three proteolytic enzymes, including an extracellular serine protease. Assays to confirm enzyme activities were conducted using established protocols (see SI for details). Briefly, phenol oxidase activity was determined using a method adapted from [42] with L-tyrosine and oxygen as substrates, with a measured activity of 2420 units/mg solid. For peroxidase, a method adapted from Chance et al. (1955) [43] was used with pyrogallol and hydrogen peroxide as substrates. The measured activity was 55 units/mg after a 10-fold dilution of the enzyme stock solution. The protease activity was determined according to Mayerhofer et al. (1973) [44] and Cupp-Enyard (2008) [45] with casein as substrate. The activity was found to be 7.5 units/mg solid powder.

2.2.3 Siderophore reactions with enzymes.

Each of the three siderophores (Fig 1) was reacted with each of the three enzymes, both as the apo-siderophore and Fe^{III}-siderophore complex at pH = 7. For phenol oxidase and protease reactions, solutions were buffered with 1 mL of phosphate buffer (25 mM, pH = 7.0). A volume of 0.3 mL of phenol oxidase (454 units/mL) or protease (7.5 units/mL) was added. The reaction was started by the addition of 0.3 mL of a 100 μM stock solution (19 μM) of apo-siderophore or Fe^{III}-siderophore complex. For peroxidase reactions, solutions were buffered with 0.5 mL of phosphate buffer (30 mM, pH = 6.8). A volume of 0.32 mL of the peroxidase enzyme solution (55 units/mL) was added. The reaction was started by adding 0.3 mL of a 100μM stock solution (23 μM) of apo-siderophore or the Fe^{III}-siderophore complex and 0.16 mL of hydrogen peroxide (H_2O_2, 0.50 %). Two further additions of 0.16 mL H_2O_2 were made at 1-hour intervals, which decreased the added siderophore concentrations to 19 μM. Controls consisted of: (1) no enzyme (addition of buffer solution instead of enzyme solution); (2) no siderophore; and (3) heat-

inactivated enzyme reactions (where the enzyme was inactivated by heating to 95˚C for 20 minutes). In the case of peroxidase experiments, a fourth control consisted of the reaction mixture without adding H_2O_2, and water was added to maintain sample volume consistent with the concentrations of the enzyme and individual components.

Experiments were conducted in an incubator maintained at 20 ºC. Preliminary experiments monitored degradation by observation of absorption spectral changes. For peroxidase and H_2O_2, quantitative protochelin degradation occurred immediately with no further changes afterwards (Fig. S4). In contrast, phenol oxidase exhibited a slower reaction that seemed to follow Michaelis-Menten kinetics. Based on these results, reaction timepoints of immediate sampling, 0.5 h, 1 h, 2 h, and 24 h, were chosen to capture the rapid initial reaction, track slower degradation, detect degradation products accumulation, and observe potential secondary reactions or structural changes. A volume of 0.16 mL was sampled and analyzed with an ultraviolet-visible (UV-vis) spectrophotometer (190–700 nm, ThermoFisher Evolution 201). The reactions were quenched by the addition of 9 parts acetonitrile to 1 part of the enzyme reaction mixture to precipitate the enzymes, and samples were centrifuged (ca. 22000 × *g* for 10 min) and diluted 1:1 with MQ water for liquid chromatography-mass spectrometry (LC-MS) analysis. All experiments were conducted in triplicate.

2.2.4 Enzyme kinetics and substrate specificity.

The reaction between protochelin and phenol oxidase appeared to follow Michaelis-Menten kinetics. Experiments were conducted to determine the maximum reaction rate (V_{max}) and Michaelis-Menten constant (K_m). The parameters V_{max} and K_m were calculated by measuring initial reaction rates (v_0) as a function of protochelin substrate concentrations (0.01 mM; 0.02 mM; 0.05 mM; 0.1 mM; 0.2 mM; 0.5 mM; 1 mM). The initial rate (v_0) was defined as the slope of the initial linear portion of the curve obtained following the product formation as a function of time (0, 0.5, and 2 h). All measurements were done in triplicate.

2.2.5 Analysis of siderophore reactions with liquid chromatography-mass spectrometry (LC-MS).

Samples were analyzed by LC-MS using a single quadrupole mass spectrometer (ISQ-EC, ThermoFisher) in combination with a diode array detector and charged aerosol detector (ThermoFisher). Separation was done with an Agilent Poroshell 120 EC-C18 column (4.6 × 100

mm, 2.7 µm) and a flow rate of 1.2 mL/min, and the column temperature was 30°C. A sample volume of 25 µL was injected and separated under a gradient of solvents A and B (A: water, 0.1% formic acid, 1% acetonitrile; B: acetonitrile, 0.1% formic acid, 2% water; gradient: 0–1.5 min 0% B, 1.5–8 min 0–100% B; 8–10 min 100% B; re-equilibration at 100% A for 4 min). Mass spectra were collected in single ion monitoring mode targeting the three added siderophores and potential degradation products (S1 Table). Siderophore degradation was followed by tracking peak areas in the enzymatic reactions and comparison to negative controls. To identify potential degradation products, select samples were analyzed with a high-resolution LC-MS/MS platform (Orbitrap Exploris 480, ThermoFisher). On the Orbitrap platform, the C18 column was a Restek Raptor C18 (2.1 × 100 mm) with a flow rate of 0.4 mL/min, and the column compartment was held at 45°C. Full-scan mass spectra (m/z = 85–1200) in positive ionization mode were collected with the resolution set to R = 60,000 (full width at half maximum at m/z = 400). Data-dependent MS/MS spectra were acquired for the top 5 most abundant ions in each cycle. Product ions were generated in HCD mode with 35 eV collision energy and an isolation window of 1.5 Da. The resolving power for MS/MS analysis was R = 15,000 (full width at half maximum at m/z = 400). Putative degradation products of the added siderophore standards were identified in high-resolution LC-MS data by searching for new LC-MS peaks in incubated samples and by mining of MS/MS spectra for characteristic siderophore groups (e.g., presence of 2,3-dihydroxybenzoid acid moieties in protochelin degradation products showing as neutral loss of *m/z* = 136.016 in MS/MS spectra [46]). Analysis of protochelin degradation products was also conducted by LC coupled to a UV-vis diode array detector by looking for new peaks with absorption maxima in the range of the absorption maxima of the 2,3-dihydroxybenzoid acid groups in protochelin (λ=315 nm [47]).

2.3 Results

2.3.1 Decrease of dissolved siderophore concentrations by enzymes.

The phenol oxidase enzyme reacted with the triscatecholamide siderophore protochelin. The reaction with apo protochelin was nearly quantitative: ~90% of the initial protochelin concentration was not detected after a 24 h reaction period (Figure 2a and Figure S1). Reaction with the Fe^{III}-protochelin complex was slower or less complete: ~50% of the initial concentration had reacted after 24 h with phenol oxidase. Expectedly, DFOB and PDMA, which do not contain phenol or catechol groups (Figure 2a), did not react appreciably with the phenol oxidase. This

trend showed statistically significant differences between apo siderophores and Fe^{III} siderophore complex reactions ($p < 0.001$) with phenol oxidases. In contrast, reactions with protease indicated no significant statistical difference ($p \geq 0.05$) for apo siderophores and Fe^{III} siderophore complexes. Experimental controls of all siderophores with the phenol oxidase and protease enzymes showed no changes in absorbance spectra (data not shown).

The reaction of peroxidase and H_2O_2 with protochelin resulted in ~80% degradation of both apo-protochelin and Fe^{III}-protochelin after a 24 h reaction period based on LC-MS quantification (Figure 2b). For the Fe^{III}-protochelin complex, the characteristic blue color of the Fe-complex turned clear after a 24 h reaction alongside the disappearance of the UV-vis spectral signature of the protochelin Fe-complex (λ = 560 nm [47, 48]). However, controls with heat-inactivated peroxidase and H_2O_2 used, or with H_2O_2 in the absence of the enzyme, also had a similar extent of degradation, indicating that a direct uncatalyzed reaction with H_2O_2 was primarily responsible for the degradation reaction and not the enzyme-catalyzed reaction (Figures S7-S9). In contrast to protochelin, both the ferric complex and apo forms of DFOB and PDMA were relatively unreactive with peroxidase and H_2O_2 (Figure 2b). Finally, protease did not significantly (< 4%) react with any of the apo siderophores or their Fe^{III}-siderophore complexes (Figure 2c).

2.3.2 Identification of siderophore degradation products.

Sample aliquots at three time points (30 minutes, 2 h, and 24 h) were collected from triplicate reactions of phenol oxidase and peroxidase enzymes with protochelin and analyzed by LC-MS/MS. When reacted with phenol oxidase, degradation products were observed, namely the oxidation of the catechol moieties to quinones (Figure 3). The observed m/z values corresponded to the sum formulas equal to the oxidation of one or two catechol moieties (protochelin-2H, protochelin-4H) by the phenol oxidase enzyme, as previously reported [34], and LC-MS/MS analysis was in agreement with the oxidation occurring in the catechol groups (Supplementary Table 2). The oxidation of the catechol groups leads to a lessened affinity for Fe^{III} due to the loss of binding moieties. Subsequent reaction products observed were based on further reaction and degradation but accounted for only minor peak areas, including the product corresponding to the oxidation of all three catechol moieties (protochelin-6H, Supplementary Table 2). Although we were not able to obtain authentic standards for the degradation products, it is interesting to note that the sum of all peak areas of protochelin degradation products amounted to ~80 % of the original protochelin

standard peak area after a 30-minute reaction but only ~10 % after a 24-hour reaction. Assuming the initial degradation products ionized similarly to the original protochelin structure, this suggested that these degradation products accounted for a majority of protochelin removal from the solution at 30 minutes. At longer reaction times, it is possible that smaller fragments with reduced ionization efficiency may have formed, which may account for the lower sum of the degradation product peak areas. For example, 2,3-dihydroxybenzoic acid has a more than 10-fold lower ionization efficiency than protochelin [46, 49-52]. No significant differences appeared between the control and reaction samples for the protochelin m/z value at the initial sampling time (0 h), but there were significant differences at 0.5 h, 2 h, and 24 h. In contrast, the degradation products showed significant differences between the control and reaction samples across these different time points (0.5, 2 h, 24 h).

In the presence of the peroxidase enzyme and H_2O_2, protochelin concentrations decreased in the reaction solution (Figures S2, S4, and S5), with most of the protochelin reacting rapidly; only ~20% of the initial protochelin concentration was detected in aliquots taken immediately after the reaction was started. However, no putative degradation products were detectable by LC-MS/MS (see discussion section for possible explanations).

2.3.3 Siderophore degradation kinetics.

The reaction between phenol oxidase and protochelin appeared to follow Michaelis-Menten kinetics (Fig 4a). The calculated K_m and V_{max} values from Lineweaver-Burk plots (Fig 4b) were K_m = 0.43 mM and V_{max} = 1.29 μM/min. Compared with other phenolics (diphenols & triphenols) reported in the literature (Table 1), our data showed the lowest K_m of all previously reported substrates [53]. For substrate specificity (V_{max}/K_m), previously reported V_{max}/K_m values of phenolic substrates were greatest for small molecules, including catechol [54, 55], or 4-methylcatechol [53]. Protochelin specificity was low (0.003 min^{-1}), which is consistent with previously reported trends [56]. After normalizing Vmax values to enzyme activity units, the normalized Vmax value and specificity in this study are similar in magnitude to the triphenolic substrates pyrogallol (0.0071 min^{-1}) [53]. On the other hand, Fe^{III}-protochelin complexes did not follow Michaelis-Menten kinetics and thus were not investigated in detail.

2.4 Discussion

2.4.1 Siderophore Degradation.

In this study, we examined the ability of three extracellular enzymes secreted by plants and a diverse array of microbes to degrade three representative siderophore structures. The results indicated that phenol oxidase and peroxidase were effective in degrading protochelin. In contrast, DFOB and PDMA, and their corresponding Fe^{III}-siderophore complexes, showed negligible reactivity. This outcome may be explained by the absence of catechol moieties in DFOB and PDMA, which are known to react with these oxidative enzymes. Considering our reaction time and pH, where DFOB [59] and PDMA [60] are generally stable, and the enzyme concentration aligns with the practical activity range in various environments, such as the soil microbiomes [25], this result emphasizes that the degradation of siderophores by enzymes may be influenced by their structure, concentration, and binding affinities.

Further investigation into phenol oxidase activity revealed that the reduction of dissolved protochelin concentration correlated with the formation of protochelin degradation products, where the 2,3-dihydroxybenzoate binding groups were oxidized to quinone groups (Figure 3b). Our results are consistent with a previous report indicating that the oxidation of protochelin to quinones followed a reversible redox reaction mechanism that may be employed by microbes to release Fe from the Fe^{III}-protochelin complexes because the quinone groups possess lesser Fe^{III} binding affinities [21]. Conversely, other studies have described the catechol groups as a "suicide substrate" for the tyrosinase enzyme, causing irreversible inactivation during catechol oxidation. This inactivation occurs through two mechanisms: (a) an attack on the nucleophilic group vicinal to the enzyme active site by quinone oxidation products [61], followed by (b) a free radical attack via reactive oxygen species formed during oxidation on the enzyme's active site [62, 63]. However, no evidence of this phenomenon was observed in our study, as the enzyme did not precipitate out of the solution.

The kinetic values of V_{max} = 1.29 μM min^{-1} and substrate specificity V_{max}/K_m = 0.003 $min^{-1,}$ as well as normalized V_{max} values from our results, compared with other phenols (including diphenols and triphenols) reported in the literature, suggested that protochelin degrades slowly and with unspecific affinity compared to smaller phenolic compounds. Earlier reports on phenol oxidases propounded that the substrate-binding site of phenol oxidases has a high affinity for smaller o-diphenols [56] such as catechol [57, 64, 65], 4-methyl catechol [66], or L-dopa [55, 67], and less

affinity for the larger o-diphenols [53] and triphenols [53, 56]. Based on this trend, a plausible explanation for our results could be steric hindrance from protochelin's triscatecholamide structure and long-tail aliphatic amides.

A diversity of phenol oxidases are known to occur widely in nature, produced by fungi (*Agaricus bisporus* [68], *Basidiomycota* [69]), bacteria (*Azotobacter chroococcum* [25, 70]), and plants (apricot [71], Chinese Toon [72], mamey [73], Hemşin apple [74], and lentil sprouts [75]). It is possible that these phenol oxidase enzymes may have a range of reactivities with protochelin depending on the enzyme sources in the environment. Although we did not study protochelin siderophore with other types of phenol oxidases (catechol oxidases, aurone synthases) or in the presence of other phenol substrates, our results showed that such enzyme-siderophore reactions may occur and thus may impact environmental Fe complexation and transport.

Additionally, Fe^{III}-protochelin complexes degraded less (~50%) when reacted with phenol oxidase, suggesting that Fe^{III} binding may have restricted direct interaction of the catechol groups with enzyme active sites, thereby reducing the rate of reaction for protochelin degradation (S6 Fig). A prior review on microbial siderophore-mediated transport noted that Fe^{III} binding by the triscatecholate siderophore enterobactin enhanced stability and improved resistance to potential degrading enzymes [3]. Because protochelin has a high affinity for Fe^{III} and can bind over a wide pH range [21, 48], we can assume minimal dissociation of complexes, resulting in potential protection of complexes from enzymic degradation under environmentally common pH values.

The peroxidase enzyme and co-substrate H_2O_2 removed protochelin from the solution rapidly (Figures S4 and S5). This outcome was not surprising, as peroxidases have previously been reportedly utilized in the biodegradation of phenolic contaminants in bioremediation studies [69, 76]. However, we did not observe any degradation products by LC-MS or LC-UV-vis, and attempts to recover protochelin or its degradation products by solid phase extraction with methanol were unsuccessful (not shown). This absence of degradation products was not likely caused by protochelin residues being trapped in the enzyme's binding sites, as no precipitates were observed in our experiments. Furthermore, the protochelin peak also rapidly diminished when reacted with H_2O_2 in the absence of peroxidase (Figure S7). In contrast, degradation was slow when only peroxidase was present in the absence of H_2O_2 (Figure S8). Thus, our results indicate that H_2O_2 promotes degradation even without catalysis by peroxidase. Because H_2O_2 may be present in

(sub)-micromolar concentrations in soil [77] and aquatic environments [78, 79], our observations may have highlighted a potential role of H_2O_2 in the degradation of the catechol-type siderophores.

In contrast to protochelin, the reaction of peroxidase (and H_2O_2) with DFOB and PDMA was insignificant. This outcome may be anticipated due to the lack of catechol groups in these siderophores and, consequently, a much higher stability towards oxidation by H_2O_2. Moreover, the hydroxamate groups in DFOB have been noted previously as inhibitors of peroxidases [80-82], where the hydroxamate moieties may form hydrogen-bond interactions with the backbone of enzymes, which is critical for their selectivity as enzyme inhibitors [83].

Protease showed no significant activity with any of our siderophores, despite being reported to play a crucial role in catalyzing the initial step of protein degradation in cellular nitrogen metabolism, for example, in the rhizosphere [84, 85]. A plausible explanation for the low reactivity of protease with protochelin, DFOB, and PDMA may lie in the modified structures of the peptide monomers, which make up these siderophores, and which render them poor substrates for protease activity. In our experiments, an increase in protease concentrations established that the observed lack of reactivity is likely due to enzyme specificity and not insufficient enzyme concentration. Additionally, the hydroxamate groups present in DFOB are recognized as effective inhibitors of proteases [86, 87]. Moreover, it was reported that the inhibition of protease activity was notably increased with higher DFOB production by *Streptomyces pilosus* ATCC 19797 in soybean medium [88], consequently enhancing their carbon source. Intracellular protease activity is crucial for processes like protein and siderophore degradation [38, 89], signaling [90], and cellular turnover [91], whereas extracellular proteases are mostly involved in plant immunity [92] and interactions with the environment [93, 94]. This process specifically, may in part explain why our extracellular protease showed nearly inert behavior toward substrates containing catechol, hydroxamate, and carboxylate groups.

The proline analog of deoxymugineic acid (PDMA) demonstrated minimal reactivity with the three extracellular enzymes (~1–4 % degradation). PDMA is a synthetic phytosiderophore analog and does not represent bacterial or fungal carboxylate siderophore structures, but it is an analog of phytosiderophores, such as deoxymugineic acid [95, 96]. PDMA demonstrates greater stability than its natural counterpart, deoxymugineic acid (DMA), due to structural modifications [97]. This enhanced stability is in part why PDMA was chosen, and because of recent interest in its use as a new effective Fe fertilizer [60, 98-100]. In particular, its relative stability may be attributed to

the substitution of the traditional azetidine-2-carboxylic acid group in deoxymugineic acid (DMA) with an L-Proline analog [40, 41], which helps decrease its degradation rate by microorganisms. Our results with extracellular enzymes are consistent with this increased structural stability. Additional studies with other compounds in the mugineic acid family may better constrain the range of susceptibilities of phytosiderophores to degradation by extracellular enzymes.

2.4.2 Impact of siderophore degradation on iron cycling.

The environmental distribution and activities of extracellular enzymes are influenced by several factors, including water table depth [101], organic carbon content (SOC) [68], pH [102], and soil depth [103]. Importantly, most enzymes are inducible, meaning that plants and microbes produce these extracellular enzymes in response to the availability of substrate and/or product. Therefore, this makes enzyme activities dynamic, changing with the concentrations of substrates or products in various microbiomes. Soil, for example, can show relatively high activities of phenol oxidase [104], peroxidase [105], and protease [106] due to the presence of abundant inducible substrates, such as proteins/peptides [107, 108], and lignin, along with other phenolic compounds [25]. Similarly, as Fe availability decreases, plants and microbes experience abiotic stress. Consequently, this stress stimulates the exudation of siderophores, which are typically found at submicromolar concentrations extracted from soil [51], and could interact with these oxidative extracellular enzymes, leading to degradation. However, the presence of other compounds, such as phenolics, could potentially interfere with the degradation process, for example, by competing for enzyme active sites, altering redox reactions, or scavenging reactive radicals, especially considering the low substrate specificity of the siderophores we tested. Given their importance in organic matter decomposition and nutrient cycling, these extracellular enzyme activities related to siderophore degradation may likely interact with the siderophores released by plants or microbes in response to Fe deficiency, thereby affecting competition for Fe by microbiomes. Further studies are required to better establish the impact of phenol oxidases and peroxidases on catechol siderophore degradation in various microbiomes, such as root environments or natural water systems.

REFERENCES

1. P. Lemanceau, Role of competition for carbon and iron in mechanisms of soil suppressiveness to Fusarium wilts, *Vascular wilt diseases of plants,* (1989): 385-396.

2. A. Robin, G. Vansuyt, P. Hinsinger, J. M. Meyer, J.-F. Briat and P. Lemanceau, 'Iron dynamics in the rhizosphere: consequences for plant health and nutrition', *Advances in agronomy*, 99 (2008): 183-225.

3. G. Winkelmann, 'Microbial siderophore-mediated transport', *Biochemical Society Transactions*, 30 (2002): 691-696.

4. C. Wandersman and P. Delepelaire, 'Bacterial iron sources: from siderophores to hemophores', *Annual review of microbiology*, 58 (2004): 611.

5. J. C. Renshaw, G. D. Robson, A. P. Trinci, M. G. Wiebe, F. R. Livens, D. Collison and R. J. Taylor, 'Fungal siderophores: structures, functions and applications', *Mycological Research*, 106 (2002): 1123-1142.

6. S. M. Kraemer, D. Crowley and R. Kretzschmar, 'Geochemical aspects of phytosiderophore-promoted iron acquisition by plants', *Advances in agronomy*, 91 (2006): 1-46.

7. J. Neilands, 'Iron absorption and transport in microorganisms', *Annual review of nutrition*, 1 (1981): 27-46.

8. P. Lemanceau, P. Bauer, S. Kraemer and J.-F. Briat, 'Iron dynamics in the rhizosphere as a case study for analyzing interactions between soils, plants and microbes', *Plant and Soil*, 321 (2009): 513-535.

9. J. Neilands, 'Siderophores: structure and function of microbial iron transport compounds', *Journal of Biological Chemistry*, 270 (1995): 26723-26726.

10. A. Albrecht-Gary and A. Crumbliss, 'Coordination chemistry of siderophores: thermodynamics and kinetics of iron chelation and release', *Metal ions in biological systems*, 35 (1998): 239-327.

11. C. Ratledge, 'Iron metabolism and infection', *Food and nutrition bulletin*, 28 (2007): S515-S523.

12. R. C. Hider and X. Kong, 'Chemistry and biology of siderophores', *Natural product reports*, 27 (2010): 637-657.

13. S. Dhungana and A. L. Crumbliss, 'Coordination chemistry and redox processes in siderophore-mediated iron transport', *Geomicrobiology Journal*, 22 (2005): 87-98.

14. A. Stintzi, C. Barnes, J. Xu and K. N. Raymond, 'Microbial iron transport via a siderophore shuttle: a membrane ion transport paradigm', *Proceedings of the National Academy of Sciences*, 97 (2000): 10691-10696.

15. O. W. Duckworth, J. R. Bargar and G. Sposito, 'Coupled biogeochemical cycling of iron and manganese as mediated by microbial siderophores', *Biometals*, 22 (2009): 605-613.

16. H. Boukhalfa and A. L. Crumbliss, 'Chemical aspects of siderophore mediated iron transport', *Biometals*, 15 (2002): 325-339.

17. J. I. Wirgau, I. Spasojević, H. Boukhalfa, I. Batinić-Haberle and A. L. Crumbliss, 'Thermodynamics, kinetics, and mechanism of the stepwise dissociation and formation of Tris (L-lysinehydroxamato) iron (III) in aqueous acid', *Inorganic chemistry*, 41 (2002): 1464-1473.

18. W. Schenkeveld, Y. Schindlegger, E. Oburger, M. Puschenreiter, S. Hann and S. Kraemer, 'Geochemical processes constraining iron uptake in strategy II Fe acquisition', *Environmental science & technology*, 48 (2014): 12662-12670.

19. W. Schenkeveld, E. Oburger, B. Gruber, Y. Schindlegger, S. Hann, M. Puschenreiter and S. Kraemer, 'Metal mobilization from soils by phytosiderophores–experiment and equilibrium modeling', *Plant and Soil*, 383 (2014): 59-71.

20. O. W. Duckworth and G. Sposito, 'Siderophore-manganese (III) interactions. I. Air-oxidation of manganese (II) promoted by desferrioxamine B', *Environmental science & technology*, 39 (2005): 6037-6044.

21. J. M. Harrington, J. R. Bargar, A. A. Jarzecki, J. G. Roberts, L. A. Sombers and O. W. Duckworth, 'Trace metal complexation by the triscatecholate siderophore protochelin: structure and stability', *Biometals*, 25 (2012): 393-412.

22. J. M. Harrington, O. W. Duckworth and K. Haselwandter, 'The fate of siderophores: antagonistic environmental interactions in exudate-mediated micronutrient uptake', *Biometals*, 28 (2015): 461-472.

23. S. M. Kraemer, 'Iron oxide dissolution and solubility in the presence of siderophores', *Aquatic sciences*, 66 (2004): 3-18.

24. L. Tian, E. Dell and W. Shi, 'Chemical composition of dissolved organic matter in agroecosystems: Correlations with soil enzyme activity and carbon and nitrogen mineralization', *Applied Soil Ecology*, 46 (2010): 426-435.

25. R. L. Sinsabaugh, 'Phenol oxidase, peroxidase and organic matter dynamics of soil', *Soil Biology and Biochemistry*, 42 (2010): 391-404.

26. C. E. Bach, D. D. Warnock, D. J. Van Horn, M. N. Weintraub, R. L. Sinsabaugh, S. D. Allison and D. P. German, 'Measuring phenol oxidase and peroxidase activities with pyrogallol, L-DOPA, and ABTS: effect of assay conditions and soil type', *Soil Biology and Biochemistry*, 67 (2013): 183-191.

27. A. Pierwola, T. Krupinski, P. Zalupski, M. Chiarelli and D. Castignetti, 'Degradation pathway and generation of monohydroxamic acids from the trihydroxamate siderophore deferrioxamine B', *Applied and Environmental Microbiology*, 70 (2004): 831-836.

28. G. Winkelmann, B. Busch, A. Hartmann, G. Kirchhof, R. Süßmuth and G. Jung, 'Degradation of desferrioxamines by Azospirillum irakense: Assignment of metabolites by HPLC/electrospray mass spectrometry', *Biometals*, 12 (1999): 255-264.

29. M. Villavicencio and J. Neilands, 'An inducible ferrichrome A-degrading peptidase from *Pseudomonas* FC-1', *Biochemistry*, 4 (1965): 1092-1097.

30. R. Warren and J. Neilands, 'Microbial degradation of the ferrichrome compounds', *Microbiology*, 35 (1964): 459-470.

31. R. Warren and J. Neilands, 'Mechanism of microbial catabolism of ferrichrome A', *Journal of Biological Chemistry*, 240 (1965): 2055-2058.

32. M. A. Fischbach, H. Lin, D. R. Liu and C. T. Walsh, 'How pathogenic bacteria evade mammalian sabotage in the battle for iron', *Nature Chemical Biology*, 2 (2006): 132-138.

33. M. Miethke and M. A. Marahiel, 'Siderophore-based iron acquisition and pathogen control', *Microbiology and molecular biology reviews*, 71 (2007): 413-451.

34. K. S. French, E. Chukwuma, I. Linshitz, K. Namba, O. W. Duckworth, M. A. Cubeta and O. Baars, 'Inactivation of siderophore iron-chelating moieties by the fungal wheat root symbiont Pyrenophora biseptata', *Environmental Microbiology Reports*, (2024): e13234.

35. D. E. Crowley, Microbial siderophores in the plant rhizosphere, *Iron nutrition in plants and rhizospheric microorganisms,* (2006): 169-198.

36. S. M. Kraemer, A. Butler, P. Borer and J. Cervini-Silva, 'Siderophores and the dissolution of iron-bearing minerals in marine systems', *Reviews in Mineralogy and Geochemistry*, 59 (2005): 53-84.

37. C. Kim, W. W. Lorenz, J. T. Hoopes and J. F. Dean, 'Oxidation of phenolate siderophores by the multicopper oxidase encoded by the Escherichia coli yacK gene', *Journal of bacteriology*, 183 (2001): 4866-4875.

38. N. Zaya, A. Roginsky, J. Williams and D. Castignetti, 'Evidence that a deferrioxamine B degrading enzyme is a serine protease', *Canadian Journal of Microbiology*, 44 (1998): 521-527.

39. M. A. McLarin and I. K. Leung, 'Substrate specificity of polyphenol oxidase', *Critical Reviews in Biochemistry and Molecular Biology*, 55 (2020): 274-308.

40. M. Suzuki, A. Urabe, S. Sasaki, R. Tsugawa, S. Nishio, H. Mukaiyama, Y. Murata, H. Masuda, M. S. Aung and A. Mera, 'Development of a mugineic acid family phytosiderophore analog as an iron fertilizer', *Nature communications*, 12 (2021): 1-13.

41. M. Suzuki, Y. Suzuki, K. Hosoda, K. Namba and T. Kobayashi, 'The phytosiderophore analogue proline-2′-deoxymugineic acid is more efficient than conventional chelators for improving iron nutrition in maize', *Soil Science and Plant Nutrition*, 70 (2024): 435-446.

42. M. Keyes and F. Semersky, 'A quantitative method for the determination of the activities of mushroom tyrosinase', *Archives of biochemistry and biophysics*, 148 (1972): 256-261.

43. B. Chance and A. Maehly, '[136] Assay of catalases and peroxidases', (1955).

44. H. Mayerhofer, R. Marshall, C. White and M. Lu, 'Characterization of a heat-stable protease of Pseudomonas fluorescens P26', *Applied microbiology*, 25 (1973): 44-48.

45. C. Cupp-Enyard, 'Sigma's non-specific protease activity assay-casein as a substrate', *JoVE (Journal of Visualized Experiments)*, (2008): e899.

46. O. Baars and D. H. Perlman, Small molecule LC-MS/MS fragmentation data analysis and application to siderophore identification, *Applications from Engineering with MATLAB Concepts,* (2016): 189.

47. O. Baars, X. Zhang, F. M. Morel and M. R. Seyedsayamdost, 'The Siderophore Metabolome of Azotobacter vinelandii', *Appl Environ Microbiol*, 82 (2015): 27-39.

48. A. K. Dubme, R. C. Hider and H. H. Khodr, 'Synthesis and Iron-Binding Properties of Protochelin, the Tris (catecholamide) Siderophore of Azotobacter vinelandii', *Chemische Berichte*, 130 (1997): 969-973.

49. S. Bieber, T. Letzel and A. Kruve, 'Electrospray ionization efficiency predictions and analytical standard free quantification for SFC/ESI/HRMS', *Journal of the American Society for Mass Spectrometry*, 34 (2023): 1511-1518.

50. K. Tang, J. S. Page and R. D. Smith, 'Charge competition and the linear dynamic range of detection in electrospray ionization mass spectrometry', *Journal of the American Society for Mass Spectrometry*, 15 (2004): 1416-1423.

51. V. Rai, N. Fisher, O. W. Duckworth and O. Baars, 'Extraction and detection of structurally diverse siderophores in soil', *Frontiers in Microbiology*, 11 (2020): 581508.

52. L. Fougere, C. Elfakir, R.-I. Chirita-Tampu and C. West, 'Advantages of HILIC mobile phases for LC–ESI–MS–MS analysis of neurotransmitters', (2013).

53. V. A. Kumar, T. K. Mohan and K. Murugan, 'Purification and kinetic characterization of polyphenol oxidase from Barbados cherry (Malpighia glabra L.)', *Food Chemistry*, 110 (2008): 328-333.

54. R. Gul Guven, K. Guven, F. Matpan Bekler, O. Acer, H. ALKAN and M. Dogru, 'Purification and characterization of polyphenol oxidase from purslane', *Food Science and Technology*, 37 (2017): 356-362.

55. N. A. M. Zaini, A. Osman, A. A. Hamid, A. Ebrahimpour and N. Saari, 'Purification and characterization of membrane-bound polyphenoloxidase (mPPO) from Snake fruit [Salacca zalacca (Gaertn.) Voss], *Food Chemistry*, 136 (2013): 407-414.

56. Y. M. Tao, L. Y. Yao, Q. Y. Qin and W. Shen, 'Purification and characterization of polyphenol oxidase from jackfruit (Artocarpus heterophyllus) bulbs', *Journal of Agricultural and Food Chemistry*, 61 (2013): 12662-12669.

57. U. Gawlik-Dziki, U. Złotek and M. Świeca, 'Characterization of polyphenol oxidase from butter lettuce (Lactuca sativa var. capitata L.)', *Food Chemistry*, 107 (2008): 129-135.

58. K. Bravo and E. Osorio, 'Characterization of polyphenol oxidase from Cape gooseberry (Physalis peruviana L.) fruit', *Food chemistry*, 197 (2016): 185-190.

59. G. H. Northover, Y. Mao, S. Blasco, R. Vilar, E. Garcia-España, C. Rocco, M. Hanif and D. J. Weiss, 'Synergistic use of siderophores and weak organic ligands during zinc transport in the rhizosphere controlled by pH and ion strength gradients', *Scientific Reports*, 12 (2022): 6774.

60. C. Rocco, M. Suzuki, R. Vilar, E. Garcia-España, S. Blasco, G. Larrouy-Maumus, C. Turnbull, M. Wissuwa, X. Cao and D. Weiss, 'Enhancing Zinc Bioavailability in Rice Using the Novel Synthetic Siderophore Ligand Proline-2′-Deoxymugineic Acid (PDMA): Critical Insights from Metal Binding Studies and Geochemical Speciation Modeling', *Journal of Agricultural and Food Chemistry*, (2025).

61. E. J. Land, C. A. Ramsden and P. A. Riley, 'The mechanism of suicide-inactivation of tyrosinase: a substrate structure investigation', *The Tohoku journal of experimental medicine*, 212 (2007): 341-348.

62. J. L. Muñoz-Muñoz, F. Garcia-Molina, P. A. García-Ruiz, M. Molina-Alarcon, J. Tudela, F. Garcia-Canovas and J. N. Rodríguez-López, 'Phenolic substrates and suicide inactivation of tyrosinase: kinetics and mechanism', *Biochemical Journal*, 416 (2008): 431-440.

63. J. L. Muñoz-Muñoz, F. Garcia-Molina, R. Varon, P. A. Garcia-Ruíz, J. Tudela, F. Garcia-Cánovas and J. N. Rodríguez-López, 'Suicide inactivation of the diphenolase and monophenolase activities of tyrosinase', *IUBMB life*, 62 (2010): 539-547.

64. J. R. Walker, Enzymatic browning in fruits: its biochemistry and control, (1995).

65. C. Queiroz, A. J. R. da Silva, M. L. M. Lopes, E. Fialho and V. L. Valente-Mesquita, 'Polyphenol oxidase activity, phenolic acid composition and browning in cashew apple (Anacardium occidentale, L.) after processing', *Food Chemistry*, 125 (2011): 128-132.

66. S. Sellés-Marchart, J. Casado-Vela and R. Bru-Martínez, 'Isolation of a latent polyphenol oxidase from loquat fruit (Eriobotrya japonica Lindl.): Kinetic characterization and comparison with the active form', *Archives of biochemistry and biophysics*, 446 (2006): 175-185.

67. L. G. Fenoll, J. N. Rodríguez-López, F. García-Molina, F. García-Cánovas and J. Tudela, 'Michaelis constants of mushroom tyrosinase with respect to oxygen in the presence of monophenols and diphenols', *The International Journal of Biochemistry & Cell Biology*, 34 (2002): 332-336.

68. B. O. Esiana, C. J. Coates, W. P. Adderley, A. E. Berns and R. Bol, 'Phenoloxidase activity and organic carbon dynamics in historic Anthrosols in Scotland, UK', *Plos one*, 16 (2021): e0259205.

69. L. Martínková, M. Kotik, E. Marková and L. Homolka, 'Biodegradation of phenolic compounds by Basidiomycota and its phenol oxidases: a review', *Chemosphere*, 149 (2016): 373-382.

70. S. Herter, M. Schmidt, M. L. Thompson, A. Mikolasch and F. Schauer, 'A new phenol oxidase produced during melanogenesis and encystment stage in the nitrogen-fixing soil bacterium Azotobacter chroococcum', *Applied microbiology and biotechnology*, 90 (2011): 1037-1049.

71. O. Arslan, A. Temur and İ. Tozlu, 'Polyphenol oxidase from Malatya apricot (Prunus armeniaca L.)', *Journal of Agricultural and Food Chemistry*, 46 (1998): 1239-1241.

72. C. Wang, J.-f. Zhang, Y. Zhang and B. Cheng, 'Characterization and inhibitors of polyphenol oxidase from Chinese Toon', *Food Biotechnology*, 27 (2013): 261-278.

73. G. Palma-Orozco, N. A. Marrufo-Hernández, J. G. Sampedro and H. Nájera, 'Purification and partial biochemical characterization of polyphenol oxidase from mango (Mangifera indica cv. Manila)', *Journal of Agricultural and Food Chemistry*, 62 (2014): 9832-9840.

74. B. Aydin, I. Gulcin and S. H. Alwasel, 'Purification and characterization of polyphenol oxidase from Hemşin apple (Malus communis L.)', *International Journal of Food Properties*, 18 (2015): 2735-2745.

75. M. Sikora, M. Świeca, M. Franczyk, A. Jakubczyk, J. Bochnak and U. Złotek, 'Biochemical properties of polyphenol oxidases from ready-to-eat lentil (Lens culinaris Medik.) sprouts and factors affecting their activities: A search for potent tools limiting enzymatic browning', *Foods*, 8 (2019): 154.

76. K. Sellami, A. Couvert, N. Nasrallah, R. Maachi, M. Abouseoud and A. Amrane, 'Peroxidase enzymes as green catalysts for bioremediation and biotechnological applications: A review', *Science of the Total Environment*, 806 (2022): 150500.

77. B. R. Petigara, N. V. Blough and A. C. Mignerey, 'Mechanisms of hydrogen peroxide decomposition in soils', *Environmental Science & Technology*, 36 (2002): 639-645.

78. L. K. Ndungu, J. H. Steele, T. L. Hancock, R. D. Bartleson, E. C. Milbrandt, M. L. Parsons, and H. Urakawa, 'Hydrogen peroxide measurements in subtropical aquatic systems and their implications for cyanobacterial blooms', *Ecological Engineering*, 138 (2019): 444-453.

79. R. Ueki, Y. Imaizumi, Y. Iwamoto, H. Sakugawa and K. Takeda, 'Factors controlling the degradation of hydrogen peroxide in river water, and the role of riverbed sand', *Science of the Total Environment*, 716 (2020): 136971.

80. C. Indiani, E. Santoni, M. Becucci, A. Boffi, K. Fukuyama and G. Smulevich, 'New Insight into the Peroxidase− Hydroxamic Acid Interaction Revealed by the Combination of Spectroscopic and Crystallographic Studies', *Biochemistry*, 42 (2003): 14066-14074.

81. E. C. O'Brien, E. Farkas, M. J. Gil, D. Fitzgerald, A. Castineras and K. B. Nolan, 'Metal complexes of salicylhydroxamic acid (H2Sha), anthranilic hydroxamic acid and benzohydroxamic acid. Crystal and molecular structure of [Cu (phen) 2 (Cl)] Cl· H2Sha, a model for a peroxidase-inhibitor complex, *Journal of Inorganic Biochemistry*, 79 (2000): 47-51.

82. K. Tsukamoto, H. Itakura, K. Sato, K. Fukuyama, S. Miura, S. Takahashi, H. Ikezawa, and T. Hosoya, 'Binding of salicylhydroxamic acid and several aromatic donor molecules to Arthromyces ramosus peroxidase, investigated by X-ray crystallography, optical difference spectroscopy, NMR relaxation, molecular dynamics, and kinetics', *Biochemistry*, 38 (1999): 12558-12568.

83. C. J. Marmion, D. Griffith and K. B. Nolan, 'Hydroxamic acids− an intriguing family of enzyme inhibitors and biomedical ligands', *European Journal of Inorganic Chemistry*, 2004 (2004): 3003-3016.

84. J. K. McDonald, 'An overview of protease specificity and catalytic mechanisms: aspects related to nomenclature and classification', *The Histochemical Journal*, 17 (1985): 773-785.

85. T. Jesmin, A. J. Margenot and R. L. Mulvaney, 'A comprehensive method for casein-based assay of soil protease activity', *Communications in Soil Science and Plant Analysis*, 53 (2022): 507-520.

86. D. Brown, W. Glass, N. Fitzpatrick, T. Kemp, W. Errington, G. Clarkson, W. Haase, F. Karsten and A. Mahdy, 'Structural variations in dinuclear model hydrolases and hydroxamate inhibitor models: synthetic, spectroscopic and structural studies', *Inorganica chimica acta*, 357 (2004): 1411-1436.

87. D. A. Brown, L. P. Cuffe, N. J. Fitzpatrick and Á. T. Ryan, 'A DFT study of model complexes of zinc hydrolases and their inhibition by hydroxamic acids', *Inorganic Chemistry*, 43 (2004): 297-302.

88. M. Mortazavi and A. Akbarzadeh, 'Improvement of desferrioxamine B production of Streptomyces pilosus ATCC 19797 with use of protease inhibitor and minerals related to its activity', *Indian Journal of Clinical Biochemistry*, 27 (2012): 274-277.

89. J. S. Ramírez-Larrota and U. Eckhard, 'An introduction to bacterial biofilms and their proteases, and their roles in host infection and immune evasion', *Biomolecules*, 12 (2022): 306.

90. R. Lucinski and M. Adamiec, 'The Role of Plant Proteases in the Response of Plants to Abiotic Stress Factors. Front', *Plant Physiol*, 1 (2023): 1330216.

91. A. Razzaq, S. Shamsi, A. Ali, Q. Ali, M. Sajjad, A. Malik and M. Ashraf, 'Microbial proteases applications', *Frontiers in bioengineering and biotechnology*, 7 (2019): 110.

92. J. L. Erickson and M. Schuster, 'Extracellular proteases from microbial plant pathogens as virulence factors', *Current Opinion in Plant Biology*, 82 (2024): 102621.

93. H. Holzgreve, M. Eick and C. Stöhr, 'Protease Activity in the Rhizosphere of Tomato Plants Is Independent from Nitrogen Status', *Root Biology*, (2019): 3.

94. Y.-Z. Zhang, W.-X. Zhang and X.-L. Chen, 'Mechanisms for Induction of Microbial Extracellular Proteases in Response to Exterior Proteins' Authors: AUTHORS INFO & AFFILIATIONS https://journals. asm. org/doi/10.1128', *ГЕНДЕРНА ТА ПСИХОСОМАТИЧНА МЕДИЦИНА*, (2022): 14-15.

95. A. Thieken and G. Winkelmann, 'Rhizoferrin: a complexone type siderophore of the mocorales and entomophthorales (Zygomycetes)', *FEMS microbiology letters*, 94 (1992): 37-41.

96. H. Drechsel, M. Tschierske, A. Thieken, G. Jung, H. Zähner and G. Winkelmann, 'The carboxylate type siderophore rhizoferrin and its analogs produced by directed fermentation', *Journal of industrial microbiology and biotechnology*, 14 (1995): 105-112.

97. D. Ueno, Y. Ito, M. Ohnishi, C. Miyake, T. Sohtome and M. Suzuki, 'A synthetic phytosiderophore analog, proline-2′-deoxymugineic acid, is efficiently utilized by dicots', *Plant and Soil*, 469 (2021): 123-134.

98. C. Rocco, M. Suzuki, R. Vilar, E. Garcia-Espana, S. Blasco, G. Larrouy-Maumus, C. Turnbull, M. Wissuwa, X. Cao, and D. Weiss, 'Application of proline-2′-deoxymugineic acid as potential fertilizer to alleviate zinc deficiency in paddy soils', (2024).

99. Z. Kaya, A. Maqbool, M. Suzuki and E. Aksoy, 'Proline-2'-deoxymugineic acid (PDMA) increases seed quality and yield by alleviating iron deficiency symptoms in soybean under calcareous-alkaline conditions', *bioRxiv*, (2024): 2024.10. 02.616232.

100. T. Wang, N. Wang, M. Suzuki, Q. Lu, S. Lang, K. Wang, L. Niu and Y. Zuo, 'Proline-2′-deoxymugineic acid, active Fe chelator enhance peanut yield by integrated improving soil-plant Fe status at molecular and ecological level', *Authorea Preprints*, (2022).

101. K. J. Minick, M. Aguilos, X. Li, B. Mitra, P. Prajapati and J. S. King, 'Effects of spatial variability and drainage on extracellular enzyme activity in coastal freshwater forested wetlands of Eastern North Carolina, USA', *Forests*, 13 (2022): 861.

102. E. Ahmed and S. J. Holmström, 'Siderophores in environmental research: roles and applications', *Microbial biotechnology*, 7 (2014): 196-208.

103. E. Ahmed and S. J. Holmström, 'The effect of soil horizon and mineral type on the distribution of siderophores in soil', *Geochimica et Cosmochimica Acta*, 131 (2014): 184-195.

104. R. G. Burns, J. L. DeForest, J. Marxsen, R. L. Sinsabaugh, M. E. Stromberger, M. D. Wallenstein, M. N. Weintraub and A. Zoppini, 'Soil enzymes in a changing environment: current knowledge and future directions', *Soil Biology and Biochemistry*, 58 (2013): 216-234.

105. M. Stursova and R. L. Sinsabaugh, 'Stabilization of oxidative enzymes in desert soil may limit organic matter accumulation', *Soil Biology and Biochemistry*, 40 (2008): 550-553.

106. H. Dong, Q. Zeng, Y. Sheng, C. Chen, G. Yu and A. Kappler, 'Coupled iron cycling and organic matter transformation across redox interfaces', *Nature Reviews Earth & Environment*, 4 (2023): 659-673.

107. E. Gamalero and B. R. Glick, 'Mechanisms used by plant growth-promoting bacteria', *Bacteria in agrobiology: plant nutrient management*, (2011): 17-46.

108. E. Gamalero and B. R. Glick, Bacterial ACC deaminase and IAA: interactions and consequences for plant growth in polluted environments, *Handbook of phytoremediation,* (2011): 763-773.

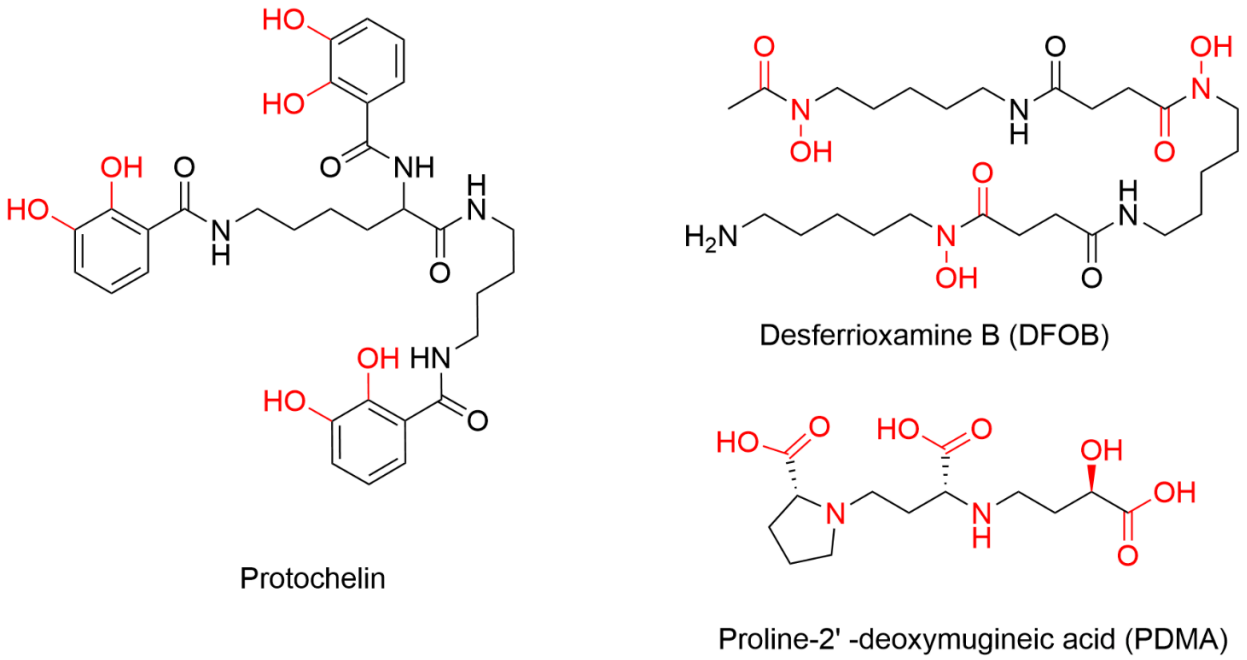

Figure 1. Structure of the three siderophores in this study. The moieties involved in Fe^{III} complexation at pH ~7 are indicated in red.

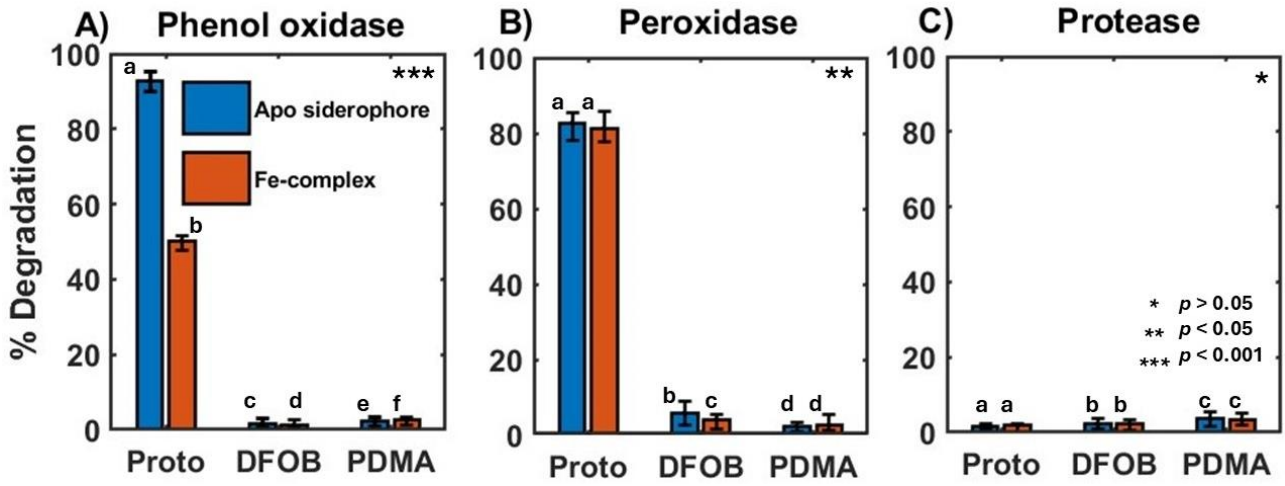

Figure 2. Percentage degradation of each of the three siderophores after reaction with (A) phenol oxidase, (B) peroxidase, and (C) protease enzymes. Blue and orange bars indicate the reaction with the apo siderophore and Fe^{III}-siderophore complex, respectively. Statistical significance was determined using a one-way ANOVA with Tukey's post hoc HSD test. Distinct letters indicate statistically significant differences between groups; asterisks (*) in the upper right corner of each plot denote the level of significance. Error bars show the range of measured degradation in three replicate experiments.

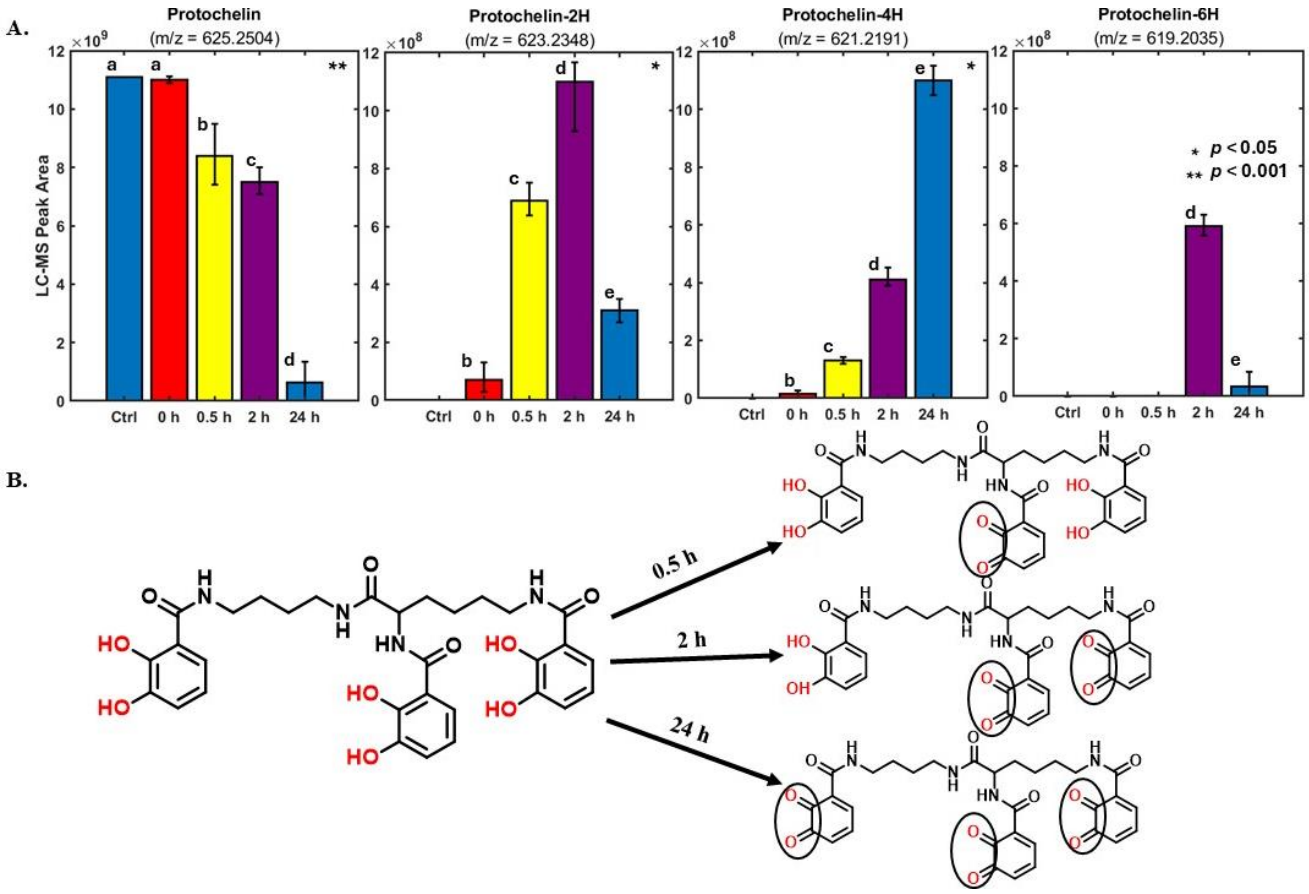

Figure 3. HR-LC-MS (+ ion mode) detected degradation of protochelin by phenol oxidase. (A) LC-MS peak areas for protochelin and protochelin degradation products for each of the four time points. Measurements of protochelin and protochelin degradation products were conducted simultaneously in the same samples. Error bars indicate a single standard deviation from triplicate biological incubations. Statistical significance was determined using a one-way ANOVA with Tukey's post hoc HSD test. Different letters indicate statistically significant differences between groups; asterisks (*) in the upper right corner of each plot denote the level of significance. (B) Structures of the identified protochelin degradation products, based on tandem mass-spectrometry fragmentation spectra. Fragments detected in the MS/MS spectra (see also S2 Table) are displayed. The catechol groups in protochelin and the quinone groups in the degradation products are highlighted with circles.

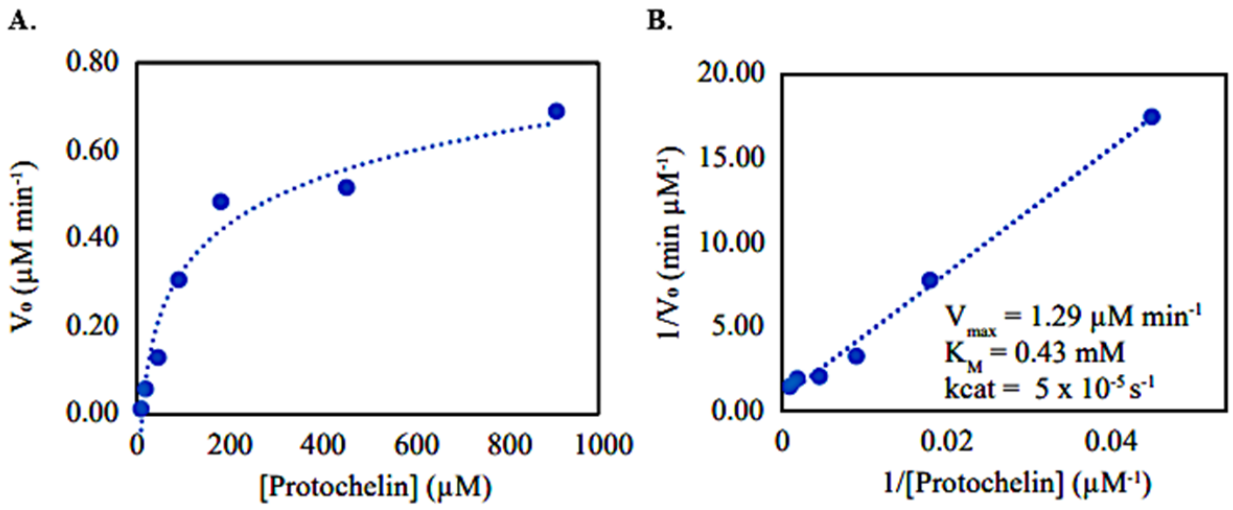

Figure 4. The protochelin oxidation with phenol oxidase followed (A) the Michaelis-Menten kinetics plot and (B) the Lineweaver-Burk calculation plot used to estimate the maximum rate of catalysis (Vmax) and substrate affinity (Km) for phenol oxidase activity on protochelin degradation.

Table 1. Kinetic parameters for the oxidation of protochelin substrate compared to other phenolic substrates by phenol oxidase. Normalized Vmax refers to Vmax normalized to enzyme activity units.

Substrate	Configuration	V_{max} (μM/min)	Normalized V_{max}	K_m (mM)	V_{max}/K_m (min^{-1})	Reference
Protochelin	tri-*o*-dihydroxy	1.29	0.0005	0.43	0.003	This study
Catechol	*o*-dihydroxy	79.5	0.002	5.2	0.0153	[53]
		109.9	0.006	8.2	13.4	[56]
		5503	0.482	4.40	1.251	[54]
		4081	0.155	3.20	1.275	[57]
Chlorogenic acid	*o*-dihydroxy	53.15	0.260	0.56	94.911	[58]
4-Methyl	*o*-dihydroxy	125	0.003	6.9	0.0181	[53]
catechol		82.1	0.004	18.2	4.5	[56]
		4504	0.394	6.75	0.6673	[54]
		5405	0.206	1.00	5.41	[57]
L-Dopa	*o*-dihydroxy	56.5	0.001	4.1	0.0138	[53]
		1655	0.145	4.60	0.3598	[54]
Pyrogallol	trihydroxy	8.8	0.0002	1.24	0.0071	[53]
		nd[a]		nd	nd	[56]
Caffeic acid	*o*-dihydroxy	48.2	0.0012	3.6	0.0134	[53]
Gallic acid	trihydroxy	nd[a]		nd	nd	[56]

nd[a] = degradation was not detected.

Chapter 3

Inactivation of siderophore iron-chelating moieties by the fungal wheat root symbiont *Pyrenophora biseptata*

3.1 Introduction

Iron is an essential but poorly available micronutrient needed as a cofactor and catalyst in many cellular and enzymatic processes. Siderophores are specialized metabolites produced and secreted by bacteria, fungi, and graminaceous plants when iron bioavailability is low. These secretions enhance iron bioavailability by binding, solubilizing, and transporting biologically unavailable ferric iron (Fe^{3+}), such as iron bound in iron oxides or humic matter. Siderophores are recognized as key agents of competition and cooperation in microbial communities and host-microbe mediated interactions [1, 2]. The ability to interfere with siderophore iron acquisition could provide a biological mechanism to gain a competitive advantage in microbial and plant community interactions, for example, by reducing iron affinity via structural modifications. Organisms may also degrade siderophores in order to metabolize them as carbon substrates.

In general, siderophores are thought to exhibit high stability towards biological degradation because of chemical modifications that protect from enzymatic degradation and because iron chelation can hinder the attack of hydrolytic enzymes [3]. However, a few studies have previously observed microbial degradation of siderophores when growing bacteria with siderophores as a carbon source [3-5]. In these studies, siderophores were only degraded when present in their free (apo) form, not bound to iron. In addition, several studies have shown the degradation of siderophore structures as part of a cellular mechanism to recover iron from siderophores: fungal esterases are known to be responsible for the hydrolysis of iron-bound fusarinines [6-8], and bacterial esterases can hydrolyze enterobactin and salmochelin iron complexes [9-11]. The siderophore hydrolysis products have lower iron affinity and promote cellular iron utilization via ligand exchange or iron reduction. Siderophore degradation products, such as mono- and bis-hydroxamates from the hydrolysis of fusarinines, also make iron more available to plants [12]. In contrast, the unmodified tris-hydroxamate siderophore desferrioxamine B (DFOB) was previously reported to be not available to maize and oat plants and provided a competitive advantage to bacteria able to utilize this siderophore for Fe acquisition [13]. The degradation or structural modification of siderophores by bacteria or fungi could thus play a critical role in iron acquisition by plants and non-siderophore producing microbes. In the following, we will use the term ‘degradation’ to describe any siderophore reactions leading to products with structural modifications that have reduced iron affinity.

In this study, we followed siderophore production and degradation by four plant and soil-associated fungi with varying ecology and substrate preference: *Phanerodontia* (*=Phanerochaete) chrysosporium* RP-78*, Phanerodontia chrysosporium* BKM-1767*, Pyrenophora* (*=Drechslera*) *biseptata,* and *Linnemannia* (*=Mortierella*) *elongata* 624. Three representative siderophore standards were chosen, representing natural diversity in siderophore structures and iron-chelating groups: the tris-hydroxamate siderophore desferrioxamine B (DFOB), the tris-catecholamide siderophore protochelin, and the carboxylate phytosiderophore proline-2'-deoxymugineic acid (PDMA) (**Figure 1**). DFOB and protochelin are bacterial siderophores, and PDMA is a synthetic analog of a plant siderophore that has been introduced as a plant iron-fertilizer [14]. In addition to analyses of the degradation of these three siderophore models, we investigated the production of fungal siderophores. The results are discussed in terms of the potential of fungi to shape siderophore dynamics in plant interactions with important consequences for iron acquisition by plants and plant microbiome members.

3.2 Experimental Procedures

3.2.1 Fungal isolates.

Four species of fungi were selected for this study: two different strains of a white rot wood decay fungus - (1) *Phanerodontia* (*=Phanerochaete*) *chrysosporium* RP-78, and (2) *Phanerodontia chrysosporium* BKM-1767 (Hjortstam & Ryvarden); a wheat root-associated symbiont – (3) *Pyrenophora* (*=Drechslera*) *biseptata* (Sacc. & Roum.), and a root endophyte isolated from eastern cottonwood - (4) *Linnemannia* (*=Mortierella*) *elongata* (Vandepol & Bonito) [15]. The strain of *Linnemania elongata* was supplied by Jessie Uehling (Oregon State University), and the two strains of *P. chrysosporium* were supplied by Dan Cullen (US Department of Agriculture Forest Products Laboratory, Madison, WI). *P. biseptata* was isolated from wheat roots in our laboratory. *L. elongata* was originally isolated from *P. deltoides* roots in North Carolina, and a culture was available in our laboratory [16]. Isolates were maintained by adding 5-mm diameter mycelial plugs taken from an actively growing colony to 0.5 mL of a mixture of sterile 50% glycerol and 0.5 mL potato dextrose broth (PDB, Difco) in cryovials. The cryovials were incubated for 24 h at 25 ºC and stored at -80˚C. Fungi were revived by transferring mycelial plugs to potato dextrose agar (PDA; Difco) plates.

3.2.2 Siderophore standards.

The siderophores were selected to represent the three most common iron binding groups found in siderophores: the trishydroxamate siderophore desferrioxamine B (DFOB, mesylate salt, MilliporeSigma), the triscatecholate siderophore protochelin, and the carboxylate siderophore proline-2'-deoxymugineic acid (PDMA) (**Figure 1**). Protochelin was synthetically prepared by the Small Molecule Synthesis Facility (SMSF) at Duke University and used as received. PDMA was kindly provided as PDMA·2HCl by Aichi Steel Corporation (Japan) [14]. Stock solutions of 10 mM were prepared in methanol for protochelin or 18 MΩ-cm water (MQ water) for DFOB and PDMA, respectively. A 10 mM standard of iron-bound DFOB (FeDFOB) was prepared by the addition of 10 mM $FeCl_3$ to a 10 mM solution of DFOB in MQ water. Siderophore stocks were immediately used or stored for up to 2 weeks at -20 ºC.

3.2.3 Preparation of fungal mycelium and growth media.

Mycelial plugs (5 mm diameter) were taken from the edge of an actively growing culture on PDA plates. The mycelial plugs were then placed on 2% malt extract agar (MEA, Difco) and grown for 7 days at 25 ºC. A new mycelial plug was taken from this culture and placed on a PDA agar plate (9-cm diameter) at 25 ºC until the mycelial growth of the fungus reached the edge of the plate, approximately 7 days. A mycelial plug from each isolate was then transferred to 1.5% malt extract broth (MEB, Difco) and incubated for 3–5 days. The cultures were then harvested by vacuum filtration with cellulose filters (Whatman #1, 11 µm), rinsed with sterile MQ water, and homogenized with a handheld homogenizer (Fisher Scientific 150) using a 7-mm probe for 1 min on low speed to achieve a homogenous inoculum for the siderophore reactions. Experiments were started by adding 2 mL of the homogenized mycelia to 13 mL of minimal salt broth (MSB) growth medium in sterile cell culture flasks (Nunc, 75 cm^2). The MSB medium was slightly modified from a previously reported medium used to stimulate production of ligninolytic enzymes by *Phlebia floridensis* [17]. A volume of 1L of MSB medium was prepared by dissolving 10 g glucose, 2 g KH_2PO_4, 0.5 g $MgSO_4·7H_2O$, 0.1 g $CaCl_2·2H_2O$, 1 mg thiamine HCl, 0.2 g ammonium tartrate, 1 mL trace metal solution containing [Zn^{2+}] = 53 µM, [Cu^{2+}] = 10 µM, [Co^{2+}] = 24 µM, [Mn^{2+}] = 225 µM, [MoO_4^{2-}] = 100µM, [BO_3^{3-}] = 10 mM), and 1mL EDTA (0.1 M) in MQ water and adjusting the pH = 4.5 ± 0.1 with NaOH and H_2SO_4. The medium was then filter sterilized (0.2 µm, PES, ThermoFisher) before use. Media were used as is (iron-deficient medium) or a

concentration of sterile filtered 300 µM $FeCl_3$ was added to the medium prior to inoculation (iron-replete media). Immediately after inoculation, a final concentration of 6.67 µM of each siderophore (10 µL of the 10 mM stock solutions) was added to the 15 mL culture flasks.

3.2.4 Siderophore degradation experiments.

Three experiments were conducted. *Experiment 1* had the purpose of comparing the ability of each of the four fungi to degrade each of the three siderophore structures. One replicate of each culture was incubated in MSB medium containing siderophores without and with added iron. A sterile MSB medium containing siderophores was used as a positive control. Samples were collected after an incubation time of 48 h. Supernatant and fungal cells were separated by centrifugation. The supernatant was further filtered using a syringe filter (0.2µm polyethersulfone, PES, membrane) and stored at -80˚C before analysis by LC-MS (see details below). Mycelium of each fungus was harvested by vacuum filtration (Whatman #1, 11 µm), rinsed with sterile 18MΩ water (MQ water), and lyophilized to determine fungal biomass. This experiment indicated *Pyrenophora biseptata* was highly effective in degrading DFOB and protochelin in contrast to the *Linnemannia elongata* and *Phanerodontia chrysosporium*. Therefore, a second experiment (Experiment 2) focused on replicating this result and taking additional time points with triplicates of *P. bispetata* in iron-limited MSB media with DFOB and protochelin. Supernatant samples were collected immediately after inoculation, after 1 day, and after 3 days by filtration (0.2 µm PES syringe filters). A sterile control containing siderophores was also set up at the same time as the incubations. The outcome of these first two experiments suggested that iron chelation protects DFOB from degradation by *P. biseptata*. To confirm this, *experiment 3* was set up in which *P. biseptata* was cultured with unbound DFOB and compared to incubations with DFOB bound to Fe (FeDFOB). These experiments were done in a modified MSB medium from which EDTA and the trace metal solution were omitted from the medium (see above). The incubation with unbound DFOB was done without any added iron in the medium; the incubation with added FeDFOB was done with the addition of 100 µM $FeCl_3$. Culture supernatants were collected after 5 d by filtration (0.2 µm PES syringe filters).

3.2.5 Analysis of siderophore degradation, formation of degradation products, and siderophore production by LC-MS.

All fungal culture supernatants were analyzed by liquid chromatography-mass spectrometry (LC-MS) using an ISQ-EC (ThermoFisher) single quadrupole mass spectrometer in combination with an Ultraviolet-visible (UV-vis) spectrophotometer and a Charged Aerosol Detector (ThermoFisher). A sample volume of 25 µL was injected and separated under a gradient of solvents A and B (unless otherwise noted A: water, 0.1% formic acid, 1% acetonitrile; B: acetonitrile, 0.1% formic acid, 2% water; gradient: 0–1.5 min 0% B, 1.5–8 min 0-100% B; 8–10 min 100% B; re-equilibration at 100% A for 4 min). Separation was accomplished with an Agilent Poroshell 120 EC-C18 column (4.6 × 100 mm, 2.7µm) and a flow rate of 1.2 mL/min, and the column temperature was 30°C. Mass spectra were collected in single ion monitoring mode targeting the three added siderophores and their degradation products (Table S1). Samples from experiment 2 were additionally analyzed with a high-resolution LC-MS/MS platform (Orbitrap Exploris 480, ThermoFisher). Sample volumes of 25 µL were injected and separated using a Restek Raptor C18 (2.1 × 100) column with a flow rate of 0.4 mL/min, and the column compartment was kept at 45°C. The LC gradient was identical to that used with the ISQ-EC described above. Full-scan mass spectra (m/z = 85–1200) were acquired in positive ionization mode with the resolution set to R = 60,000 (full width at half maximum at m/z = 400) and data-dependent MS/MS acquisition of the top 5 most abundant ions in each cycle. Product ions were generated in HCD mode with 35 eV collision energy and an isolation window of 1.5 Da. The resolving power for MS/MS analysis was R = 15,000 (full width at half maximum at m/z = 400). Siderophore degradation was followed by tracking peak areas of the three siderophores added. Putative degradation products of the added siderophore standards were identified in high-resolution LC-MS data by searching for new LC-MS peaks in incubated samples with related *m/z* values (e.g., simple mass differences, such as –O in new product compared to original siderophore standard; similar mass defects) and MS/MS spectra (e.g., presence of 2,3-dihydroxybenzoid acid moieties in protochelin degradation products showing as neutral loss of *m/z* = 136.016 in MS/MS spectra [18]). Analysis of protochelin degradation products was also done by LC-UV-vis by looking for new peaks with absorption maxima in the range of the absorption maxima of the 2,3-dihydroxybenzoid acid groups in protochelin (λ = 315 nm [19]). Untargeted siderophore analysis was done using high-resolution LC–MS/MS by searching for the specific ^{54}Fe-^{56}Fe isotope pattern

associated with Fe-siderophore complexes, along with searching for the specific mass difference between the apo-siderophore and the Fe-siderophore complex, and siderophore-characteristic MS/MS fragmentation patterns as [18, 20]. In addition, the production of fungal siderophores was assayed using the Chrome Azurol S (CAS) assay [21].

3.2.6 Enzyme extraction from P. biseptata cell-pellets and siderophore degradation assays.

The mycelium of the fungus was grown in MSB medium with and without added iron, as described for Experiment 1 (see 'Siderophore degradation experiments' above). The supernatant and cell pellet were separated by centrifugation. The supernatant was sterile filtered (0.2 μM PES membrane syringe filter) for assays of siderophore degradation. Crude cell-pellet enzyme extracts for assays of siderophore degradation by intracellular enzymes were prepared using a protocol previously reported for mycelium of the fungus *Magnaporthe oryzae* [22]. Cell pellets were freeze-dried, and 500 mg of freeze-dried sample was ground using a mortar and pestle with liquid nitrogen. Samples were resuspended with 2 mL of a lysis buffer containing 50 mM HEPES (pH=7.5), 0.5% Nonidet P-40, 250 mM NaCl, 10% (v/v) glycerol, 2 mM EDTA (pH 8.0), and a protease inhibitor cocktail (cOmplete^{TM}, Roche) [22]. To assay for siderophore degradation, a concentration of 20 μM of DFOB, FeDFOB, or protochelin was added to 5mL of liquid supernatant or 5mL MSB before incubating for 3 days at 100 rpm. Samples were then filtered (0.2 μm) and analyzed by LC-MS.

3.3 Results

3.3.1 Decrease of dissolved siderophore concentrations during fungal incubations.

The mycelium of each of the four fungi was incubated with the three siderophores added at a concentration of 6.67 μM in MSB medium. The incubation time was 2 days in iron-limited (Figure 2) and iron-replete MSB media (Figure S1). We found that the activity of *P. biseptata* led to an approximately 50% decrease of DFOB concentrations in iron-limited medium (Figure 2), in contrast to the two strains of *P. chrysosporium* and *L. elongata,* which did not change DFOB concentrations significantly. For protochelin, the siderophore was almost completely removed from solution with *P. biseptata,* whereas the two *Phanerodontia* strains and *L. elongata* showed no or minor changes in dissolved protochelin concentrations. PDMA concentrations were less affected by *P. biseptata* compared to DFOB and protochelin, with ~30% decrease in solution. The

other fungi showed no (*P. chrysosprium* strains) or minor (*L. elongata*) ability to decrease dissolved concentrations of this siderophore. Comparable results were obtained with incubations in iron-replete MSB medium (Figure S1) except in the case of DFOB, for which the concentration decrease was much smaller with *P. biseptata* (~15%). Taken together, these results suggested a specialized ability of *P. biseptata* to remove diverse siderophore structures from the solution. The presence of iron reduced the ability of *P. biseptata* to remove DFOB from the solution.

3.3.2 Degradation of DFOB by P. biseptata.

To confirm the above results and further investigate potential degradation products and mechanisms, a second incubation experiment was conducted with *P. biseptata,* where supernatants from triplicate cultures in iron-limited MSB medium were sampled at three timepoints (immediately after inoculation, 24, and 72 h) and subsequently analyzed by high-resolution LC-MS. The results confirmed a significant decrease in dissolved DFOB concentrations (~25% after 24 h and ~70% after 72h) and, at the same time, formation of putative DFOB degradation products was observed (Figure 3A). The three main observed putative degradation products had *m/z* values in agreement with the sum formulas of DFOB, less than one to three oxygen atoms (DFOB-O, DFOB-2O, and DFOB-3O). The timepoints were consistent with DFOB-O formed first, followed by DFOB-2O, and finally DFOB-3O. The relatively minor modifications of the DFOB structure were not expected to strongly impact ionization behavior in LC-ESI-MS. Therefore, the peak area sum of the degradation products was used to estimate whether most of the DFOB concentration decrease in solution could be explained by the formation of these three degradation products. After 24 and 72 h, the peak area sum of the three degradation products accounted for ~80% and ~55% of the dissolved DFOB loss, respectively. This good agreement between the DFOB peak area decrease and the increase in peak areas of DFOB degradation products suggested that the major fraction of DFOB reacted in the supernatant solution and was not lost via sorption to cell surfaces or sequestered as substrates.

MS/MS spectra showed fragmentation of the three degradation products consistent with DFOB, in which one, two, or three hydroxamate groups were reduced to amides (Figure 3C**,** Supplementary Table 2). Fragmentation spectra show that the reduction of the hydroxamate groups in DFOB-O occurred in any of the three hydroxamate positions, leading to three degradation products which were not chromatographically separated (Figure 3C, Supplementary Table 2). The

same was true for DFOB-2O, in which any two of the three hydroxamate groups were reduced to amides. In the final degradation product, DFOB-3O, all three hydroxamate moieties were reduced to amides. Because the three hydroxamate moieties are the iron chelating groups in DFOB, their loss is expected to lead to a loss of iron chelating ability in the degradation products. Indeed, a fraction of DFOB was bound to iron under our LC-MS conditions, as shown by an LC-MS peak corresponding to FeDFOB. In contrast, DFOB-3O did not show any corresponding Fe chelates in LC-MS. DFOB-O and DFOB-2O showed increasingly lower peak area fractions of Fe chelates compared to the respective apo siderophores. It should be noted that the analysis of Fe chelation via LC-MS does not equate to the speciation of DFOB and DFOB degradation products in the culture media supernatants due to a different pH in the LC-MS mobile phase, which contained 0.1% formic acid (pH ~3).

To test for potential cellular or extracellular enzymes that could lead to DFOB degradation, sterile spent medium and crude enzyme cell extracts from *P. biseptata* mycelium were prepared and incubated with DFOB for 72 h, but no degradation of DFOB was detected in these experiments by LC-MS (data not shown). It was then tested if the presence of iron affected DFOB degradation by *P. biseptata* as suggested by the initial experiments (see above). It was found that when *P. biseptata* was incubated with FeDFOB in Fe-replete MSB medium, there was no significant degradation (Figure 3B).

3.3.3 Degradation of protochelin by P. biseptata.

Protochelin concentrations in solution decreased rapidly in incubations with *P. biseptata* mycelium (Figure 4A): in the first timepoint, taken immediately after inoculation, ~1% of the initial protochelin concentration was detected in the spent medium solution, and after 24 and 72 h incubation, less than 0.1% was detected. The main detected protochelin degradation products indicated sum formulas equal to protochelin-2H, and additional minor degradation products, including protochelin-4H and protochelin-6H. Analysis of MS/MS spectra showed that these compounds consisted of the protochelin structure with one, two, or three catechol groups oxidized to quinones (Figure 4B). Extracted ion chromatograms of the main degradation product with *m/z* = 623.2348 (protochelin-2H) showed three distinct peaks (retention times: 4.15, 4.23, and 4.39 min) with about equal intensities, indicating that any one of the three catechol groups in protochelin was oxidized, leading to three different degradation products. As in the case of DFOB, the

degradation of protochelin involved the iron-chelating moieties in the siderophore, leading to a loss of the ability of the siderophore to bind iron. Peak areas of protochelin degradation products were around 1% of the protochelin standard in the first timepoint and less than 0.1% in the 24 and 72 h timepoints, suggesting that the majority of protochelin removal from solution was not accounted for by these degradation products. This agreed with the analysis of LC-UV-vis data, which showed only minor new UV-vis active catechol or quinone degradation products, but not to the extent that these degradation products could account for a significant fraction of protochelin removed from solution. This suggested that the bulk protochelin may have adsorbed onto cell surfaces. It is also possible that additional degradation products were not detected because they may have consisted of hydrophobic compounds that did not elute from the column.

3.3.4 Siderophore production and degradation.

Beyond these degradation studies with the three siderophore models, we investigated which siderophores the tested fungi produce and whether they may undergo degradation by fungal activity similar to the siderophore standards. Siderophore assays (CAS assays) with iron-limited MSB medium showed that of the four studied fungi, only *P. biseptata* was CAS positive. Following the initial CAS results, LC-MS/MS analyses were conducted to discover siderophores after 72 h incubation with *P. biseptata* mycelium in iron-limited and iron-replete media. Siderophore production was detected in iron-limited medium but was suppressed or not detected in iron-replete medium. The main detected siderophores were matching in mass and MS/MS fragmentation to the known fungal siderophores neocoprogen I, neocoprogen II [23], coprogen [24], and dimerum acid [25, 26] (Figure 5A, Figure S2A-D, Supplementary Table 3). Minor peaks were detected for several additional, structurally closely related, siderophores (Supplementary Table 3). All detected siderophores from *P. biseptata* were in the coprogen family of structures. Coprogens are linear fungal trishydroxamate siderophores with the same iron-chelating moieties as those in DFOB. Interestingly, as for DFOB, putative degradation products were detected with sum formulas less one, two, or three oxygen atoms (Figure 5B). MS/MS spectra showed that these structures were identical to those of the four main siderophores with one, two, or three hydroxamate groups reduced to amides, analogous to the observed DFOB degradation (Figure 5C, Figure S3, Supplementary Tables 4-8).

3.4 Discussion

In this study, we investigated the degradation of three representative siderophore structures by the mycelium of ecologically and taxonomically diverse species of fungi found associated with plants and soil. The four isolates were selected because they are known to be prolific producers of extracellular enzymes for the acquisition of carbon (*P. chrysosporium* RP-78 and BKM-1767) [27, 28] or because they can colonize plants and can affect plant growth, as in the case of *P. biseptata* [29] and *L. elongata* [16, 30]. We found that *P. biseptata* incubations in iron-limited MSB medium were associated with a significant decrease in dissolved concentrations of DFOB, protochelin, and, to a lesser degree, PDMA. *P. biseptata* also produced its own coprogen-type siderophores in iron-limited MSB medium. This suggested a notable biology of *P. biseptata* surrounding siderophore degradation, production, and Fe acquisition. Closer investigation of the activity of *P. biseptata s*howed that the decrease in dissolved DFOB concentration was linked to the formation of DFOB degradation products in which one, two, or three of the iron-chelating hydroxamate groups were reduced to amides. No indication of enzymatic degradation was found during incubations of DFOB with cell lysates or sterile supernatant medium, and a multi-step mechanism might have been involved in the degradation, in which fungal cells needed to remain intact. No degradation was observed with FeDFOB in iron-replete medium, suggesting that either iron chelation protected the hydroxamate groups or that the biochemical mechanisms leading to DFOB degradation were not active under iron-replete conditions. We also found that *P. biseptata* produced coprogen-type siderophores, primarily neocoprogen I and neocoprogen II. Coprogens share similarity with DFOB in that they are linear trishydroxamate siderophores, and *P. biseptata* degraded the siderophores it produced, like it degraded DFOB. The reduction of tris-hydroxamate siderophores by *P. biseptata* can be expected to have important implications for iron availability to plants. It has been shown via plant ^{55}Fe radioisotope tracer short-term uptake experiments that DFOB was not available to maize and oat plants [13]. In contrast, mono- and bis-hydroxamates are plant available because of their reduced strength and lower reduction potential, which enables plant uptake via ligand exchange or reductive iron-uptake [1, 12].

A few previous studies demonstrated that bacteria were able to degrade DFOB as part of an ability to grow on DFOB as the sole carbon source. DFOB degradation proceeded by hydrolysis of the amide bonds in DFOB via a serine protease in the nitrogen-fixing bacterium *Mesorhizobium*

loti [5] or a specific DFOB hydrolase in multiple strains of nitrogen-fixing bacteria, *Azospirillum* [3], but the hydroxamate groups remained intact. Another study showed that the trishydroxamate ferrichrome A was utilized by the soil bacterium *Pseudomonas sp.* isolate FC1 as a carbon source and involved degradation via hydrolysis of the peptide bonds to yield simpler hydroxamate structures [4]. The presence of Fe and the formation of Fe-siderophore chelates protected siderophores from the degradation reaction. A separate mechanism was involved in several studies, which have shown the enzymatic degradation of iron-fusarinine complexes as part of a cellular mechanism to recover iron from these siderophores in the cytosol or the periplasm [6-8]. The degradation involved fungal esterases that hydrolyze the cyclic tris-hydroxamate fusarinine C at the ester bonds to form mono-and bis-hydroxamate products. The reaction products had lower iron affinities, which promoted cellular iron utilization [8].

In contrast to our study, these previous reports showed hydrolysis of the amide bonds or ester bonds in siderophores while the hydroxamate groups remained intact. However, to our knowledge, siderophore degradation via microbial reduction of hydroxamate groups to amides has not been reported previously, and may have important implications for metal uptake and the fate of siderophores in soil environments. Because of the potential implications, we provide some preliminary discussion exploring putative mechanisms for observed changes in dissolved siderophore concentration and structure. However, we specifically note that definitively establishing the mechanism of DFOB degradation was outside the scope of this work and is the subject of ongoing studies in this laboratory.

An abiotic auto-decomposition reaction of Fe^{II}-DFOB complexes was previously observed under anaerobic conditions in which the oxidation of two Fe^{II} ions was coupled to the reduction of a hydroxamate group to an amide (**Eq. 1**) [31, 32].

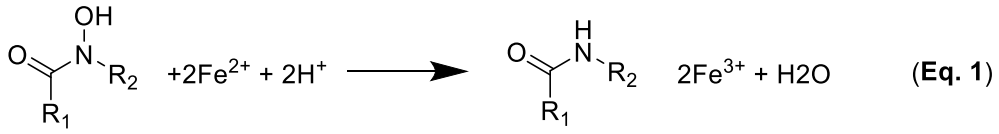

The initial reaction rate was rapid under neutral to acidic pH values, such as those found in the fungal incubations in our study (pH=4.5). A mechanism as described in Eq. 1 could explain the observed DFOB and coprogen siderophore degradation if Fe^{II} was generated in our aerobic experiments. Under aerobic conditions, DFOB was present as free DFOB or as Fe^{III}-DFOB chelate. Generally, fungi can acquire iron from siderophores via (1) a non-reductive system that

utilizes Fe^{III}-siderophore transporters or ligand-exchange of Fe^{III} at the cell surface, and (2) by reduction of the Fe^{III}-siderophore complex to a weak and labile Fe^{II} complex at the plasma membrane, followed by Fe^{II} exchange with permeases or oxidases for cellular uptake [1, 33, 34]. Iron acquisition mechanisms by fungi have been elucidated in detail with the *Saccharomyces cerevisiae* model. *S. cerevisiae* does not produce siderophores, but is capable of acquiring Fe from siderophores via non-reductive and reductive uptake pathways [35]. The reductive system involves plasma membrane-bound ferric reductases (FREs) that are produced under conditions of iron (and in some cases copper) limitation, primarily Fre1p and Fre2p. Fe reduction is followed by either transport of Fe^{II} via a high-affinity ferrous transporter or re-oxidation of Fe^{II} to Fe^{III} via a multicopper ferroxidase (Fet3) and transport via a permease (Ftr1) [34, 35]. A broad substrate specificity of Fre1p and Fre2p enables *S. cerevisiae* to acquire iron from a wide range of sources, including iron bound to hydroxamate siderophores, such as DFOB, and catechol siderophores, such as enterobactin [34-36]. The reduction of stable and inert Fe^{III}–tris hydroxamate siderophore chelates by physiologic reductants such as NADPH becomes possible by coupling the reduction with chelation of the Fe^{II} ion in a high-affinity transporter, combined with a hydrophobic environment and reduced pH at the cell surface [34, 37]. Iron-reduction thus enables ligand exchange both thermodynamically and kinetically to access siderophore-bound iron [37]. To get preliminary evidence on whether fungal reductive iron acquisition led to DFOB degradation, we cultured *S. cerevisiae* S288C under the same conditions as *P. biseptata*. LC-MS analysis of Fe-limited *S. cerevisiae* S288C supernatants after 72 h of incubation indeed showed significant formation of the DFOB-O degradation product, although compared to the *P. biseptata* incubations, only a minor fraction of DFOB had reacted (~4%) (Figure S4). The DFOB-2O and DFOB-3O degradation products were not detected, likely because they were below the detection limit. Orthologs of the *S. cerevisiae* reductive iron uptake system are present in other fungi and possibly widely distributed among fungi [38]: a *FreB* metalloreductase is involved in the *Aspergillus fumigatus* iron starvation response [39], and the black fungus pathogen *Cladophialophora carrionii* has been found to secrete the extracellular ferricrocin while also expressing reductive iron uptake genes similar to *S. cerevisiae* [40]. As pointed out by [40], the oxidase-permease components of the reductive iron uptake system of *S. cerevisiae* are also conserved in other human pathogens, including *Candida albicans* [41], *Cryptococcus neoformans* [42], and in the plant pathogens *Ustilago maydis* [43], and *Fusarium graminearum* [44]. There is no available whole-genome sequence of *P. biseptata*, but the

wide distribution of high-affinity iron-reductive-uptake systems in fungi supports the hypothesis that our mechanism may involve the formation of ferrous iron species. If the discussed mechanistic link between high-affinity reductive iron uptake and degradation of hydroxamate siderophores is correct, any fungal plant symbionts that utilize the high-affinity reductive iron-uptake system in the presence of tris-hydroxamate siderophores may be expected to enhance iron bioavailability to plants by forming bis- and mono-hydroxamates in competitive low-iron environments.

Taken together, reductive iron acquisition was a plausible explanation for the observed degradation reaction in our study. We hypothesized that reductive iron uptake activity by *P. biseptata* involved the formation of transient Fe^{II}-DFOB or Fe^{II}-coprogen, followed by a re-oxidation of Fe^{II} to Fe^{III} and reduction of a siderophore hydroxamate group. If such a mechanism was involved in DFOB degradation, we need to be able to explain the observation of DFOB degradation in Fe-limited medium, whereas FeDFOB complexes were not degraded in Fe-replete medium. Fe-limited media are not completely iron-free but contain iron as trace contaminants, enabling significant growth of fungal cultures, which can explain degradation in Fe-limited media. Conversely, Fe replete media are not expected to result in degradation of FeDFOB because of suppression of the FRE ferric reductases and high-affinity ferrous iron transporters involved in Fe acquisition from FeDFOB in Fe replete conditions [34]. Supporting a suppression of iron starvation response in Fe-replete medium, *P. biseptata* did not produce coprogen siderophores.

The specific activity to degrade as well as produce tris-hydroxamate siderophores by *P. biseptata* suggested a biological role linked to efficient uptake of iron. The reduction of the iron-chelating hydroxamate groups (Eq. 1) leads to a progressive loss of Fe chelating ability, enhancing reactivity for further Fe reduction or ligand-exchange, but comes at the cost of the fungal siderophore being degraded. Therefore, this activity may be beneficial in the presence of high siderophore concentrations, for example, in the presence of siderophores from competing organisms. Supporting this idea, the reductive iron uptake from tris-hydroxamate siderophores has been reported to be preferred at high siderophore concentrations, while non-reductive uptake mechanisms are prevalent at low siderophore concentrations [34, 45]. Nearly all fungi are capable of taking up Fe via the non-reductive uptake system that is specific for iron-siderophore chelates [34, 46]. It can be hypothesized that *P. biseptata* adapted to growing in both an environment with low iron-chelator concentrations and low iron-availability by producing its own siderophores, and

taking up iron in an environment of high siderophore concentration from the activity of competing bacteria and fungi using a reductive uptake system.

Aside from DFOB, *P. biseptata* also rapidly removed protochelin from solution. Minor degradation peaks could be identified and showed oxidation of the 2,3-dihydroxybenzoate groups to quinone groups. The oxidation of quinones in protochelin was previously observed by cyclic voltammetry and interpreted as a reversible, redox-mediated method to release Fe from the Fe^{III}-protochelin complexes because the quinone groups have greatly reduced Fe^{III} binding affinities [47]. Most of the protochelin removed from the solution was not accounted for by potential degradation products in our study, either because it was taken up and metabolized internally by the fungus, or because it was adsorbed, or degradation products evaded detection. Experiments to recover protochelin by cell extraction with methanol were not successful, implying potential degradation following adsorption of protochelin on the surface of fungal cells. Our previous studies with protochelin have shown a propensity of the hydrophobic protochelin to adsorb to particles and colloids in soil extract solutions [47], and the catechol groups can also react in oxidative polymerization processes, forming hydrophobic products [19, 48]. The rapid removal of the bulk of protochelin within minutes after addition to the fungal mycelium, without the observation of corresponding degradation products in solution, suggested that protochelin or protochelin degradation products may have adsorbed on cellular surfaces. Given the strong removal of DFOB and protochelin by *P. bispetata* in contrast to the other three tested fungi, it appears that the observed oxidation of protochelin may have involved reductive iron uptake at the *P. biseptata* plasma membrane, similar to that discussed above for DFOB. Reductive iron uptake from chelates with the tris-catechol siderophore enterobactin has been reported previously with *S. cerevisiae* and involved the same ferric reductases that can also reduce Fe^{III} bound to DFOB (FRE1, FRE2) [36]. In the presence of oxygen, high iron redox activity at the cell surface may have resulted in the rapid formation of polymeric protochelin oxidation products.

Common to the observed DFOB and protochelin degradation in our study was that the reaction occurred specifically in the iron-chelating groups, so that siderophores were compromised in their Fe binding ability. The impact is that iron becomes more available to plants and microbes that are not able to access iron-siderophore chelates. The observed siderophore degradation by *P. biseptata* may be a widespread ability among fungi, and we hypothesize that degradation involves fungal reductive iron acquisition systems. Future studies will need to test and mechanistically

establish this hypothesized link between high-affinity reductive iron uptake and siderophore degradation, as well as consequences for iron availability to plants.

REFERENCES

1. G. Winkelmann, 'Ecology of siderophores with special reference to the fungi', *Biometals*, 20 (2007): 379-392.

2. J. Kramer, Ö. Özkaya and R. Kümmerli, 'Bacterial siderophores in community and host interactions', *Nature Reviews Microbiology*, 18 (2020): 152-163.

3. G. Winkelmann, B. Busch, A. Hartmann, G. Kirchhof, R. Süßmuth and G. Jung, 'Degradation of desferrioxamines by Azospirillum irakense: assignment of metabolites by HPLC/electrospray mass spectrometry', *Biometals*, 12 (1999): 255-264.

4. R. Warren and J. Neilands, 'Microbial degradation of the ferrichrome compounds', *Microbiology*, 35 (1964): 459-470.

5. N. Zaya, A. Roginsky, J. Williams and D. Castignetti, 'Evidence that a deferrioxamine B degrading enzyme is a serine protease', *Canadian Journal of Microbiology*, 44 (1998): 521-527.

6. F. Ecker, H. Haas, M. Groll and E. M. Huber, 'Iron scavenging in Aspergillus species: Structural and biochemical insights into fungal siderophore esterases', *Angewandte Chemie International Edition*, 57 (2018): 14624-14629.

7. M. Gründlinger, F. Gsaller, M. Schrettl, H. Lindner and H. Haas, 'Aspergillus fumigatus SidJ mediates intracellular siderophore hydrolysis', *Applied and environmental microbiology*, 79 (2013): 7534-7536.

8. C. Kragl, M. Schrettl, B. Abt, B. Sarg, H. H. Lindner and H. Haas, 'EstB-mediated hydrolysis of the siderophore triacetylfusarinine C optimizes iron uptake of Aspergillus fumigatus', *Eukaryotic Cell*, 6 (2007): 1278-1285.

9. M. Caza, A. Garénaux, F. Lépine and C. M. Dozois, 'Catecholate siderophore esterases Fes, IroD and IroE are required for salmochelins secretion following utilization, but only IroD contributes to virulence of extra-intestinal pathogenic Escherichia coli', *Molecular microbiology*, 97 (2015): 717-732.

10. X. Zeng, Y. Mo, F. Xu and J. Lin, 'Identification and characterization of a periplasmic trilactone esterase, Cee, revealed unique features of ferric enterobactin acquisition in C ampylobacter', *Molecular microbiology*, 87 (2013): 594-608.

11. Q. Perraud, L. Moynié, V. Gasser, M. Munier, J. Godet, F. Hoegy, Y. Mély, G. t. L. Mislin, J. H. Naismith and I. J. Schalk, 'A key role for the periplasmic PfeE esterase in iron acquisition via the siderophore enterobactin in Pseudomonas aeruginosa', *ACS chemical biology*, 13 (2018): 2603-2614.

12. W. Hördt, V. Römheld and G. Winkelmann, 'Fusarinines and dimerum acid, mono-and dihydroxamate siderophores from Penicillium chrysogenum, improve iron utilization by strategy I and strategy II plants', *Biometals*, 13 (2000): 37-46.

13. E. Bar-Ness, Y. Hadar, Y. Chen, V. Romheld and H. Marschner, 'Short-term effects of rhizosphere microorganisms on Fe uptake from microbial siderophores by maize and oat', *Plant physiology*, 100 (1992): 451-456.

14. M. Suzuki, A. Urabe, S. Sasaki, R. Tsugawa, S. Nishio, H. Mukaiyama, Y. Murata, H. Masuda, M. S. Aung and A. Mera, 'Development of a mugineic acid family phytosiderophore analog as an iron fertilizer', *Nature communications*, 12 (2021): 1-13.

15. G. Bonito, H. Reynolds, M. S. Robeson, J. Nelson, B. P. Hodkinson, G. Tuskan, C. W. Schadt and R. Vilgalys, 'Plant host and soil origin influence fungal and bacterial assemblages in the roots of woody plants', *Molecular ecology*, 23 (2014): 3356-3370.

16. L. E. Becker and M. A. Cubeta, 'Increased flower production of Calibrachoa x hybrida by the soil fungus Mortierella elongata', *Journal of Environmental Horticulture*, 38 (2020): 114-119.

17. D. S. Arora and P. K. Gill, 'Production of ligninolytic enzymes by Phlebia floridensis', *World Journal of Microbiology and Biotechnology*, 21 (2005): 1021-1028.

18. O. P. Baars, David H., Small Molecule LC-MS/MS Fragmentation Data Analysis and Application to Siderophore Identification, In ed. J. Valdman *Applications from Engineering with MATLAB Concepts,* (Rijeka, Croatia, 2016): 191-214.

19. O. Baars, X. Zhang, F. M. Morel and M. R. Seyedsayamdost, 'The Siderophore Metabolome of Azotobacter vinelandii', *Appl Environ Microbiol*, 82 (2015): 27-39.

20. O. Baars, F. M. M. Morel and D. H. Perlman, 'ChelomEx: Isotope-Assisted Discovery of Metal Chelates in Complex Media Using High-Resolution LC-MS', *Analytical Chemistry*, 86 (2014): 11298-11305.

21. A. W. Smith, 6.13 Iron Starvation and Siderophore-Mediated iron Transport, In eds. J. K. Peter Williams and S. George. *Methods in Microbiology,* (1998): 331-342.

22. Y. Oh, W. L. Franck, S.-O. Han, A. Shows, E. Gokce, D. C. Muddiman and R. A. Dean, 'Polyubiquitin is required for growth, development and pathogenicity in the rice blast fungus Magnaporthe oryzae', (2012).

23. M. Hossain, M. Jalal, B. Benson, C. Barnes, and D. Van der Helm, 'Structure and conformation of two coprogen-type siderophores. Neocoprogen I and neocoprogen II', *Journal of the American Chemical Society*, 109 (1987): 4948-4954.

24. E. Mawji, M. Gledhill, J. A. Milton, G. A. Tarran, S. Ussher, A. Thompson, G. A. Wolff, P. J. Worsfold and E. P. Achterberg, 'Hydroxamate Siderophores: Occurrence and Importance in the Atlantic Ocean', *Environmental Science & Technology*, 42 (2008): 8675-8680.

25. S. M. Lehner, L. Atanasova, N. K. N. Neumann, R. Krska, M. Lemmens, I. S. Druzhinina and R. Schuhmacher, 'Isotope-Assisted Screening for Iron-Containing Metabolites Reveals a High Degree of Diversity among Known and Unknown Siderophores Produced by Trichoderma spp', *Applied and Environmental Microbiology*, 79 (2013): 18-31.

26. S. Bertrand, G. Larcher, A. Landreau, P. Richomme, O. Duval and J.-P. Bouchara, 'Hydroxamate siderophores of Scedosporium apiospermum', *Biometals*, 22 (2009): 1019-1029.

27. R. Haapala and S. Linko, 'Production of Phanerochaete chrysosporium lignin peroxidase under various culture conditions', *Applied microbiology and biotechnology*, 40 (1993): 494-498.

28. A. Ray, S. Saykhedkar, P. Ayoubi-Canaan, S. D. Hartson, R. Prade and A. J. Mort, 'Phanerochaete chrysosporium produces a diverse array of extracellular enzymes when grown on sorghum', *Applied Microbiology and Biotechnology*, 93 (2012): 2075-2089.

29. K. Peraza-Jiménez, S. De la Rosa-García, J. J. Huijara-Vasconselos, M. Reyes-Estebanez and S. Gómez-Cornelio, 'Enzymatic bioprospecting of fungi isolated from a tropical rainforest in Mexico', *Journal of Fungi*, 8 (2021): 22.

30. J. Uehling, A. Gryganskyi, K. Hameed, T. Tschaplinski, P. Misztal, S. Wu, A. Desirò, N. Vande Pol, Z. Du and A. Zienkiewicz, 'Comparative genomics of Mortierella elongata and its bacterial endosymbiont Mycoavidus cysteinexigens', *Environmental Microbiology*, 19 (2017): 2964-2983.

31. E. Farkas, É. A. Enyedy, L. Zékány and G. Deák, 'Interaction between iron (II) and hydroxamic acids: oxidation of iron (II) to iron (III) by desferrioxamine B under anaerobic conditions', *Journal of inorganic biochemistry*, 83 (2001): 107-114.

32. D. Kim, O. W. Duckworth and T. J. Strathmann, 'Hydroxamate siderophore-promoted reactions between iron (II) and nitroaromatic groundwater contaminants', *Geochimica et Cosmochimica Acta*, 73 (2009): 1297-1311.

33. L. Pecoraro, X. Wang, D. Shah, X. Song, V. Kumar, A. Shakoor, K. Tripathi, P. W. Ramteke and R. Rani, 'Biosynthesis pathways, transport mechanisms and biotechnological applications of fungal siderophores', *Journal of Fungi*, 8 (2021): 21.

34. C. C. Philpott, 'Iron uptake in fungi: a system for every source', *Biochimica et Biophysica Acta (bba)-molecular cell research*, 1763 (2006): 636-645.

35. C. W. Yun, T. Ferea, J. Rashford, O. Ardon, P. O. Brown, D. Botstein, J. Kaplan and C. C. Philpott, 'Desferrioxamine-mediated iron uptake in Saccharomyces cerevisiae: evidence for two pathways of iron uptake', *Journal of Biological Chemistry*, 275 (2000): 10709-10715.

36. C. W. Yun, M. Bauler, R. E. Moore, P. E. Klebba and C. C. Philpott, 'The role of the FRE family of plasma membrane reductases in the uptake of siderophore-iron in Saccharomyces cerevisiae', *Journal of Biological Chemistry*, 276 (2001): 10218-10223.

37. S. Dhungana and A. L. Crumbliss, 'Coordination Chemistry and Redox Processes in Siderophore-Mediated Iron Transport', *Geomicrobiology Journal*, (2005): 87-98.

38. D. J. Kosman, 'Molecular mechanisms of iron uptake in fungi', *Molecular microbiology*, 47 (2003): 1185-1197.

39. M. Blatzer, U. Binder and H. Haas, 'The metalloreductase FreB is involved in adaptation of Aspergillus fumigatus to iron starvation', *Fungal genetics and Biology*, 48 (2011): 1027-1033.

40. A. M. Bailão, K. L. P. d. Silva, D. Moraes, B. Lechner, H. Lindner, H. Haas, C. M. A. Soares and M. G. Silva-Bailão, 'Iron Starvation Induces Ferricrocin Production and the Reductive

Iron Acquisition System in the Chromoblastomycosis Agent Cladophialophora carrionii', *Journal of Fungi*, 9 (2023): 727.

41. N. Ramanan and Y. Wang, 'A high-affinity iron permease essential for Candida albicans virulence', *Science*, 288 (2000): 1062-1064.

42. W. H. Jung, A. Sham, T. Lian, A. Singh, D. J. Kosman and J. W. Kronstad, 'Iron source preference and regulation of iron uptake in Cryptococcus neoformans', *PLoS pathogens*, 4 (2008): e45.

43. H. Eichhorn, F. Lessing, B. Winterberg, J. Schirawski, J. Kamper, P. Muller and R. Kahmann, 'A ferroxidation/permeation iron uptake system is required for virulence in Ustilago maydis', *The Plant Cell*, 18 (2006): 3332-3345.

44. Y. S. Park, J. H. Kim, J. H. Cho, H. I. Chang, S. W. Kim, H. D. Paik, C. W. Kang, T. H. Kim, H. C. Sung and C. W. Yun, 'Physical and functional interaction of FgFtr1–FgFet1 and FgFtr2–FgFet2 is required for iron uptake in Fusarium graminearum', *Biochemical Journal*, 408 (2007): 97-104.

45. E. Lesuisse, P.-L. Blaiseau, A. Dancis and J.-M. Camadro, 'Siderophore uptake and use by the yeast Saccharomyces cerevisiae', *Microbiology*, 147 (2001): 289-298.

46. T. Hsiang and D. L. Baillie, 'Comparison of the yeast proteome to other fungal genomes to find core fungal genes', *Journal of molecular evolution*, 60 (2005): 475-483.

47. V. Rai, N. Fisher, O. W. Duckworth and O. Baars, 'Extraction and detection of structurally diverse siderophores in soil', *Frontiers in Microbiology*, 11 (2020): 581508.

48. R. Pinnataip and B. P. Lee, 'Oxidation chemistry of catechol utilized in designing stimuli-responsive adhesives and antipathogenic biomaterials', *ACS omega*, 6 (2021): 5113-5118.

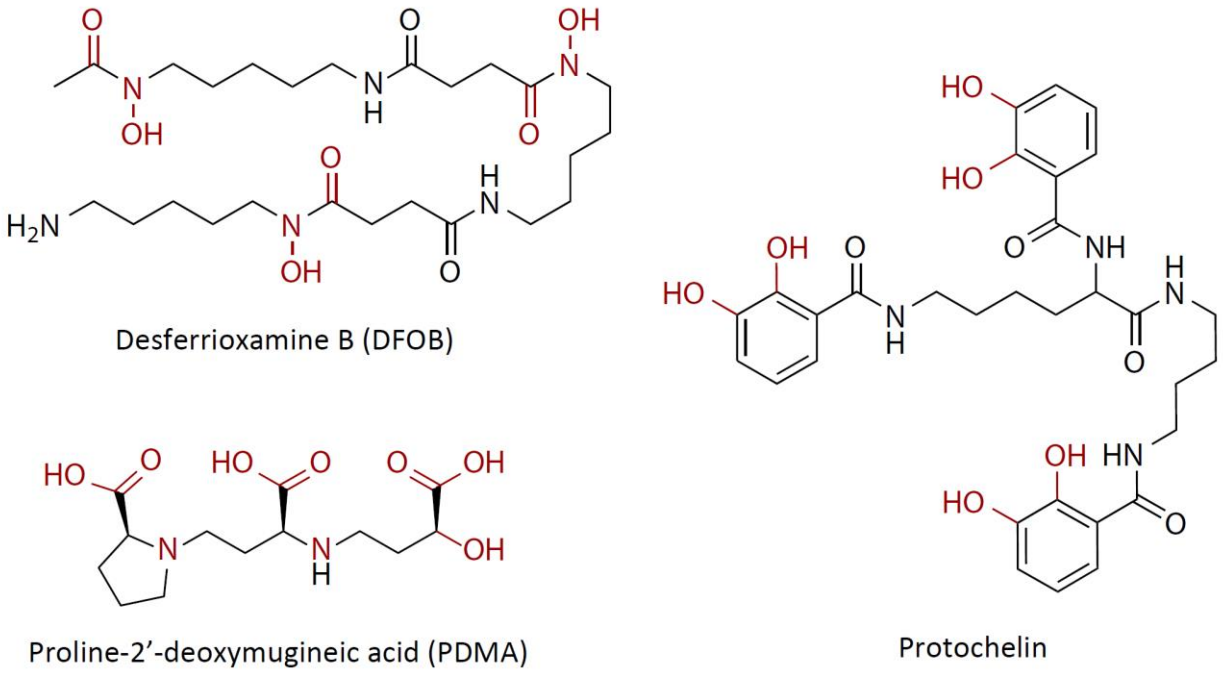

Figure 1. Structures of model siderophores used in the degradation experiments. The different moieties involved in Fe complexation are indicated in red.

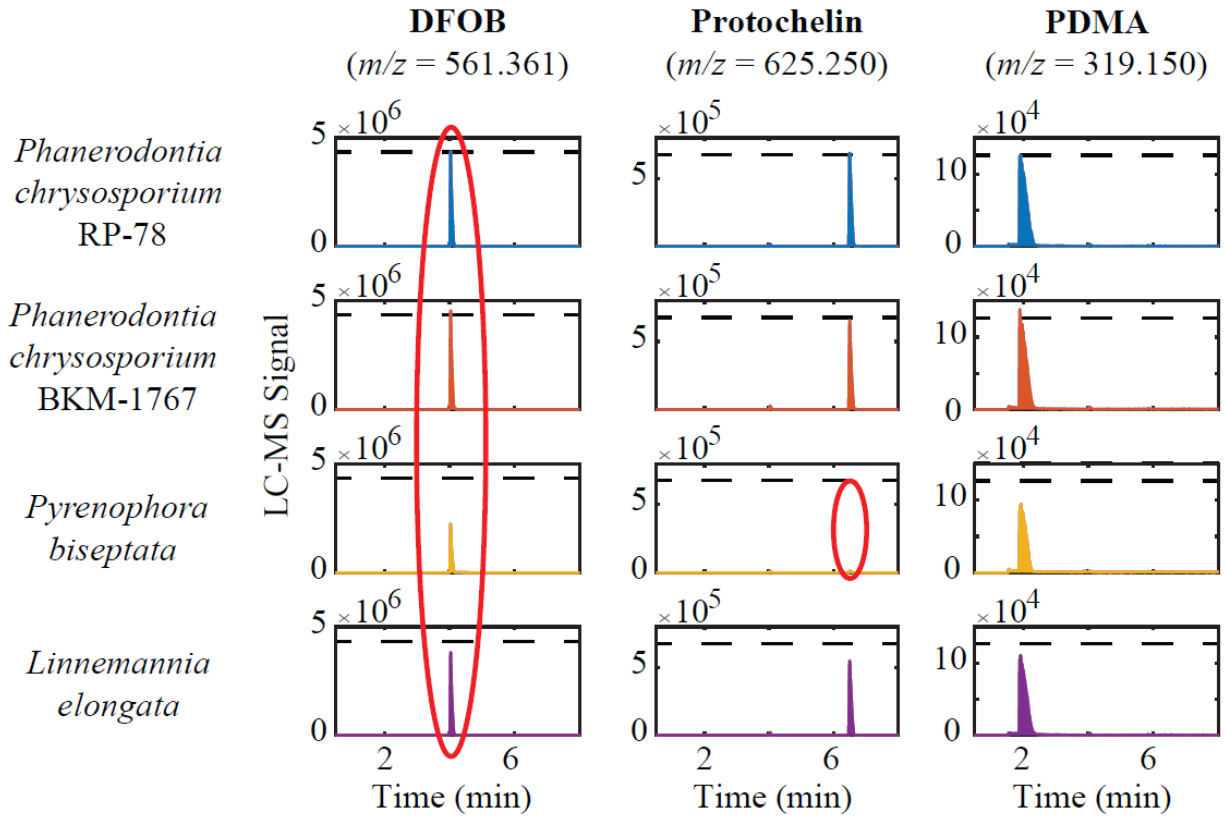

Figure 2. LC-MS peaks showing dissolved siderophores after incubation in iron-limited MSB media for each of the four mycelial slurries after 2 days in comparison to initial peak heights (dashed line). LC–MS, liquid chromatography–mass spectrometry; MSB, minimal salt broth.

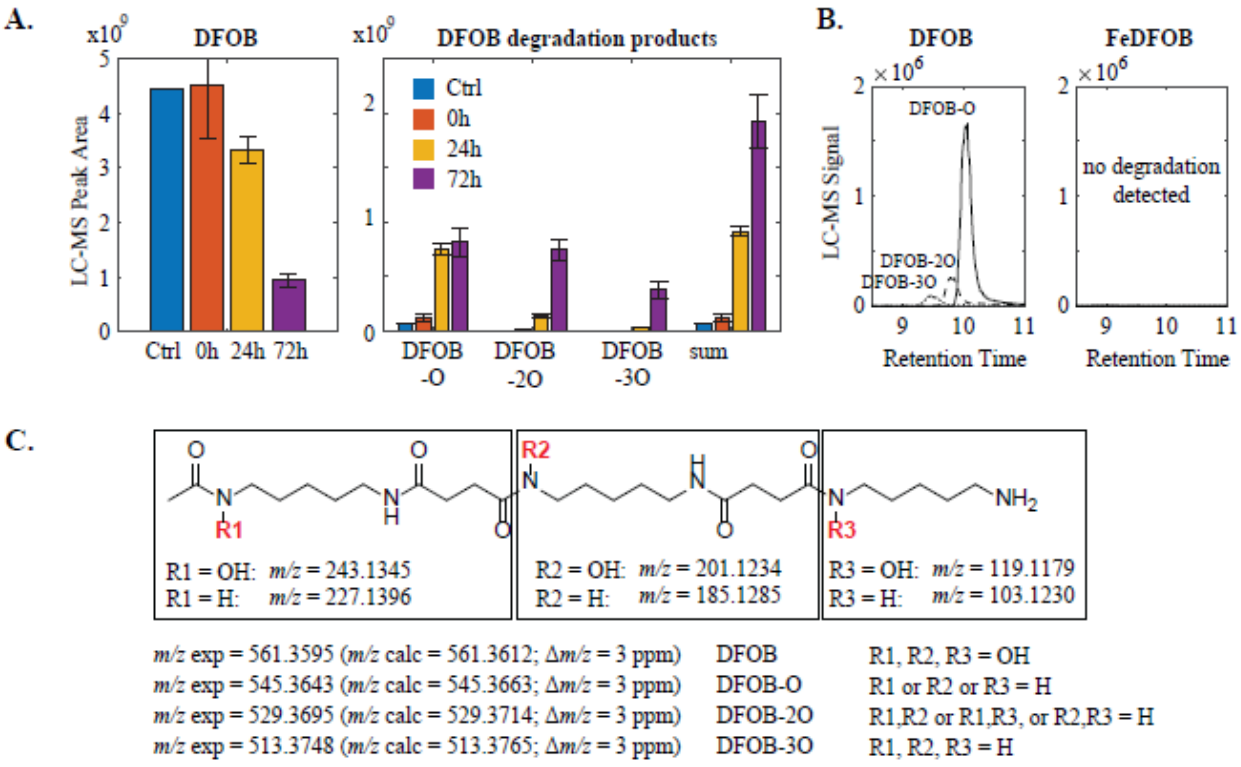

Figure 3. Degradation of DFOB by *P. biseptata*. (A) LC-MS peak areas for DFOB and DFOB degradation products for each of the three time points. Measurements of DFOB and DFOB degradation products were done simultaneously in the same samples. Error bars indicate standard deviations from triplicate biological incubations. (B) LC-MS chromatograms for the three degradation products after 5 days of incubation in iron-limited media with DFOB and iron-replete media with FeDFOB. (C) Structures of the observed DFOB degradation products derived from tandem mass-spectrometry fragmentation spectra. Fragments observed in MS/MS spectra (see also Table S2) are shown and correspond to the intact iron-chelating hydroxamates or to the corresponding structures in which hydroxamates were reduced to amides. DFOB, desferrioxamine B; LC–MS, liquid chromatography–mass spectrometry.

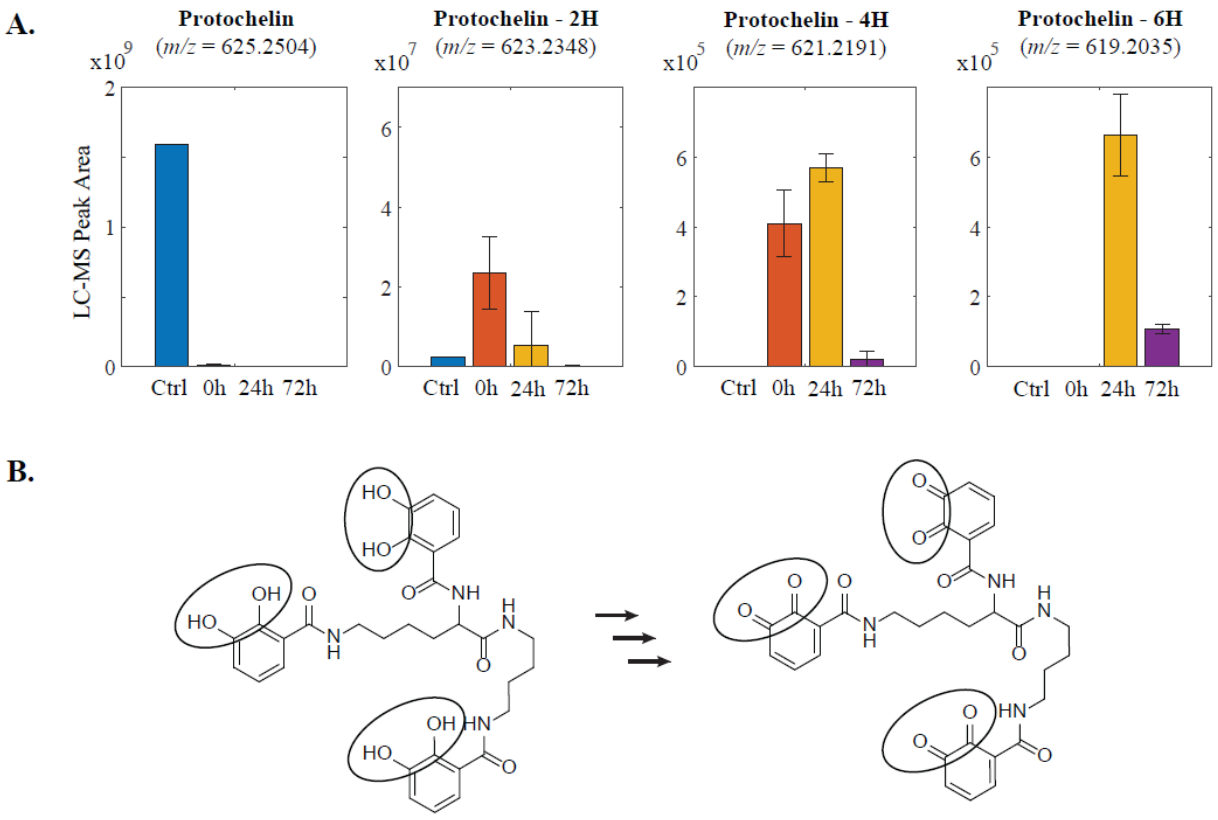

Figure 4. Removal of protochelin from supernatant solutions by *Pyrenophora biseptata* and detected degradation products (A). Iron chelating catechol moieties in protochelin and the quinone moieties in the degradation products, which lose their iron-chelating effectiveness, are circled. Error bars indicate standard deviations from triplicate biological incubations. Structures of the protochelin degradation products were derived from tandem mass-spectrometry fragmentation spectra (B).

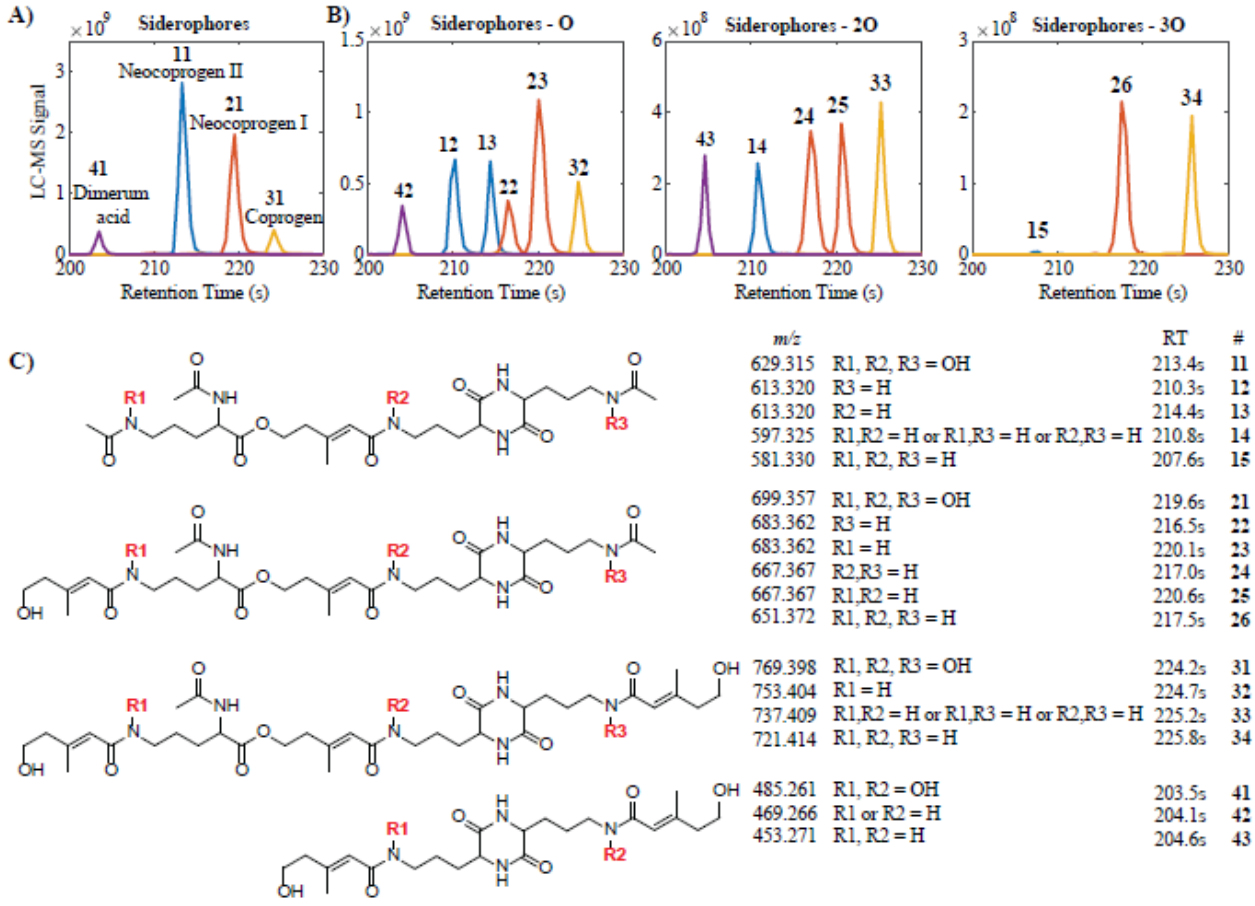

Figure 5. Siderophores produced by *Pyrenophora biseptata* (A) and related structures which had sum formulas with one, two, or three oxygen less (B). Analysis of MS/MS spectra (Figure S3, Tables S3-S8) showed that the structures of these related compounds were identical to those of the four main siderophores with one, two, or three hydroxamate groups reduced to their corresponding amides, similar to the observed DFOB degradation (C). DFOB, desferrioxamine B; MS/MS, tandem mass spectrometry.

Chapter 4

Mechanism of Hydroxamate Reduction in Reductive Iron uptake by diverse fungi

4.1 Introduction

The bioavailability of microbial iron (Fe) is partially regulated by biogenic complexing agents that facilitate its transport and uptake for cellular growth and maintenance. Siderophores are specialized metabolites and chelating agents produced and exuded by bacteria [1], fungi [2], and graminaceous plants [3] in response to Fe stress. These molecules not only promote Fe uptake, they also impact the interplay of competition and cooperation within microbial communities and in host-microbe interactions [4, 5].

Although siderophores are usually stable and resistant to biological degradation [6], several studies have documented microbial degradation of siderophores [7-10]. The resulting hydrolysis products of these siderophores possess a lower affinity for Fe, which may facilitate cellular Fe uptake via ligand exchange or Fe reduction. By effectively lowering Fe affinity through structural modifications, siderophores support the survival of diverse microbial species and drive plant-microbe interactions that can shape ecosystems within microbial and plant communities [11, 12].

Siderophore-mediated pathways for Fe uptake have been widely investigated [2, 7, 13, 14]. Fungi typically possess two strategies to acquire Fe from siderophores. The first strategy involves a non-reductive system that employs Fe^{III}-siderophore permease transporters or facilitates ligand-exchange of Fe^{III} at the cell surface [15], whereas the second strategy is a reductive system involving plasma membrane-bound ferric reductases (FREs, primarily Fre1p and Fre2p) produced under Fe-limited (and, in some cases, copper) conditions [16]. In the reductive system, Fe reduction is followed by either transport of Fe^{II} via a high-affinity ferrous permease transporter or reoxidation of Fe^{II} to Fe^{III} via a multicopper ferroxidase (Fet3) and transport via a ferric permease (Ftr1) [17-20].

A notable recent finding by French et al. (2024)[21] was the inactivation of the trishydroxamate siderophore, desferrioxamine B (DFOB), by the wheat root-associated fungus *Pyrenophora biseptata* through specific modification of Fe-binding moieties. These authors hypothesized that the Fe acquisition system in *P. biseptata* follows a reductive Fe uptake mechanism related to siderophore degradation. The proposed system reportedly proceeded through transient Fe^{II}-DFOB formation with subsequent Fe^{II} to Fe^{III} reoxidation and concomitant reduction of a siderophore hydroxamate group to an amide [21]. These results suggest a novel integration between ligand degradation and reductive Fe uptake. However, the specific mechanism(s) responsible for these transformations have not been fully elucidated.

Therefore, to demonstrate and document the mechanistic link(s) between high-affinity reductive Fe uptake and degradation of hydroxamate siderophores, we employed ferrozine [23] as a Fe^{II} trapping agent in our experiments. Ferrozine has been utilized in previous studies for Fe^{II} determination in quantification assays [24-31], astrocyte cultured cells [32], Fenton reactions [33], aqueous biological solutions [34], tracking Fe^{II} oxidation kinetics in the presence of Fe oxyhydroxides at acidic pH [35], and assessing Fe-reducing capacity of the wood decay fungi *Meruliporia incrassata*, *Gloeophyllum trabeum*, *Coniophora puteana*, and *Serpula lacrymans* [36-38], the ectomycorrhizal fungus *Paxillus involutus* during protein acquisition [39], and the yeasts *Candida albicans* and *Nakaseomyces glabratus* [40]. During the formation of stable complexes with Fe^{II}, in a 3:1 ratio of ferrozine to Fe^{II} [41], ferrozine can inhibit the reoxidation of Fe^{II} to Fe^{III}, thereby preventing the reduction of hydroxamate groups in desferrioxamine B (DFOB) to amides.

The reductive uptake of Fe in *P. biseptata* has also been documented in the unicellular yeast *Saccharomyces cerevisiae,* which utilizes a reductive Fe uptake system without producing siderophores [16, 17]. Similarly, the human pathogenic fungi *Cladophialophora carrionii* [42] and *Aspergillus fumigatus* [43] express genes involved in reductive Fe uptake in response to Fe starvation. Furthermore, *Candida albicans* [44] and *Cryptococcus neoformans* [45], possess conserved oxidase-permease genes similar to those characterized in *S. cerevisiae* involved in Fe uptake [18]. The plant pathogenic fungi *Ustilago maydis* [46] and *Fusarium graminearum* [47] also demonstrate genetic adaptations similar to those of the reductive Fe uptake system.

In this study, we initially investigated the relationship between DFOB degradation, siderophore production, including coprogens, neocoprogen I, neocoprogen II, and dimerum acid, and their degradation by *P. biseptata* in two experiments to better elucidate the high-affinity reductive uptake mechanism(s) of Fe acquisition in the absence or presence of ferrozine. We tested the hypothesis that reoxidation of Fe^{II} directly contributes to the degradation of DFOB and similar endogenous hydroxamate siderophores to amides during the reductive Fe uptake mechanism of *P. biseptata*. Our experimental approach involved the use of ferrozine to immobilize Fe^{II} and examine how Fe^{II} reoxidation reduces hydroxamates to amides. An additional experiment was conducted with the well characterized *S. cerevisiae* wild type and five mutant strains impaired in iron uptake and six additional isolates of unicellular and filamentous fungi representing a range of genetic diversity and evolutionary relatedness in the Ascomycota and Basidiomycota (Table 1). The patterns of DFOB degradation in relation to the reductive Fe uptake system observed in *P.*

biseptata were used to test the hypothesis that this Fe acquisition and transport process will be identified in ecologically and taxonomically diverse fungi in the Ascomycota and Basidiomycota.

4.2 Materials and methods

4.2.1 Fungal isolates/strain.

Thirteen isolates/strains of fungi were selected for this study (Table 1). Filamentous fungi were maintained by adding five 5-mm diameter mycelial plugs taken from the edge of an actively growing colony to 0.5 mL potato dextrose broth (PDB, Difco) in 2.0 mL cryovials (Thermo Fisher Scientific Inc.). Cryovials were incubated for 24 h at 25 ºC, sterile 50% glycerol was added to each tube, gently vortexed, and stored at -80˚C. The yeasts were maintained in cryovials with 0.5 mL YPD (Yeast Extract Peptone Dextrose) media, incubated for 24 h at 25 ºC, and 0.5 mL sterile 50% glycerol was added to each tube, gently vortexed, and stored at -80˚C. All fungi were revived from storage by transferring mycelial plugs or yeast cells to potato dextrose agar (PDA, Difco) plates.

4.2.2 Siderophore and ferrozine standards.

The trishydroxamate siderophore desferrioxamine B (DFOB) was selected based on the results of French et al. (2024)[21] and purchased as the mesylate salt (MilliporeSigma) (Figure 1A). A 10 mM stock solution of DFOB was prepared in 18 MΩ-cm water (MQ water), and a 10 mM standard of Fe-bound DFOB (Fe^{III}-DFOB) was prepared by the addition of 10 mM $FeCl_3$ to a 10 mM solution of DFOB in MQ water. The mixture was left to stand for 1 h in the dark at 20˚C with occasional shaking at 20 min intervals and centrifuged at ca. 22000 × *g* for 3 min. Ferrozine was purchased from Sigma-Aldrich and used as received (Figure 1B), and a stock solution of 1 mM was prepared in MQ water. DFOB siderophore and ferrozine stocks were immediately used or stored for up to two weeks at -20 ºC.

4.2.3 Preparation of fungal mycelium and growth media.

Mycelial plugs (5-mm diameter) were taken from the edge of an actively growing culture on PDA plates. The mycelial plugs were placed on 2% malt extract agar (MEA, Difco) and grown for 7 d at 25 ºC. A new mycelial plug was excised from this culture and placed on a PDA plate (9-cm diameter) at 25 ºC until mycelial growth reached the edge of the plate, approximately 7 d. A mycelial plug from each isolate was then transferred to 1.5% malt extract broth (MEB, Difco) and

incubated for 3–5 d. Fungal mycelium was harvested by vacuum filtration with cellulose filters (Whatman #1, 11 µm), rinsed with sterile MQ water, and homogenized with a handheld homogenizer (Fisher Scientific 150) using a 7-mm probe for 1 min on low speed to achieve a homogenous source of mycelium for the all reaction experiments with DFOB siderophore. Experiments were conducted by adding 2 mL of the homogenized mycelium to 13 mL of minimal salt broth (MSB) medium [21] in sterile cell culture flasks (Nunc, 75 cm^2) in the absence of 500 µM ferrozine. When 7.5 mL ferrozine (500 µM) was added to the reaction solution, 5.5 mL of minimal salt broth (MSB) medium was used in sterile cell culture flasks (Nunc, 75 cm^2). MSB medium was utilized to stimulate siderophore production by *P. biseptata* [21]. This medium was prepared as previously described [21]. A volume of 1 L of MSB medium was prepared by dissolving 10 g glucose, 2 g KH_2PO_4, 0.5 g $MgSO_4 \cdot 7H_2O$, 0.1 g $CaCl_2 \cdot 2H_2O$, 1 mg thiamine HCl, 0.2 g ammonium tartrate, 1 mL trace metal solution containing $[Zn^{2+}]$ = 53 µM, $[Cu^{2+}]$ = 10 µM, $[Co^{2+}]$ = 24 µM, $[Mn^{2+}]$ = 225 µM, $[MoO_4^{2-}]$ = 100µM, $[BO_3^{3-}]$ = 10 mM), and 1mL EDTA (0.1 M) in MQ water and adjusting the pH = 4.5 ± 0.1 with NaOH and H_2SO_4. The medium was filter sterilized (0.2 µm, PES, ThermoFisher) before use. Immediately after adding homogenized mycelium, a final concentration of 20 µM of unbound DFOB or Fe^{III}-DFOB complex (3 mL of the 100 µM stock solutions) was added to the 15 mL culture flasks.

4.2.4 Siderophore degradation experiments.

Three experiments were conducted. Experiment 1 compared the ability of *P. biseptata* to degrade the DFOB siderophore with or without ferrozine in the solution. Three replicates of each fungal culture were incubated in an MSB medium containing DFOB siderophores without and with added Fe. Sterile MSB media containing DFOB and Fe^{III}-DFOB complex, without and with added ferrozine, were used as controls. Samples were collected after incubating culture flasks for 0, 24, and 72 h. The supernatant and fungal cells were separated by centrifugation (ca. 22000 × *g* for 10 min), and the supernatant was passed through a syringe filter (0.2 µm polyethersulfone, PES, membrane) and stored at -80˚C before analysis by LC-MS (see details below). The mycelium of *P. biseptata* from each culture flask was harvested by vacuum filtration (Whatman #1, 11 µm), rinsed with sterile 18 MΩ•cm water (MQ water), and lyophilized to determine fungal biomass. This experiment indicated that *P. biseptata* effectively degraded DFOB in the absence of ferrozine, contrary to the samples with ferrozine, whether they contained Fe or not. Based on these results, a

second experiment (Experiment 2) was conducted to determine whether the production of coprogens, neocoprogen I, neocoprogen II, and dimerum acid siderophores, and their degradation by *P. biseptata* are influenced by ferrozine, particularly without DFOB in the culture solution. Three replicate cultures of *P. bispetata* in Fe-limited MSB medium, without and with added Fe (as $FeCl_3$), were incubated, without and with added ferrozine, in the absence of DFOB. Supernatant samples were collected immediately after inoculation with fungal mycelium, after 1 and 3 d by filtration (0.2 µm PES syringe filters). Sterile MSB medium with no added fungal mycelium was included in this experiment as a control treatment.

The results of these two experiments suggest the involvement of Fe^{II} in the degradation of DFOB and other hydroxamate-type siderophores produced by *P. biseptata*. To further investigate whether the link between Fe^{II} formation, reoxidation, and hydroxamate-type siderophore degradation observed in *P. biseptata* occurs in ecologically and taxonomically diverse unicellular and filamentous fungi, a third experiment was conducted with additional fungal isolates/strains that included *S. cerevisiae* wild type and five mutant strains with impaired iron transport mechanisms, and six additional isolates (*Sporobolomyces ruberrimus*, *Ustilago nunavutica*, *Vishniacozyma victoriae*, *Aspergillus flavus* aflatoxin and non-aflatoxin producing, and *Phanerodontia chrysosporium*) and *P. biseptata* as a positive control. Each fungal species was cultured with unbound DFOB in minimal salt broth (MSB) medium and compared to incubations with DFOB bound to Fe (Fe^{III}-DFOB complex) in MSB medium, with and without ferrozine added. Sterile MSB media containing DFOB and Fe^{III}-DFOB complex, with and without added ferrozine, were used as negative controls. The incubation with unbound DFOB was done without any added Fe in the medium; the incubation with added Fe^{III}-DFOB was done with the addition of 20 µM $FeCl_3$. Culture supernatants were collected after 3 and 7 d by filtration (0.2 µm PES syringe filters).

4.2.5 Siderophore degradation, formation of degradation products, and siderophore production analysis by LC-MS.

All fungal culture supernatants were analyzed by liquid chromatography-mass spectrometry (LC-MS) using an ISQ-EC (ThermoFisher) single quadrupole mass spectrometer in combination with an ultraviolet-visible (UV-vis) spectrophotometer and a charged aerosol detector (ThermoFisher) to determine the presence of siderophores and their degradation products. In

addition to the added DFOB, results from the chrome azurol S (CAS) assay [48] for *P. biseptata* suggested the production of endogenous siderophores [21]. A sample volume of 25 µL was injected and separated under a gradient of solvents A and B (unless otherwise noted A: water, 0.1% formic acid, 1% acetonitrile; B: acetonitrile, 0.1% formic acid, 2% water; gradient: 0–1.5 min 0% B, 1.5–8 min 0–100% B; 8–10 min 100% B; re-equilibration at 100% A for 4 min). Separation was accomplished with an Agilent Poroshell 120 EC-C18 column (4.6 × 100 mm, 2.7µm) and a flow rate of 1.2 mL/min, and the column temperature was 30°C. Mass spectra were collected in single ion monitoring mode targeting the three added siderophores and their degradation products (Table S1). Aliquot samples (0, 24, and 72 h) were analyzed with a high-resolution LC-MS/MS platform (Orbitrap Exploris 480, ThermoFisher). Sample volumes of 25 µL were injected and separated using a Restek Raptor C18 (2.1 × 100 mm) column with a flow rate of 0.4 mL/min, and the column compartment was kept at 45°C. The LC gradient was identical to that used with the ISQ-EC described above. Full-scan mass spectra (m/z = 85–1200) were acquired in positive ionization mode with the resolution set to R = 60,000 (full width at half maximum at m/z = 400) and data-dependent MS/MS acquisition of the five most abundant ions in each cycle. Product ions were generated in HCD mode with 35 eV collision energy and an isolation window of 1.5 Da. The resolving power for MS/MS analysis was R = 15,000 (full width at half maximum at m/z = 400). Structures of siderophores were analyzed by high-resolution LC-MS/MS by searching for the specific ^{54}Fe-^{56}Fe isotope pattern associated with Fe-siderophore complexes, along with searching for specific mass difference between the apo-siderophore and the Fe-siderophore complex, and siderophore-characteristic MS/MS fragmentation patterns [49, 50].

Siderophore degradation was followed by tracking peak areas of DFOB and fungal siderophores produced (Coprogen, Neocoprogen I & Neocoprogen II). Putative degradation products of the added siderophore standard and produced fungal siderophores were identified in both LC-MS and high-resolution LC-MS data by searching for new LC-MS peaks in incubated samples with related m/z values (e.g., simple mass differences, such as loss of an oxygen atom in new product compared to original siderophore standard; similar mass defects) and MS/MS spectra (e.g., presence of 2,3-dihydroxybenzoid acid moieties in protochelin degradation products showing as neutral loss of m/z = 136.016 in MS/MS spectra [51]).

4.3 Results

4.3.1 Degradation of DFOB as a function of time.

The mycelium of *P. biseptata* was incubated for 3 d with 20 µM DFOB in MSB medium in apo and Fe^{III} complex forms. Our findings from experiment 1 (Figure 2) indicated that *P. biseptata* activity resulted in approximately a 50% decrease in DFOB concentration in the Fe-limited medium when ferrozine was absent (Figure 2a). This observation is consistent with and supports the results of French et al. (2024)[21]. In contrast, when ferrozine was present in the culture medium, DFOB concentrations remained unchanged. Comparable results were also observed with the Fe^{III}-DFOB complex incubations in Fe-limited MSB medium. After 24 h, a stable magenta color was observed when ferrozine was present (Figure S1), indicating Fe reduction and Fe^{II}-Ferrozine complex formation. Overall, these results suggest that *P. biseptata* reduced Fe^{III} to Fe^{II} while degrading DFOB in solution. In contrast, the presence of ferrozine in culture samples appeared to interfere with the reduction of DFOB concentration by *P. biseptata*, suggesting an association between Fe^{II} formation to DFOB degradation.

4.3.2 DFOB degradation product formation during incubation with P. biseptata without and with ferrozine.

Figure 2a shows the mass spectrometer peak areas for DFOB and its degradation products at three timepoints (immediately after inoculation (time 0), 24, and 72 h) of incubation with *P. biseptata*. The findings showed a significant decrease in dissolved DFOB concentrations (approximately 24% and 65% after 24 and 72 h, respectively) when ferrozine was not present in the solution. At the same time, formation of putative DFOB degradation products was observed (Figure 2B), consistent with prior findings [21]. The three main degradation products observed had *m/z* values that corresponded to the sum formulas of DFOB with 1 to 3 fewer oxygen atoms (DFOB-O, DFOB-2O, and DFOB-3O). The formation of DFOB-O occurred first, followed by DFOB-2O, and finally DFOB-3O. The relatively minor modifications to the DFOB structure were not expected to significantly impact ionization behavior in LC-ESI-MS. Consequently, the combined peak areas of degradation products were used to estimate whether decreased DFOB concentration in solution could be attributed to the detected three degradation products. After 24 and 72 h, the sum of peak areas of the three degradation products accounted for approximately 80% and 55% of the dissolved DFOB loss, respectively. This consistent relationship between the

decrease in the DFOB peak area and the increase in the peak areas of the degradation products suggests that a major fraction of DFOB reacted in the supernatant solution rather than being lost due to sorption to cell surfaces or being sequestered as substrates.

MS/MS spectra indicated fragmentation of the three degradation products consistent with DFOB, in which one, two, or three hydroxamate groups were reduced to amides (Figure 2B, Supplementary Table 1). The fragmentation spectra revealed that the reduction of hydroxamate groups in DFOB-O could have occurred at any of the three hydroxamate positions, resulting in three degradation products that could not be chromatographically separated (Figure 2B, Supplementary Table 1**)**. The same was true for DFOB-2O, where two of the three hydroxamate groups were reduced to amides. In the final degradation product, DFOB-3O, all three hydroxamate moieties were reduced to amides. Since the three hydroxamate groups serve as the Fe^{III} binding moieties in DFOB, their loss resulted in a diminished ability to complex Fe^{III} in the degradation product. Additionally, when *P. biseptata* was incubated with either DFOB or Fe^{III}-DFOB in Fe-limited MSB medium containing ferrozine, no degradation of DFOB was detected in these experiments, as evidenced by the LC-MS analysis (Figure 3A). This further suggests that ferrozine may inhibit DFOB degradation in solution.

4.3.3 Siderophore production and degradation without and with ferrozine.

In addition to analyzing DFOB degradation, we investigated the ability of *P. biseptata* to produce and degrade endogenous siderophores, including coprogens, neocoprogen I, neocoprogen II, and dimerum acid [21], in a Fe-limited medium in both the presence and absence of ferrozine. Our findings revealed that siderophore production occurred only in Fe-limited medium when ferrozine was absent. In contrast, siderophore production was suppressed or not detected when ferrozine was present, as well as in Fe-replete medium, regardless of ferrozine presence. The masses of detected fungal siderophores corresponded with those described by [21], belonging to the family of trihydroxamate siderophores, which possess the same Fe-binding moieties as those found in DFOB, including coprogen [52], neocoprogen I, neocoprogen II [53], and dimerum acid [54, 55] (Figure 3A, Supplementary Table 2). Putative degradation products were detected with sum formulas containing less than one, two, or three oxygen atoms (Figure 3B). MS/MS spectra indicated that these structures were identical to the original four main siderophores, with one, two, or three

hydroxamate groups being reduced to amides, which were similar to and consistent with degradation patterns observed for DFOB (Figure 3C, Supplementary Tables 3-7).

4.3.4 DFOB degradation during incubation with other diverse fungi without ferrozine.

Beyond these degradation studies with *P. biseptata*, we investigated whether DFOB may undergo similar degradation by fungal activity using a diverse array of fungi, and to test whether the relationship between Fe^{II} formation and DFOB degradation is common among fungi. DFOB degradation product (DFOB-O) was detected by LC-MS analyses (Figure 4) when ferrozine was absent in solution, revealed after 72 h incubation with *S. cerevisiae* wild type (WT), five mutants of *S. cerevisiae* impaired in iron uptake (Arn1, Arn2, Fre1, Fre2, Sit1), *Sporobolomyces ruberrimus*, *Ustilago nunavutica*, *Vishniacozyma victoriae*, *Aspergillus flavus* 201 (aflatoxin+), and *A. flavus* 278 (aflatoxin-) mycelia in Fe-limited medium. *Phanerodontia chrysosporium* was used as a negative control based on a prior study [21]. Conversely, the presence of ferrozine in experimental cultures with isolates showed the formation of Fe^{II} (Figure 4), but no detection of DFOB-O degradation product. Further investigation into Fe^{II} and DFOB-O formation indicated a significant correlation ($R^2 = 0.94$; $p < 0.00001$) between the reduction of Fe^{III} to Fe^{II} in the presence of ferrozine and the formation of DFOB degradation products in the absence of ferrozine (Figure 5). Interestingly, *P. chrysosporium* showed a contrasting effect with no DFOB degradation and Fe^{II} formation, regardless of whether ferrozine was absent or present in the solution.

4.4 Discussion

4.4.1 Mechanism of Fe uptake by P. biseptata.

French et al. (2024)[21] reported on DFOB degradation by the wheat root-associated fungus *P. biseptata* and hypothesized that the observed reduction of hydroxamates to amides was associated with a reductive Fe uptake mechanism. In this study, we examined and investigated this hypothesis in detail by deploying ferrozine to inhibit Fe^{II} reoxidation. Ferrozine forms stable complexes with Fe^{II} when introduced into the reaction solution, potentially preventing reoxidation of Fe^{II} and concomitant reduction of the DFOB hydroxamate groups to an amide. Our results suggest that *P. biseptata* reduces Fe^{III} to Fe^{II}, prior to or during uptake, followed by Fe^{II} involvement in degrading DFOB and other siderophores through reoxidation. *P. biseptata* grown in Fe-limited MSB medium without ferrozine showed a significant decrease in dissolved DFOB

concentration and, to a lesser extent, Fe^{III}-DFOB complexes. The decrease in DFOB was accompanied by the formation of DFOB degradation products, where one, two, or three of the Fe-chelating hydroxamate groups were reduced to amides. Conversely, when ferrozine was present, complexation with Fe^{II}-ferrozine occurred, preventing reoxidation of Fe^{II}, resulting in no degradation of DFOB and Fe^{III}-DFOB. Our chemical equilibrium calculations, conducted using MINEQL+ software [56], along with prior studies [57, 58], confirmed that both Fe^{III}-DFOB and Fe^{II}-Ferrozine complexes were the thermodynamically predominant (>99%) forms of Fe^{III} and Fe^{II} in our experiments. Taken together, these findings confirm Fe^{III} reduction from Fe^{III}-DFOB, followed by Fe^{II} reoxidation as the biochemical mechanism that leads to DFOB degradation. Supplementary DFOB degradation assay with crude cell-pellet enzyme extracts revealed that the hydroxamate moiety reduction process appeared to occur without any extracellular enzymatic involvement, which is consistent with previous research [21].

Additionally, *P. biseptata* produced coprogen-type siderophores in Fe-limited conditions without ferrozine, generating neocoprogen I and II, typical linear trishydroxamate siderophores, which were also degraded similarly to DFOB. This siderophore production and degradation process may be an integral aspect of the reductive Fe uptake mechanisms, where siderophore production complements Fe acquisition by mobilizing Fe^{III}, which is then reduced to Fe^{II}, causing siderophore degradation and facilitating Fe uptake to microbial or plant cells. Our results provide additional evidence involving Fe reduction to uptake processes through coordinated siderophore production and degradation.

DFOB degradation has previously been observed as an abiotic auto-decomposition reaction of Fe^{II}-DFOB complexes under anaerobic conditions (Eq. 1) [57, 59, 60]. In this system, physiological reductases such as flavine mononucleotide (FMN) and nicotinamide-adenine dinucleotide phosphate (NADPH) play a crucial role by coupling the reduction of stable Fe^{III}–tris hydroxamate siderophore chelates with chelation of the Fe^{II} ion in a high-affinity transporter [19, 61-63]. This process is facilitated by a hydrophobic environment and reduced pH at the cell surface, consequently allowing for both thermodynamic and kinetic ligand exchange, making siderophore-bound Fe accessible [61, 63].

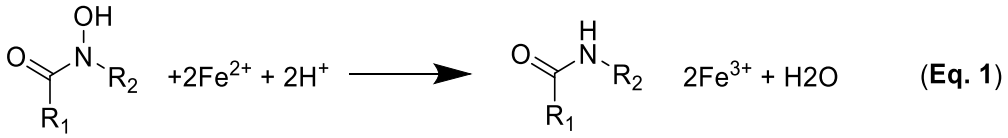

(**Eq. 1**)

To our knowledge, no research studies have specifically elucidated the mechanism(s) underlying biotic degradation of DFOB where hydroxamate groups are reduced to an amide. Previous studies have reported evidence of DFOB degradation by nitrogen-fixing bacteria, including *Azospirillum* [64], *Mesorhizobium loti* [9, 10], and the soil bacteria *Pseudomonas sp.* isolate FC1 [8, 65] and *Pseudomonas sp*. isolate DFBC#5 [66], indicating an ability to use DFOB as a sole carbon source. While these studies primarily showed hydrolysis of the amide or ester bonds in siderophores, the hydroxamate groups remained intact. Taken together, our study clarifies the mechanisms of DFOB degradation and the direct relationship in the reductive Fe uptake system of *P. biseptata*, emphasizing the implications for metal uptake and complex dynamics of siderophore activity. Further studies are needed to better understand the relative contribution and importance of this mechanism of microbes in the soil.

4.4.2 Evidence of a similar mechanism of reductive Fe uptake in other fungi.

Furthermore, the identification of DFOB-O degradation product in ecologically and taxonomically diverse fungi without ferrozine, and Fe^{II} formation when ferrozine was present in solution, showed a highly significant correlation ($R^2 = 0.94$; $p < 0.00001$) (Figure 5) that supports the existence of coupled Fe reduction and hydroxamate degradation in fungi that belong to well recognized species represented in different fungal phyla with varying ecology, growth, life history, and trophic (nutrient acquisition) behavior. Although only a minor fraction of DFOB (~1-3%) (Figure S2) had reacted in incubations with *S. cerevisiae* wild type and its mutants, *Sporobolomyces ruberrimus*, *Ustilago nunavutica*, *Vishniacozyma victoriae*, *Aspergillus flavus* 201 (aflatoxin+), *A. flavus* 278 (aflatoxin-), compared to *P. biseptata* (Figure 2). This result supports our hypothesis that the mechanism of DFOB degradation to amides is common within the context of Fe acquisition and transport for fungi. Conversely, the degradation products DFOB-2O and DFOB-3O were not observed, likely because they were below the detection limit of the analytical instruments. The ability of these fungi to utilize other Fe uptake mechanisms, such as

uptake of intact Fe-siderophore complexes, may be explained by the limited extents of siderophore degradation, although additional experiments are needed to explore these processes.

For this study, we included the model unicellular budding yeast *S. cerevisiae* in the phylum Ascomycota due to the availability of well-characterized mutant strains that varied in Fe acquisition and uptake mechanisms to address the influence of reductive Fe uptake in DFOB degradation and test its prevalence in diverse fungi. Although no siderophore production was detected in the *S. cerevisiae* wild type and Fe acquisition and uptake mutant strains, we found that these strains have the innate capacity to sequester Fe by potentially using alternative Fe acquisition strategies, including non-reductive Fe uptake systems as previously described [15, 67-69]. This mode of uptake may compete with conventional reductive Fe assimilation pathways, potentially accounting for the reduced degradation of DFOB observed in our cultures. This process may confer a competitive advantage in Fe-scarce environments, influencing microbial community diversity and structure and resource partitioning. We subsequently examined the unicellular saprobic yeast *Vishniacozyma victoriae*, the saprobic endophytic plant-associated unicellular yeast, *Sporobolomyces ruberrimus,* and the dimorphic (possessing a unicellular yeast and filamentous mycelial stage) plant pathogen *Ustilago nunavutica*, which are distantly related to the budding yeast *S. cerevisiae* and belong to the phylum Basidiomycota. They were also tested for their ability to utilize the reductive Fe systems, siderophore production, and degradation, as observed with *S. cerevisiae*.

No siderophore production was detected in these fungi, but they were able to reduce Fe and degrade DFOB in solution. Interestingly, species of the dimorphic plant pathogenic fungi *Ustilago maydis* and *Ustilago sphaerogena*, which are closely related to *Ustilago nunavutica,* synthesize Ferrichrome and Ferrichrome A, hydroxamate-type siderophores [70-72]. These siderophores are well-documented for their high affinity for Fe^{III}, suggesting potential for similar Fe acquisition mechanisms in less-characterized species like *Ustilago nunavutica*. The endophytic unicellular yeast *V. victoriae* has been previously used as a biological control agent to suppress plant diseases caused by *Botrytis cinerea* in kiwifruit [73], and *Phlyctema vagabunda* in apples [74]. The mechanism of biological management of these diseases with *V. victoriae* has been hypothesized to involve Fe homeostasis and redox balance regulation, which suppresses fungal pathogen growth while enhancing host plant defenses. The dual capacity to regulate micronutrient dynamics and inhibit plant pathogens highlights the ecological utility of *V. victoriae* and related

endophytes in sustainable agriculture. Moreover, *Sporobolomyces ruberrimus* can modulate oxidative stress responses in the model plant *Arabidopsis thaliana* [75], by influencing Fe uptake without disrupting homeostasis of essential micronutrients [76, 77]. These findings underscore the ecological role of fungal-mediated Fe mobilization in promoting plant health, particularly under abiotic stress, and suggest that *S. ruberrimus* may act as a regulatory tool for soil Fe availability and plant resilience.

Our experimental setup also included the filamentous fungi *Aspergillus flavus* and *Phanerodontia chrysosporium*. *A. flavus* is a toxin producing fungal plant pathogen that impacts animals and humans on a global scale, particularly in developing countries [78]. The Fe acquisition and uptake genes are well studied in *A. flavus*, and the gene cluster for reductive iron Assimilation (RIA) pathway is known, functionally analogous to those are also found in *S. cerevisiae* [79]. Although we did not test for and quantify aflatoxin production in this study, previous studies have reported a connection between Fe availability and aflatoxin production, with Fe influencing the expression of aflatoxin biosynthetic genes [80-82]. Notably, aflatoxin production in the strains used in this study is well characterized, even though our study did not confirm this in experiments.

Notably, *A. flavus* also shares the same non-ribosomal peptide synthetase genes (e.g., sidD, sidF, sidG) as *A. fumigatus*, strongly suggesting it could produce ferricrocin, a ferrichrome-type siderophore [83], triacetylfusarinine C (TAFC), a fusarinine-hydroxamate siderophore [84], and aspergillic acid, a hydroxamate-type siderophore [79]. While we did not assess the production of these siderophores directly, it is possible that their production competed with and interfered in the DFOB degradation process, potentially explaining the observed levels of DFOB reactivity in our experiments.

Furthermore, *Phanerodontia chrysosporium* was selected as an internal negative control in this study, based on prior knowledge of its inability to degrade DFOB [21]. *P. chrysosporium* does not produce siderophores; instead, it expresses genes related to non-reductive Fe acquisition, such as TonB-like transporters [85]. As anticipated, no DFOB degradation was observed when cultured with *P. chrysosporium*.

Collectively, these findings underscore the complex interactions between fungal physiology, Fe acquisition strategies, and ecological function. The production and degradation of siderophores, along with alternative Fe uptake mechanisms, play crucial roles in influencing fungal survival and competition across diverse environments. Our data suggests a common association

between the reductive Fe uptake mechanism and DFOB degradation among fungi, regardless of their ecological classification. While key genes involved in reductive Fe uptake remain incompletely characterized in many fungi, especially beyond well-studied models like *Saccharomyces cerevisiae*, the observed patterns point to conserved functional themes across fungal taxa.

4.4.3 Implications.

Understanding the mechanisms underlying fungal Fe acquisition sheds light on microbial adaptation in Fe-limited environments and reveals how these strategies shape broader biogeochemical and ecological processes. The connection between reductive Fe uptake systems and siderophore metabolism emphasizes the role of photogenically diverse fungi in potentially influencing nutrient availability and microbial interactions, including those with plants. These insights open new avenues for the targeted use of fungi in agriculture, such as promoting plant growth or managing soil nutrients, as well as in environmental applications like bioremediation and ecosystem restoration.

REFERENCES

1. C. Ratledge and L. G. Dover, 'Iron metabolism in pathogenic bacteria', *Annual reviews in microbiology*, 54 (2000): 881-941.

2. G. Winkelmann, 'Molecular recognition and transport of siderophores in fungi', *Iron transport in microbes, plants and animals*, (1987): 317-336.

3. H. Marschner and V. Römheld, 'Strategies of plants for acquisition of iron', *Plant and soil*, 165 (1994): 261-274.

4. G. Winkelmann, 'Ecology of siderophores with special reference to the fungi', *Biometals*, 20 (2007): 379-392.

5. J. Kramer, Ö. Özkaya and R. Kümmerli, 'Bacterial siderophores in community and host interactions', *Nature Reviews Microbiology*, 18 (2020): 152-163.

6. G. Winkelmann and H. Drechsel, 'Microbial siderophores', *Biotechnology*, 7 (1997): 199-246.

7. G. Winkelmann, B. Busch, A. Hartmann, G. Kirchhof, R. Süßmuth and G. Jung, 'Degradation of desferrioxamines by Azospirillum irakense: Assignment of metabolites by HPLC/electrospray mass spectrometry', *Biometals*, 12 (1999): 255-264.

8. R. Warren and J. Neilands, 'Microbial degradation of the ferrichrome compounds', *Microbiology*, 35 (1964): 459-470.

9. N. Zaya, A. Roginsky, J. Williams and D. Castignetti, 'Evidence that a deferrioxamine B degrading enzyme is a serine protease', *Canadian journal of microbiology*, 44 (1998): 521-527.

10. A. Pierwola, T. Krupinski, P. Zalupski, M. Chiarelli and D. Castignetti, 'Degradation pathway and generation of monohydroxamic acids from the trihydroxamate siderophore deferrioxamine B', *Applied and environmental microbiology*, 70 (2004): 831-836.

11. G. Winkelmann, 'Microbial siderophore-mediated transport', *Biochemical Society Transactions*, 30 (2002): 691-696.

12. J. C. Renshaw, G. D. Robson, A. P. Trinci, M. G. Wiebe, F. R. Livens, D. Collison and R. J. Taylor, 'Fungal siderophores: structures, functions and applications', *Mycological Research*, 106 (2002): 1123-1142.

13. G. Winkelmann, 'Importance of siderophores in fungal growth, sporulation and spore germination', *Frontiers in mycology*, (1991): 49-65.

14. H. Boukhalfa and A. L. Crumbliss, 'Chemical aspects of siderophore mediated iron transport', *Biometals*, 15 (2002): 325-339.

15. E. Lesuisse, P.-L. Blaiseau, A. Dancis and J.-M. Camadro, 'Siderophore uptake and use by the yeast Saccharomyces cerevisiae', *Microbiology*, 147 (2001): 289-298.

16. C. W. Yun, T. Ferea, J. Rashford, O. Ardon, P. O. Brown, D. Botstein, J. Kaplan and C. C. Philpott, 'Desferrioxamine-mediated iron uptake in Saccharomyces cerevisiae: evidence for two pathways of iron uptake', *Journal of Biological Chemistry*, 275 (2000): 10709-10715.

17. D. J. Kosman, 'Molecular mechanisms of iron uptake in fungi', *Molecular microbiology*, 47 (2003): 1185-1197.

18. C. W. Yun, M. Bauler, R. E. Moore, P. E. Klebba and C. C. Philpott, 'The role of the FRE family of plasma membrane reductases in the uptake of siderophore-iron in Saccharomyces cerevisiae', *Journal of Biological Chemistry*, 276 (2001): 10218-10223.

19. C. C. Philpott, 'Iron uptake in fungi: a system for every source', *Biochimica et Biophysica Acta (bba)-molecular cell research*, 1763 (2006): 636-645.

20. L. Pecoraro, X. Wang, D. Shah, X. Song, V. Kumar, A. Shakoor, K. Tripathi, P. W. Ramteke and R. Rani, 'Biosynthesis pathways, transport mechanisms and biotechnological applications of fungal siderophores', *Journal of Fungi*, 8 (2021): 21.

21. K. S. French, E. Chukwuma, I. Linshitz, K. Namba, O. W. Duckworth, M. A. Cubeta and O. Baars, 'Inactivation of siderophore iron-chelating moieties by the fungal wheat root symbiont Pyrenophora biseptata', *Environmental Microbiology Reports*, (2024): e13234.

22. P. Crous, S. Denman, J. Taylor, L. Swart, C. Bezuidenhout, L. Hoffman, M. Palm and J. Groenewald, 'Cultivation and diseases of Proteaceae: Leucadendron, Leucospermum and Protea. 2nd edn.[CBS Biodiversity Series no. 13.]', *Utrecht: CBSKNAW Fungal Biodiversity Centre*, (2013).

23. L. L. Stookey, 'Ferrozine---a new spectrophotometric reagent for iron', *Analytical chemistry*, 42 (1970): 779-781.

24. C. R. Gibbs, 'Characterization and application of ferrozine iron reagent as a ferrous iron indicator', *Analytical Chemistry*, 48 (1976): 1197-1201.

25. M. Pascual-Reguera, I. Ortega-Carmona and A. Molina-Dıaz, 'Spectrophotometric determination of iron with ferrozine by flow-injection analysis', *Talanta*, 44 (1997): 1793-1801.

26. E. Viollier, P. Inglett, K. Hunter, A. Roychoudhury and P. Van Cappellen, 'The ferrozine method revisited: Fe (II)/Fe (III) determination in natural waters', *Applied geochemistry*, 15 (2000): 785-790.

27. B. S. Berlett, R. L. Levine, P. B. Chock, M. Chevion and E. R. Stadtman, 'Antioxidant activity of Ferrozine–iron–amino acid complexes', *Proceedings of the National Academy of Sciences*, 98 (2001): 451-456.

28. K. I. Berker, K. Güçlü, B. Demirata and R. Apak, 'A novel antioxidant assay of ferric reducing capacity measurement using ferrozine as the colour forming complexation reagent', *Analytical Methods*, 2 (2010): 1770-1778.

29. J. Im, J. Lee and F. E. Löffler, 'Interference of ferric ions with ferrous iron quantification using the ferrozine assay', *Journal of microbiological methods*, 95 (2013): 366-367.

30. T. M. Jeitner, 'Optimized ferrozine-based assay for dissolved iron', *Analytical biochemistry*, 454 (2014): 36-37.

31. M. Ma, H. Wang, J. Xu, Y. Huang, D. Yuan, X. Zhang and Q. Song, 'An in situ analyzer for two-dimensional Fe (II) distribution in sediment pore water based on ferrozine coloration and computer imaging densitometry', *ACS omega*, 5 (2020): 31551-31558.

32. J. Riemer, H. H. Hoepken, H. Czerwinska, S. R. Robinson and R. Dringen, 'Colorimetric ferrozine-based assay for the quantitation of iron in cultured cells', *Analytical biochemistry*, 331 (2004): 370-375.

33. Z. Yang, Y. Yan, A. Yu, B. Pan and J. J. Pignatello, 'Revisiting the phenanthroline and ferrozine colorimetric methods for quantification of Fe (II) in Fenton reactions', *Chemical Engineering Journal*, 391 (2020): 123592.

34. S. Pepper, M. Borkowski, M. Richmann and D. Reed, 'Determination of ferrous and ferric iron in aqueous biological solutions', *Analytica chimica acta*, 663 (2010): 172-177.

35. A. M. Jones, P. J. Griffin, R. N. Collins and T. D. Waite, 'Ferrous iron oxidation under acidic conditions–The effect of ferric oxide surfaces', *Geochimica et Cosmochimica Acta*, 145 (2014): 1-12.

36. B. Goodell, G. Daniel, J. Jellison and Y. Qian, 'Iron-reducing capacity of low-molecular-weight compounds produced in wood by fungi', (2006).

37. C. Oviedo, D. Contreras, J. Freer and J. Rodríguez, 'A screening method for detecting iron reducing wood-rot fungi', *Biotechnology letters*, 25 (2003): 891-893.

38. A. C. Steenkjær Hastrup, T. Ø. Jensen and B. Jensen, 'Detection of iron-chelating and iron-reducing compounds in four brown rot fungi', *Holzforschung*, 67 (2013): 99-106.

39. F. Shah, M. Gressler, S. Nehzati, M. Op De Beeck, L. Gentile, D. Hoffmeister, P. Persson and A. Tunlid, 'Secretion of iron (III)-reducing metabolites during protein acquisition by the ectomycorrhizal fungus Paxillus involutus', *Microorganisms*, 9 (2020): 35.

40. F. Gerwien, A. Safyan, S. Wisgott, S. Brunke, L. Kasper and B. Hube, 'The fungal pathogen Candida glabrata does not depend on surface ferric reductases for iron acquisition', *Frontiers in Microbiology*, 8 (2017): 1055.

41. G. L. Smith, A. A. Reutovich, A. K. Srivastava, R. E. Reichard, C. H. Welsh, A. Melman and F. Bou-Abdallah, 'Complexation of ferrous ions by ferrozine, 2, 2′-bipyridine and 1, 10-phenanthroline: Implication for the quantification of iron in biological systems', *Journal of Inorganic Biochemistry*, 220 (2021): 111460.

42. A. M. Bailão, K. L. P. d. Silva, D. Moraes, B. Lechner, H. Lindner, H. Haas, C. M. A. Soares and M. G. Silva-Bailão, 'Iron Starvation Induces Ferricrocin Production and the Reductive Iron Acquisition System in the Chromoblastomycosis Agent Cladophialophora carrionii', *Journal of Fungi*, 9 (2023): 727.

43. M. Blatzer, U. Binder and H. Haas, 'The metalloreductase FreB is involved in adaptation of *Aspergillus fumigatus* to iron starvation', *Fungal genetics and Biology*, 48 (2011): 1027-1033.

44. N. Ramanan and Y. Wang, 'A high-affinity iron permease essential for Candida albicans virulence', *Science*, 288 (2000): 1062-1064.

45. W. H. Jung, A. Sham, T. Lian, A. Singh, D. J. Kosman and J. W. Kronstad, 'Iron source preference and regulation of iron uptake in Cryptococcus neoformans', *PLoS pathogens*, 4 (2008): e45.

46. H. Eichhorn, F. Lessing, B. Winterberg, J. Schirawski, J. Kamper, P. Muller and R. Kahmann, 'A ferroxidation/permeation iron uptake system is required for virulence in Ustilago maydis', *The Plant Cell*, 18 (2006): 3332-3345.

47. Y. S. Park, J. H. Kim, J. H. Cho, H. I. Chang, S. W. Kim, H. D. Paik, C. W. Kang, T. H. Kim, H. C. Sung and C. W. Yun, 'Physical and functional interaction of FgFtr1–FgFet1 and FgFtr2–FgFet2 is required for iron uptake in Fusarium graminearum', *Biochemical Journal*, 408 (2007): 97-104.

48. A. W. Smith, 6.13 Iron starvation and siderophore-mediated iron transport, *Methods in microbiology,* (1998): 331-342.

49. O. Baars, F. o. M. Morel and D. H. Perlman, 'ChelomEx: Isotope-assisted discovery of metal chelates in complex media using high-resolution LC-MS', *Analytical chemistry*, 86 (2014): 11298-11305.

50. O. Baars and D. H. Perlman, Small molecule LC-MS/MS fragmentation data analysis and application to siderophore identification, *Applications from Engineering with MATLAB Concepts,* (2016): 189.

51. O. Baars, X. Zhang, F. M. Morel and M. R. Seyedsayamdost, 'The siderophore metabolome of Azotobacter vinelandii', *Applied and Environmental Microbiology*, 82 (2016): 27-39.

52. E. Mawji, M. Gledhill, J. A. Milton, G. A. Tarran, S. Ussher, A. Thompson, G. A. Wolff, P. J. Worsfold and E. P. Achterberg, 'Hydroxamate Siderophores: Occurrence and Importance in the Atlantic Ocean', *Environmental Science & Technology*, 42 (2008): 8675-8680.

53. M. Hossain, M. Jalal, B. Benson, C. Barnes, and D. Van der Helm, 'Structure and conformation of two coprogen-type siderophores. Neocoprogen I and neocoprogen II', *Journal of the American Chemical Society*, 109 (1987): 4948-4954.

54. S. M. Lehner, L. Atanasova, N. K. N. Neumann, R. Krska, M. Lemmens, I. S. Druzhinina and R. Schuhmacher, 'Isotope-Assisted Screening for Iron-Containing Metabolites Reveals a High Degree of Diversity among Known and Unknown Siderophores Produced by Trichoderma spp', *Applied and Environmental Microbiology*, 79 (2013): 18-31.

55. S. Bertrand, G. Larcher, A. Landreau, P. Richomme, O. Duval and J.-P. Bouchara, 'Hydroxamate siderophores of Scedosporium apiospermum', *Biometals*, 22 (2009): 1019-1029.

56. W. D. Schecher and D. C. McAvoy, 'MINEQL+: a software environment for chemical equilibrium modeling', *Computers, Environment and Urban Systems*, 16 (1992): 65-76.

57. E. Farkas, É. A. Enyedy, L. Zékány and G. Deák, 'Interaction between iron (II) and hydroxamic acids: oxidation of iron (II) to iron (III) by desferrioxamine B under anaerobic conditions', *Journal of inorganic biochemistry*, 83 (2001): 107-114.

58. I. Spasojević, S. K. Armstrong, T. J. Brickman and A. L. Crumbliss, 'Electrochemical behavior of the Fe (III) complexes of the cyclic hydroxamate siderophores alcaligin and desferrioxamine E', *Inorganic chemistry*, 38 (1999): 449-454.

59. D. Kim, O. W. Duckworth and T. J. Strathmann, 'Hydroxamate siderophore-promoted reactions between iron (II) and nitroaromatic groundwater contaminants', *Geochimica et Cosmochimica Acta*, 73 (2009): 1297-1311.

60. D. Kim, O. W. Duckworth and T. J. Strathmann, 'Reactions of aqueous iron–DFOB (desferrioxamine B) complexes with flavin mononucleotide in the absence of strong iron (II) chelators', *Geochimica et Cosmochimica Acta*, 74 (2010): 1513-1529.

61. S. Dhungana and A. L. Crumbliss, 'Coordination Chemistry and Redox Processes in Siderophore-Mediated Iron Transport', *Geomicrobiology Journal*, (2005): 87-98.

62. F. Hallé and J. M. Meyer, 'Iron release from ferrisiderophores: A multi-step mechanism involving a NADH/FMN oxidoreductase and a chemical reduction by FMNH2', *European journal of biochemistry*, 209 (1992): 621-627.

63. J. P. Adjimani and E. Owusu, 'Nonenzymatic NADH/FMN-dependent reduction of ferric siderophores', *Journal of inorganic biochemistry*, 66 (1997): 247-252.

64. G. Winkelmann, B. Busch, A. Hartmann, G. Kirchhof, R. Süßmuth and G. Jung, 'Degradation of desferrioxamines by Azospirillum irakense: assignment of metabolites by HPLC/electrospray mass spectrometry', *Biometals*, 12 (1999): 255-264.

65. R. Warren and J. Neilands, 'Mechanism of microbial catabolism of ferrichrome A', *Journal of Biological Chemistry*, 240 (1965): 2055-2058.

66. S. C. Harwani, A. Roginsky, Y. Vallejo and D. Castignetti, 'Further characterization and proposed pathway of deferrioxamine B catabolism', *BioMetals*, 10 (1997): 205-213.

67. E. Lesuisse, M. Simon-Casteras and P. Labbe, 'Siderophore-mediated iron uptake in Saccharomyces cerevisiae: the SIT1 gene encodes a ferrioxamine B permease that belongs to the major facilitator superfamily', *Microbiology*, 144 (1998): 3455-3462.

68. P. Heymann, J. F. Ernst and G. Winkelmann, 'Identification of a fungal triacetylfusarinine C siderophore transport gene (TAF1) in Saccharomyces cerevisiae as a member of the major facilitator superfamily', *Biometals*, 12 (1999): 301-306.

69. P. Heymann, J. F. Ernst and G. Winkelmann, 'Identification and substrate specificity of a ferrichrome-type siderophore transporter (Arn1p) in Saccharomyces cerevisiae', *FEMS microbiology letters*, 186 (2000): 221-227.

70. D. Ecker, C. Passavant and T. Emery, 'Role of two siderophores in Ustilago sphaerogena: Regulation of biosynthesis and uptake mechanisms', *Biochimica et Biophysica Acta (BBA)-Molecular Cell Research*, 720 (1982): 242-249.

71. A. D. Budde and S. A. Leong, 'Characterization of siderophores from Ustilago maydis', *Mycopathologia*, 108 (1989): 125-133.

72. C. Voisard, J. Wang, J. L. McEvoy, P. Xu and S. A. Leong, 'urbsl, a gene regulating siderophore biosynthesis in Ustilago maydis, encodes a protein similar to the erythroid transcription factor GATA-1', *Molecular and Cellular Biology*, 13 (1993): 7091-7100.

73. L. Nian, Y. Xie, H. Zhang, M. Wang, B. Yuan, S. Cheng and C. Cao, 'Vishniacozyma victoriae: an endophytic antagonist yeast of kiwifruit with biocontrol effect to Botrytis cinerea', *Food Chemistry*, 411 (2023): 135442.

74. X. Sepúlveda, D. Silva, R. Ceballos, S. Vero, M. D. López and M. Vargas, 'Endophytic yeasts for the biocontrol of Phlyctema vagabunda in apples', *Horticulturae*, 8 (2022): 535.

75. A. Domka, R. Jędrzejczyk, R. Ważny, M. Gustab, M. Kowalski, M. Nosek, J. Bizan, M. Puschenreiter, M. Vaculík and J. Kováč, 'Endophytic yeast protect plants against metal toxicity by inhibiting plant metal uptake through an ethylene-dependent mechanism', *Plant, Cell & Environment*, 46 (2023): 268-287.

76. R. J. Jędrzejczyk, M. Gustab, R. Ważny, A. Domka, P. J. Jodłowski, M. Sitarz, P. Bezkosty, M. Kowalski, D. Pawcenis and K. Jarosz, 'Iron inactivation by Sporobolomyces ruberrimus and its potential role in plant metal stress protection. An in vitro study, *Science of the Total Environment*, 870 (2023): 161887.

77. A. T. Morales-Vargas, V. López-Ramírez, C. Álvarez-Mejía and J. Vázquez-Martínez, 'Endophytic fungi for crops adaptation to abiotic stresses', *Microorganisms*, 12 (2024): 1357.

78. B. N. Adhikari, R. Bandyopadhyay and P. J. Cotty, 'Degeneration of aflatoxin gene clusters in Aspergillus flavus from Africa and North America', *Amb Express*, 6 (2016): 1-16.

79. B. Adhikari, K. Callicott, and P. Cotty, Conservation and Loss of a Putative Iron Utilization Gene Cluster among Genotypes of Aspergillus flavus. Microorganisms 2021, 9, 137, (2021).

80. R. Tiwari, V. Mittal, T. Bhalla, S. Saini, G. Singh and D. Vadehra, 'Effect of metal ions on aflatoxin production by Aspergillus parasiticus', *Folia microbiologica*, 31 (1986): 124-128.

81. I. Caceres, A. Al Khoury, R. El Khoury, S. Lorber, I. P. Oswald, A. El Khoury, A. Atoui, O. Puel and J.-D. Bailly, 'Aflatoxin biosynthesis and genetic regulation: A review', *Toxins*, 12 (2020): 150.

82. L. Yao, F. Ban, S. Peng, D. Xu, H. Li, H. Mo, L. Hu, and X. Zhou, 'Exogenous iron induces NADPH oxidases-dependent ferroptosis in the conidia of Aspergillus flavus', *Journal of agricultural and food chemistry*, 69 (2021): 13608-13617.

83. I. Happacher, M., Aguiar, M., Alilou, B. Abt, T. J. Baltussen, C. Decristoforo, W. J. Melchers and H. Haas, 'The siderophore ferricrocin mediates iron acquisition in Aspergillus fumigatus', *Microbiology Spectrum*, 11 (2023): e00496-23.

84. E. D. Mulvihill, N. M. Moloney, R. A. Owens, S. K. Dolan, L. Russell and S. Doyle, 'Functional investigation of iron-responsive microsomal proteins, including MirC, in Aspergillus fumigatus', *Frontiers in Microbiology*, 8 (2017): 418.

85. E. M. Assmann, L. M. M. Ottoboni, A. Ferraz, J. Rodríguez and M. P. De Mello, 'Iron-responsive genes of Phanerochaete chrysosporium isolated by differential display reverse transcription polymerase chain reaction', *Environmental Microbiology*, 5 (2003): 777-786.

86. Y. Guo, W.-C. Au, M. Shakoury-Elizeh, O. Protchenko, M. Basrai, W. A. Prinz and C. C. Philpott, 'Phosphatidylserine is involved in the ferrichrome-induced plasma membrane trafficking of Arn1 in Saccharomyces cerevisiae', *Journal of Biological Chemistry*, 285 (2010): 39564-39573.

87. G. Giaever and C. Nislow, 'The yeast deletion collection: a decade of functional genomics', *Genetics*, 197 (2014): 451-465.

88. C. Philpott, O. Protchenko, Y. Kim, Y. Boretsky and M. Shakoury-Elizeh, 'The response to iron deprivation in Saccharomyces cerevisiae: expression of siderophore-based systems of iron uptake', *Biochemical Society Transactions*, 30 (2002): 698-702.

89. X. Shi, C. Stoj, A. Romeo, D. J. Kosman and Z. Zhu, 'Fre1p Cu2+ reduction and Fet3p Cu1+ oxidation modulate copper toxicity in Saccharomyces cerevisiae', *Journal of Biological Chemistry*, 278 (2003): 50309-50315.

90. E. Georgatsou, L. A. Mavrogiannis, G. S. Fragiadakis and D. Alexandraki, 'The yeast Fre1p/Fre2p cupric reductases facilitate copper uptake and are regulated by the copper-modulated Mac1p activator', *Journal of Biological Chemistry*, 272 (1997): 13786-13792.

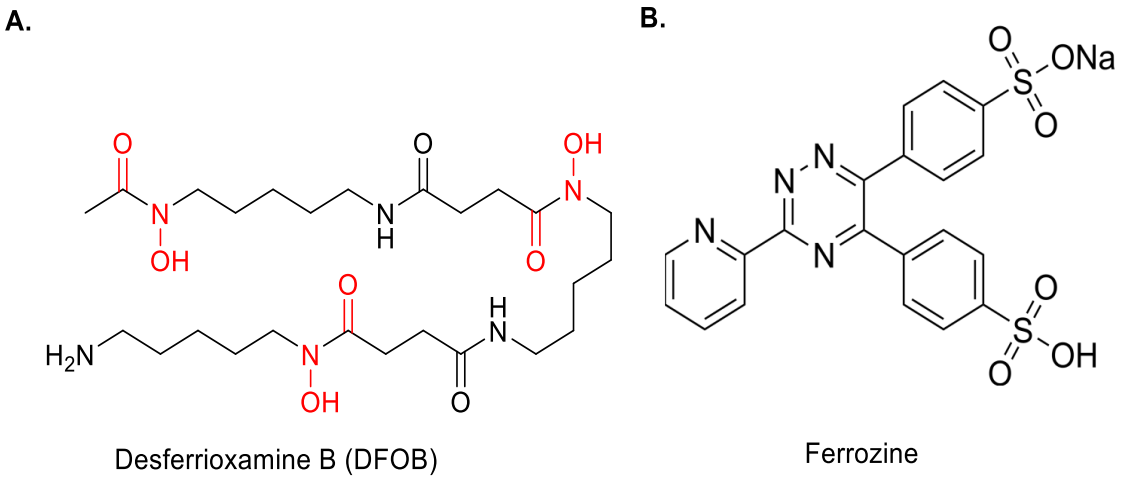

Figure 1. Chemical structures of DFOB siderophore with different moieties involved in Fe complexation are indicated in red (A), and ferrozine (B) used in siderophore degradation experiments.

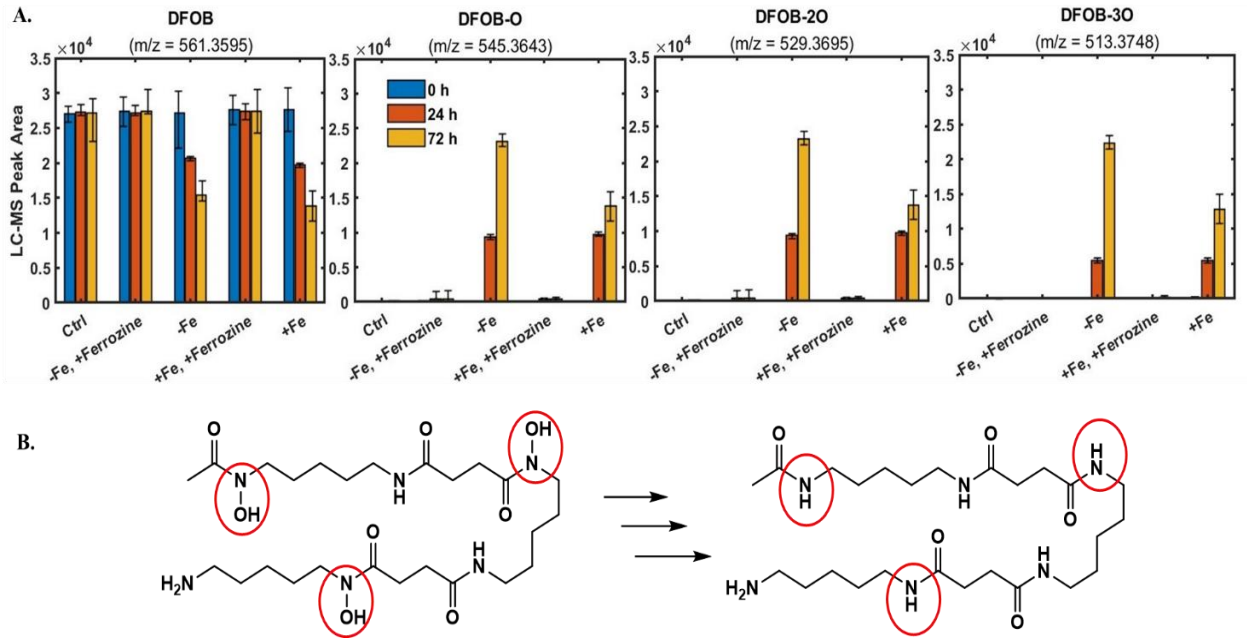

Figure 2. Incubation of *P. biseptata* in Fe-limited medium with DFOB and Fe^{III}-DFOB. (A) LC-MS peak areas for DFOB and degradation products at three time points (0 h, 24 h, and 72 h), after 3 d incubation in Fe-limited medium with DFOB and Fe^{III}-DFOB, shown with error bars representing standard deviations from three replicates per treatment. Measurements of DFOB and DFOB degradation products were done simultaneously in the same samples. Conditions: pH = 4.5 ± 0.1, [DFOB] or [Fe^{III}-DFOB] = 20 µM, T = 25˚C. (B) Structures of observed DFOB degradation products derived from tandem mass-spectrometry fragmentation spectra, highlighting MS/MS spectra fragments (see Table S3) that correspond to intact Fe-chelating hydroxamates and their reduced amide forms.

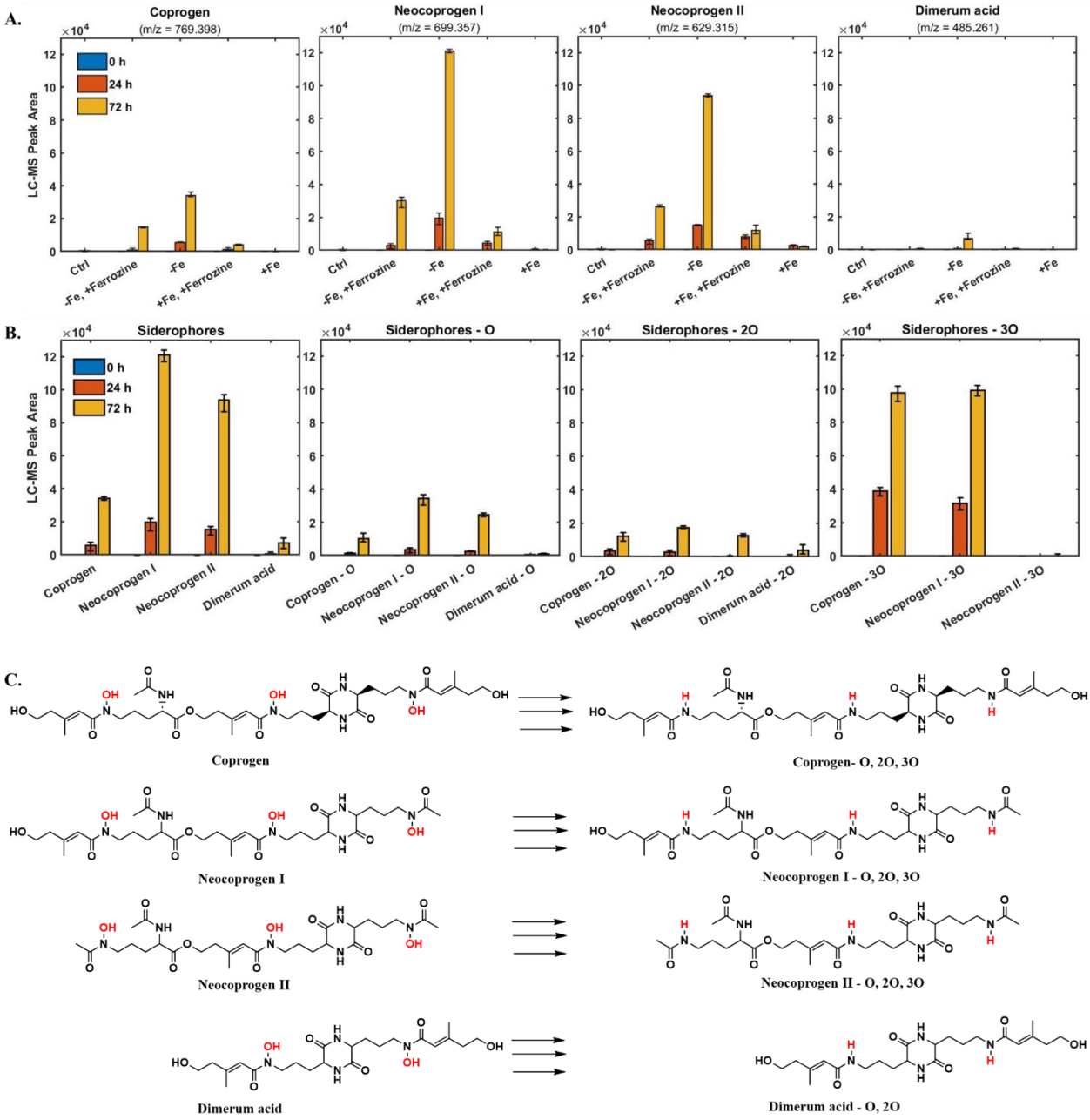

Figure 3. Siderophores produced by *P. biseptata* as a function of time (0 h, 24 h, 72 h) after 3 d incubation in Fe-limited medium with DFOB and Fe^{III}-DFOB, shown with error bars representing standard deviations from three replicates of each treatment. Conditions: pH = 4.5 ± 0.1, c = 20 µM DFOB or Fe^{III}-DFOB, T = 25˚C. A. Related peak areas of structures which had sum formulas with fewer than one, two, or three oxygen B. Structures of these related compounds were identical to those of the four main siderophores with one, two, or three hydroxamate groups reduced to their corresponding amides confirmed by analysis of MS/MS spectra (Figure S3, Tables S3-S6), like the observed DFOB (C).

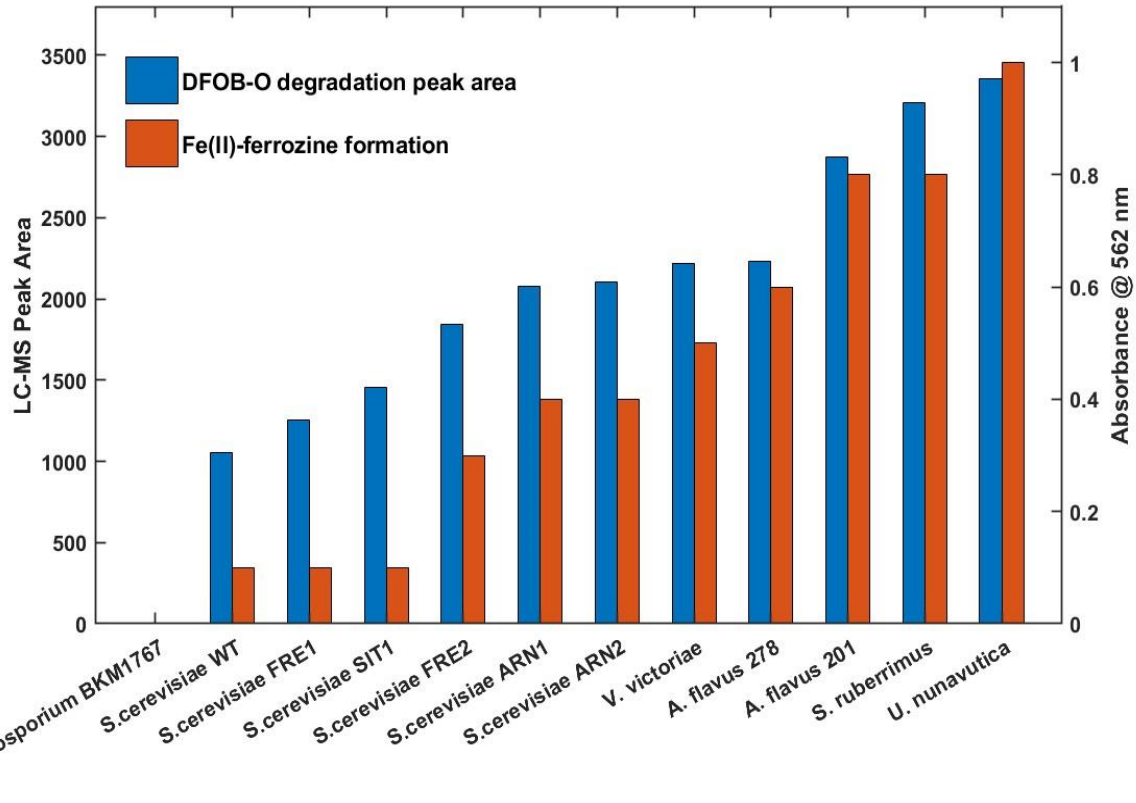

Figure 4. Degradation of DFOB by *Saccharomyces cerevisiae* wild type (WT), *S. cerevisiae* mutants impaired in Fe uptake (FRE1, FRE2, ARN1, ARN2, and SIT1), *Sporobolomyces ruberrimus*, *Ustilago nunavutica*, *Vishniacozyma victoriae*, *Aspergillus flavus* 201 (aflatoxin+), *A. flavus* 278 (aflatoxin-), and *Phanerodontia chrysosporium*) in samples without ferrozine. LC-MS peak areas for DFOB degradation product (DFOB-O) (blue) in samples without ferrozine and spectrophotometric values of Fe^{II}-ferrozine complex formation (orange) in samples with ferrozine present after 72 h incubation. Fe^{II}-ferrozine complexation and DFOB degradation product formation were measured simultaneously from three biological replicates of each treatment.

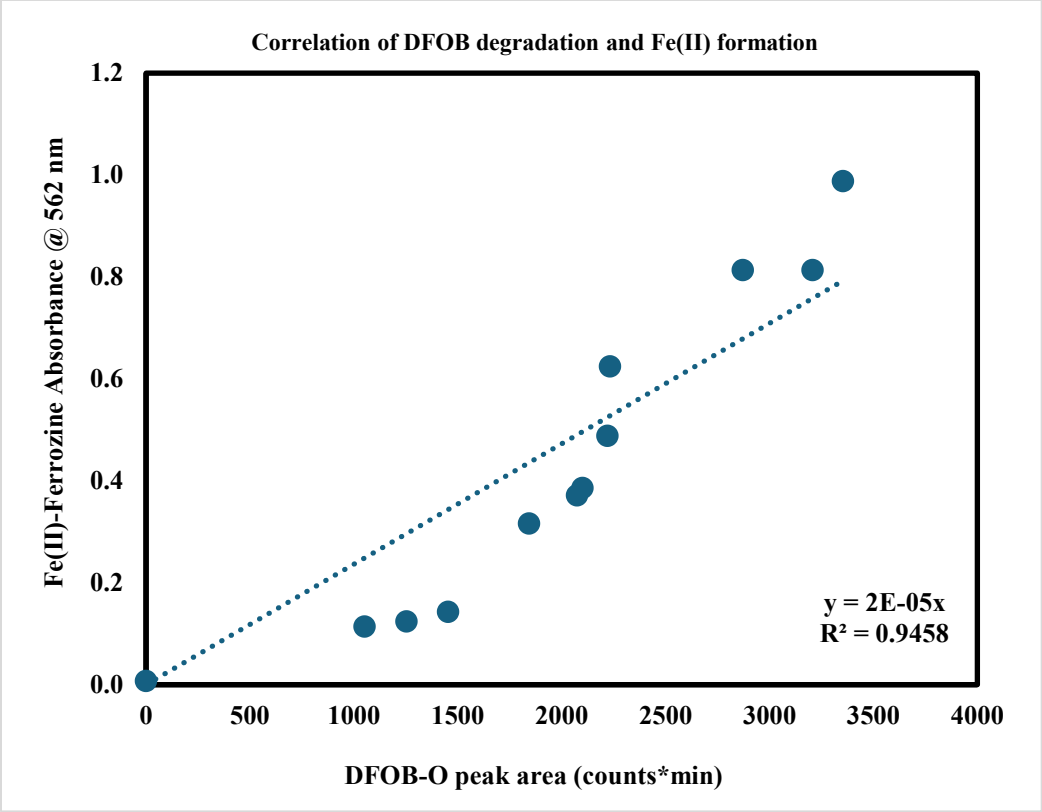

Figure 5. Correlation of DFOB degradation product generated and Fe^{II} formation by diverse fungi (*Saccharomyces cerevisiae* wild type (WT), *S. cerevisiae* mutants impaired in Fe uptake (FRE1, FRE2, ARN1, ARN2, and SIT1), *Sporobolomyces ruberrimus*, *Ustilago nunavutica*, *Vishniacozyma victoriae*, *Aspergillus flavus* 201 (aflatoxin+), *A. flavus* 278 (aflatoxin-), and *Phanerodontia chrysosporium*). LC-MS peak areas for DFOB degradation product (DFOB-O) after 72 h incubation in samples without ferrozine were compared to spectrophotometric values of Fe^{II}-ferrozine complexes formed in samples with ferrozine present.

Table 1. Taxonomic classification, ecology/life history, and source of isolates/strains used in this study.

Isolate	Phylum	Ecology and life history	Source
Aspergillus flavus 201	Ascomycota	Pathogen of cotton, maize, and peanuts, Saprobic, seed and soil associated, no aflatoxin production, and filamentous growth.	I. Carbone[5]
Aspergillus flavus 278	Ascomycota	Pathogen of cotton, maize, and peanuts. Saprobic, seed and soil associated, aflatoxin production, and filamentous growth.	I. Carbone[5]
Phanerodontia chrysosporium BKM-1767	Basidiomycota	Non-pathogenic, saprobic, white rot decay of wood, and filamentous growth.	D. Cullen[6]
Pyrenophora biseptata	Ascomycota	Leaf and root pathogen of wheat and other grasses, a toxin producer, saprobic, and filamentous growth.	O. Barrs[1], P. Fernandez[2], and K. French[3]
Saccharomyces cerevisiae S288C wild type	Ascomycota	Baker's yeast, domesticated, non-pathogenic, and saprobic with functional Arn1, Arn2, and Sit1 non-reductive transporters and Fre1 and Fre2 chelator reductive uptake genes.	C. Heil[1,16, 19, 86]
Saccharomyces cerevisiae Arn1 mutant	Ascomycota	Arn1 family transporter gene deletion replaced with a KanMX cassette, confirmed by resistance to geneticin G418 antibiotic.	C. Heil[1,87,69]
Saccharomyces cerevisiae Arn2 mutant	Ascomycota	Arn2 family transporter gene triacetylfusarinine C deletion.	C. Heil[1,87,68]
Saccharomyces cerevisiae Sit1 mutant	Ascomycota	Sit1- Ferrioxamine B specific transporter gene deletion.	C. Heil[1,87,67,88]
Saccharomyces cerevisiae Fre1 mutant	Ascomycota	Fre1- ferric/cupric-chelate reductase gene deletion.	C. Heil[1,87,89]
Saccharomyces cerevisiae Fre2 mutant	Ascomycota	Fre2 - ferric/cupric-chelate reductase gene deletion.	C. Heil[1,87,90]
Sporobolomyces ruberrimus	Basidiomycota	Non-pathogenic leaf and seed endophyte of plants, unicellular yeast stage, and saprobic.	M.A. Cubeta[1] and L. Becker[4]
Ustilago nunavutica	Basidiomycota	Leaf, flower, and root pathogen of wheat and other grasses, saprobic unicellular yeast, and parasitic filamentous stages (dimorphic).	M.A. Cubeta[1] and L. Becker[4]
Vishniacozyma victoriae	Basidiomycota	Mostly non-pathogenic, saprobic unicellular yeast found in lower temperature environments in soil and on lichens, mosses, and plants, recent association with asthma.	M.A. Cubeta[1] and L. Becker[4]

Table References:

[1] Authors in this study.

[2] Department of Plant and Microbial Biology, North Carolina State University, Raleigh.

[3] Department of Crop, Soil, and Environmental Sciences. University of Arkansas, Fayetteville.

[4] Department of Plant Pathology and Plant-Microbe Biology, Cornell University, Ithaca, NY.

[5] Center for Integrated Fungal Research, North Carolina State University, Raleigh.

[6] US Department of Agriculture Forest Products Laboratory, Madison, WI.

Chapter 5
Summary and Conclusions

5.1 Summary of Major Findings

This dissertation elucidated the fate of siderophores with regard to their degradation, either by extracellular enzyme activities or reductive Fe uptake systems, as well as structural changes influenced by these reactions that facilitate or hinder Fe transport and competition in circumneutral pH. To achieve this, complementary analytical techniques were leveraged, including wet chemistry, reaction kinetics, liquid chromatography coupled with mass spectrometry (LC-MS), high resolution-MS, and spectroscopy analyses (e.g., molecular/atomic scale analyses, UV-visible spectrophotometry, nuclear magnetic resonance (NMR)). Combining these analytical techniques revealed that siderophore degradation by oxidative extracellular enzymes depended on structure, binding state, and pH. In addition, the reactivity of free apo-siderophores is substantially greater than that of their Fe-bound complexes. Further investigation indicated that H_2O_2 promotes degradation even without catalysis by peroxidase, highlighting a crucial role of H_2O_2 in the degradation of the catechol-type siderophores. Reaction kinetics for the protochelin degradation reactions were rapid and suggested the potential for catechol siderophore degradation via extracellular enzymes in microbiomes, even though the presence of other compounds, such as phenolics, could potentially interfere with the degradation process. The extracellular enzyme activities highlighted their role in influencing competition for Fe by microbiomes through degradation of catecholate siderophores released by plants or microbes in response to Fe deficiency.

The second discovery is that *P. biseptata*, a melanized fungus from wheat roots, effectively degrades DFOB by substantially inactivating siderophore Fe-chelating moieties under Fe-limiting conditions at acidic to circumneutral pH. Interestingly, LC-MS, Tandem MS/MS, and spectroscopy analysis show similar loss of hydroxamate chelating groups forming from their own tris-hydroxamate siderophores (Neocoprogen I and II, Coprogen, Dimerum acid). These results suggest that the reason for the trishydroxamate siderophores' degradation is likely the formation of transient ferrous iron, followed by reduction of the siderophore hydroxamate groups during fungal high-affinity reductive Fe uptake in the supernatant solution. The results also suggest that the new siderophore inactivating activity of the wheat symbiont *P. biseptata* has implications for the availability of Fe to plants and the surrounding microbiome in siderophore-rich environments.

The third finding is that the mechanism of trishydroxamate siderophore degradation by *P. biseptata* has a direct relationship with the reductive Fe uptake system and is widespread among

fungi. The rationale can be attributed to the reduction of Fe^{III} to Fe^{II} by *P. biseptata,* probably as part of its uptake mechanism, and that degrades DFOB and other siderophores. Ferrozine was utilized as a trapping agent to inhibit Fe^{II} reoxidation by forming stable complexes when introduced into the reaction solution, thereby quenching the reduction of the DFOB hydroxamate groups to an amide and confirming our hypothesis. Taken together, the fate of siderophores in Fe transport and cycling reveals that incorporation of oxidative enzymes and other intrinsic systems within the organisms for Fe nutrition.

5.2 Environmental Implications

The findings of this dissertation have important implications for understanding plant-microbe interactions, Fe cycling, and broader nutrient dynamics in the environment. Siderophores are chemically and structurally diverse, and as such, can enhance or alter their reactivity depending on environmental conditions [1, 2]. Due to their high affinity for Fe, inner-sphere complexation mechanisms, and resistance to structural changes, siderophores are employed by both plants and microbes, making them likely to influence Fe availability, virulence, and competition in the rhizosphere over extended periods, particularly under Fe-limited, circumneutral pH conditions.

The results reveal that extracellular oxidative enzymes play a significant role in the degradation of siderophores, with degradation rates varying between 2% and 90%. This enzymatic breakdown likely constrains the influence of Fe-siderophore complexes, reducing their persistence in the environment and either limiting or facilitating access to these complexes by non-enzyme producing organisms. It is well recognized that both plants and microbes are prolific producers of extracellular enzymes [3, 4], and they also exude siderophores [5-7] for nutrition and to enhance competitive advantage. Hence, this degradation pathway may release metabolic intermediates that can serve as alternative carbon and nitrogen sources [8-11], thereby linking the turnover of siderophores to broader microbial nutrient cycling processes.

Moreover, the results also show that the reductive Fe system involving Fe^{III} reduction [12, 13], followed by Fe^{II} reoxidation [14, 15], contributes to the degradation of hydroxamate siderophores such as DFOB, particularly by fungi. Previous research indicated that the siderophore degradation process can enhance Fe availability for plants, as demonstrated by the accessibility of mono- and bis-hydroxamates that facilitate plant uptake through ligand exchange or reductive Fe uptake [16, 17]. These reductive processes likely operate alongside enzymatic degradation, further influencing

siderophore fate and Fe dynamics in soil. Additionally, this research data show variable DFOB decomposition across microbial taxa, yet measurable reduced Fe (Fe^{II}) (> 50%) was consistently observed, supporting the ubiquity of the reductive Fe uptake mechanism phenomenon among fungi, as well as the idea that siderophores can function as natural Fe fertilizers, as seen in recent work [18-20].

Although no research has investigated the intricate relationship between siderophore degradation and the reductive Fe uptake mechanism, altogether, these findings underscore the dynamic role of siderophores in mediating biogeochemical processes. Their production, degradation, and interaction with enzymatic and redox systems are key to microbial competition, nutrient availability, and plant health.

5.3 Suggestions for Future Work

This dissertation advances our understanding of the fate, structure, and reactivity of siderophores at circumneutral pH. However, several avenues remain open for further exploration to broaden the scope and depth of some research questions.

5.3.1 Role of competitive phenolic substrates.

All enzyme-siderophore experiments presented here were conducted in the absence of competing substrates, even though other phenolic compounds are commonly present in natural environments. Phenolics can significantly influence siderophore reactivity by interfering with, inhibiting, or outcompeting enzymatic degradation mechanisms [21-23]. Therefore, future research should incorporate a diverse set of phenolic substrates to examine their impact on enzyme-siderophore interactions. Real-time kinetic studies should also be employed to assess differences in substrate specificity, inhibitory mechanisms, and competitive binding under a broader pH range (4.5–9). This would enhance our understanding of how natural substrate complexity affects siderophore degradation and function.

5.3.2 Fe^{II} dynamics and mechanistic insights.

Additionally, our incubation studies showed that Fe^{II} concentrations increased over time, indicating active Fe reductive processes. Fungi are known to acquire Fe through multiple pathways, including non-reductive systems [24, 25], reductive mechanisms involving Fe^{II} formation

[26], and ferroxidation by multicopper ferroxidases [27] such as Fet3 in *S. cerevisiae* [28]. To determine the Fe^{II} formation over time, ferrozine-based spectrophotometric assays were used to monitor Fe^{II}-ferrozine complex formation. These results suggested that Fe^{II} reoxidation plays a crucial role in the siderophore degradation, as it reduces the hydroxamate groups to amides, thereby diminishing their chelation potential.

Nevertheless, to refine our understanding of Fe redox dynamics in siderophore degradation, future studies should consider incorporating radioisotope-labeled Fe (^{55}Fe and ^{59}Fe), as previously employed in studies involving the determination of Fe reduction and transport from siderophores in plants [29-35] and microbes [36, 37]. Coupling radioisotope tracking with ferrozine assays, UV-vis spectroscopy, and Fourier Transform Ion Cyclotron Resonance Mass Spectrometry (FT-ICR MS) could provide enhanced resolution of the localization and behavior of Fe^{III} and Fe^{II} species in real time.

5.3.3 Genetic modulation of Fe uptake pathways.

LC-MS and UV-vis analyses of DFOB degradation over three days in *S. cerevisiae* mutants (Arn1, Arn2, Sit1, Fre1, Fre2) samples revealed only limited DFOB transformation. Notably, mutants lacking Arn1 and Arn2 gene components of the non-reductive Fe uptake pathway exhibited slightly higher reactivity. These findings imply that more genetic modifications may enhance DFOB degradation efficiency.

To test this, future work should involve the use of multiple-gene deletion mutants to assess the relative contributions of non-reductive versus reductive Fe uptake systems. For instance, deleting all non-reductive genes (e.g., Arn1, Arn2, Arn3) in a single mutant, like in prior study [26] could clarify the role of reductive mechanisms in DFOB degradation, and vice versa. Such studies would not only elucidate the genetic basis of siderophore reactivity but could also inform the refinement of siderophore cycling models and their application in complex environments such as soils and rhizospheres. By pursuing these lines of inquiry, future research can build on the foundations laid here to deepen our understanding of siderophore-mediated Fe cycling, with important implications for microbial ecology, biogeochemistry, and sustainable agriculture.

5.4 Final Thoughts

The results presented in this dissertation advance the current understanding of siderophore structure and reactivity, thereby enhancing knowledge of Fe transport and uptake in circumneutral pH environments. Moreover, it demonstrates the effectiveness of integrating molecular-scale analyses with high-throughput analytical techniques to address complex challenges in natural systems.

REFERENCES

1. J. C. Renshaw, G. D. Robson, A. P. Trinci, M. G. Wiebe, F. R. Livens, D. Collison and R. J. Taylor, 'Fungal siderophores: structures, functions and applications', *Mycological Research*, 106 (2002): 1123-1142.

2. R. C. Hider and X. Kong, 'Chemistry and biology of siderophores', *Natural product reports*, 27 (2010): 637-657.

3. R. Haapala and S. Linko, 'Production of Phanerochaete chrysosporium lignin peroxidase under various culture conditions', *Applied microbiology and biotechnology*, 40 (1993): 494-498.

4. A. Ray, S. Saykhedkar, P. Ayoubi-Canaan, S. D. Hartson, R. Prade and A. J. Mort, 'Phanerochaete chrysosporium produces a diverse array of extracellular enzymes when grown on sorghum', *Applied Microbiology and Biotechnology*, 93 (2012): 2075-2089.

5. M. Saha, S. Sarkar, B. Sarkar, B. K. Sharma, S. Bhattacharjee and P. Tribedi, 'Microbial siderophores and their potential applications: a review', *Environmental Science and Pollution Research*, 23 (2016): 3984-3999.

6. B. Xie, X. Wei, C. Wan, W. Zhao, R. Song, S. Xin and K. Song, 'Exploring the biological pathways of siderophores and their multidisciplinary applications: A comprehensive review', *Molecules*, 29 (2024): 2318.

7. A. Kamath, A. Sharma, A. Shukla, P. Parmar and D. Patel, 'Fortifying plant fortresses: siderophores in defense against Cercospora leaf spot disease in Vigna radiata L', *Frontiers in Microbiology*, 15 (2025): 1492139.

8. R. Warren and J. Neilands, 'Microbial degradation of the ferrichrome compounds', *Microbiology*, 35 (1964): 459-470.

9. R. Warren and J. Neilands, 'Mechanism of microbial catabolism of ferrichrome A', *Journal of Biological Chemistry*, 240 (1965): 2055-2058.

10. G. Winkelmann, B. Busch, A. Hartmann, G. Kirchhof, R. Süßmuth and G. Jung, 'Degradation of desferrioxamines by Azospirillum irakense: Assignment of metabolites by HPLC/electrospray mass spectrometry', *Biometals*, 12 (1999): 255-264.

11. A. Pierwola, T. Krupinski, P. Zalupski, M. Chiarelli and D. Castignetti, 'Degradation pathway and generation of monohydroxamic acids from the trihydroxamate siderophore deferrioxamine B', *Applied and Environmental Microbiology*, 70 (2004): 831-836.

12. D. J. Kosman, 'Iron metabolism in aerobes: managing ferric iron hydrolysis and ferrous iron autoxidation', *Coordination chemistry reviews*, 257 (2013): 210-217.

13. N. G. De Luca and P. M. Wood, 'Iron uptake by fungi: contrasted mechanisms with internal or external reduction', (2000).

14. X. Shi, C. Stoj, A. Romeo, D. J. Kosman and Z. Zhu, 'Fre1p Cu2+ reduction and Fet3p Cu1+ oxidation modulate copper toxicity in Saccharomyces cerevisiae', *Journal of Biological Chemistry*, 278 (2003): 50309-50315.

15. D. J. Kosman, 'Molecular mechanisms of iron uptake in fungi', *Molecular microbiology*, 47 (2003): 1185-1197.

16. W. Hördt, V. Römheld and G. Winkelmann, 'Fusarinines and dimerum acid, mono-and dihydroxamate siderophores from Penicillium chrysogenum, improve iron utilization by strategy I and strategy II plants', *Biometals*, 13 (2000): 37-46.

17. G. Winkelmann, 'Ecology of siderophores with special reference to the fungi', *Biometals*, 20 (2007): 379-392.

18. Z. Kaya, A. Maqbool, M. Suzuki and E. Aksoy, 'Proline-2'-deoxymugineic acid (PDMA) increases seed quality and yield by alleviating iron deficiency symptoms in soybean under calcareous-alkaline conditions', *bioRxiv*, (2024): 2024.10. 02.616232.

19. C. Rocco, M. Suzuki, R. Vilar, E. Garcia-España, S. Blasco, G. Larrouy-Maumus, C. Turnbull, M. Wissuwa, X. Cao and D. Weiss, 'Enhancing Zinc Bioavailability in Rice Using the Novel Synthetic Siderophore Ligand Proline-2′-Deoxymugineic Acid (PDMA): Critical Insights from Metal Binding Studies and Geochemical Speciation Modeling', *Journal of Agricultural and Food Chemistry*, (2025).

20. D. Ueno, Y. Ito, M. Ohnishi, C. Miyake, T. Sohtome and M. Suzuki, 'A synthetic phytosiderophore analog, proline-2′-deoxymugineic acid, is efficiently utilized by dicots', *Plant and Soil*, 469 (2021): 123-134.

21. G. Grass, K. Thakali, P. E. Klebba, D. Thieme, A. Müller, G. n. F. Wildner and C. Rensing, 'Linkage between catecholate siderophores and the multicopper oxidase CueO in Escherichia coli', *Journal of bacteriology*, 186 (2004): 5826-5833.

22. S. Shalaby and B. A. Horwitz, 'Plant phenolic compounds and oxidative stress: integrated signals in fungal–plant interactions', *Current genetics*, 61 (2015): 347-357.

23. M. J. Zwetsloot, J. M. Ucros, K. Wickings, R. C. Wilhelm, J. Sparks, D. H. Buckley and T. L. Bauerle, 'Prevalent root-derived phenolics drive shifts in microbial community composition and prime decomposition in forest soil', *Soil Biology and Biochemistry*, 145 (2020): 107797.

24. E. Lesuisse, P.-L. Blaiseau, A. Dancis and J.-M. Camadro, 'Siderophore uptake and use by the yeast Saccharomyces cerevisiae', *Microbiology*, 147 (2001): 289-298.

25. E. Lesuisse, M. Simon-Casteras and P. Labbe, 'Siderophore-mediated iron uptake in Saccharomyces cerevisiae: the SIT1 gene encodes a ferrioxamine B permease that belongs to the major facilitator superfamily', *Microbiology*, 144 (1998): 3455-3462.

26. C. W. Yun, M. Bauler, R. E. Moore, P. E. Klebba and C. C. Philpott, 'The role of the FRE family of plasma membrane reductases in the uptake of siderophore-iron in Saccharomyces cerevisiae', *Journal of Biological Chemistry*, 276 (2001): 10218-10223.

27. K. Takemura, V. Kolasinski, M. Del Poeta, N. F. Vieira de Sa, A. Garg, I. Ojima, M. Del Poeta and N. Pereira de Sa, 'Iron acquisition strategies in pathogenic fungi', *mBio*, (2025): e01211-25.

28. C. W. Yun, T. Ferea, J. Rashford, O. Ardon, P. O. Brown, D. Botstein, J. Kaplan and C. C. Philpott, 'Desferrioxamine-mediated iron uptake in Saccharomyces cerevisiae: evidence for two pathways of iron uptake', *Journal of Biological Chemistry*, 275 (2000): 10709-10715.

29. C. Reid, D. Crowley, H. Kim, P. Powell and P. Szaniszlo, 'Utilization of iron by oat when supplied as ferrated synthetic chelate or as ferrated hydroxamate siderophore', *Journal of Plant Nutrition*, 7 (1984): 437-447.

30. Y. Mino, T. Ishida, N. Ota, M. Inoue, K. Nomoto, T. Takemoto, H. Tanaka and Y. Sugiura, 'Mugineic acid-iron (III) complex and its structurally analogous cobalt (III) complex: characterization and implication for absorption and transport of iron in gramineous plants', *Journal of the American Chemical Society*, 105 (1983): 4671-4676.

31. F. Awad, V. Römheld and H. Marschner, 'Mobilization of ferric iron from a calcareous soil by plant-borne chelators (Phytosiderophores)', *Journal of plant nutrition*, 11 (1988): 701-713.

32. D. E. Crowley, V. Römheld, H. Marschner and P. J. Szaniszlo, 'Root-microbial effects on plant iron uptake from siderophores and phytosiderophores', *Plant and Soil*, 142 (1992): 1-7.

33. B. Duijff, W. De Kogel, P. Bakker and B. Schippers, 'Influence of pseudobactin 358 on the iron nutrition of barley', *Soil Biology and Biochemistry*, 26 (1994): 1681-1688.

34. G. V. Johnson, A. Lopez and N. La Valle Foster, 'Reduction and transport of Fe from siderophores', *Plant and Soil*, 241 (2002): 27-33.

35. S. Cesco, A. D. Rombolà, M. Tagliavini, Z. Varanini and R. Pinton, 'Phytosiderophores released by graminaceous species promote 59 Fe-uptake in citrus', *Plant and Soil*, 287 (2006): 223-233.

36. L. J. Liermann, B. E. Kalinowski, S. L. Brantley and J. G. Ferry, 'Role of bacterial siderophores in dissolution of hornblende', *Geochimica et Cosmochimica Acta*, 64 (2000): 587-602.

37. R. M. Boiteau, S. J. Fansler, Y. Farris, J. B. Shaw, D. W. Koppenaal, L. Pasa-Tolic and J. K. Jansson, 'Siderophore profiling of co-habitating soil bacteria by ultra-high resolution mass spectrometry', *Metallomics*, 11 (2019): 166-175.

APPENDICES

Appendix A
(Supplementary Information for Chapter 2)

Supplementary Methods

Enzyme activity assays.

(a) Phenol oxidase. Three milliliters of the reaction mixture to determine the phenol oxidase activity consisted of 1 mL 50 mM potassium phosphate buffer (pH 7.0), 1 mL 0.001 M L-tyrosine, and 900 µL of ultra-pure water. The enzyme assay sample reaction in a 15 mL centrifuge tube was left to stand for 4-5 minutes to be oxygenated before adding 100 µL of 200-400 units/mL of phenol oxidase enzyme. The absorbance at 280 nm was monitored for 10 minutes using a Thermo-scientific Evolution 201 UV-Vis spectrophotometer (Waltham, MA, USA). Enzyme activity was calculated based on the rate of absorbance increase, proportional to enzyme concentration, and linear during 5-10 minutes after an initial lag. One unit causes a change in absorbance at 280 nm of 0.001 per minute at 25°C, pH 6.5-7.4, under the specified conditions.

(b) Peroxidase. Three milliliters of the reaction mixture to determine the peroxidase activity consisted of 320 µL 100 mM potassium phosphate buffer, pH 7.01, 160 µL 0.50% hydrogen peroxide, 320 µL 0.1 M pyrogallol, 2.1 mL of ultra-pure water, and 100 µL peroxidase enzyme solution. The blank sample consisted of 320 µL 100 mM potassium phosphate buffer, pH 7.01, 160 µL 0.50% hydrogen peroxide, 320 µL 0.1 M pyrogallol, and 2.2 mL ultrapure water only. In the 3.00 mL reaction mix, the final concentrations are 14 mM phosphate buffer (pH 7.01), 0.16 M 0.027% (v/v) hydrogen peroxide, 0.1 M 0.5% (w/v) pyrogallol, and 0.45–0.75-unit peroxidase enzyme. The absorbance at 420 nm was monitored for 3 minutes using a UV-Vis spectrophotometer, as described above. The enzymatic activity was calculated by considering the linear part of the curve (optical density vs. time). One unit of enzyme activity was defined as the amount of enzyme that produces an absorbance increase of 0.001/minute/mL at 25ºC. This unit is equivalent to ~18 µM units per minute at 25 °C. The enzymatic activity was calculated as the mean of three experiments for all tested conditions.

(c) Protease. The protease activity was determined by a method previously used by Mayerhofer et al. (1973). The final concentration for the assay mixture: 1 mL 8.6 mM borate solution, 1 mL (5.1 mg/mL) (0.6 %) casein solution, 500 µL 0.29 mM calcium acetate solution, and 500 µL 30 Units/mL protease enzyme solution. The reaction mixture was filtered after 10 minutes, and the optical density of the filtrate at 275 nm (OD test) was measured using UV-Vis spectrophotometry,

as described above. The protease activity was calculated in activity units (U). One activity unit was defined as the amount of enzyme that is required to hydrolyze casein to give 1 μM of tyrosine in 1 min at pH 7.0 and a temperature of 25 ℃. One unit causes an increase of optical density at 275 nm corresponding to one micromole of tyrosine per minute.

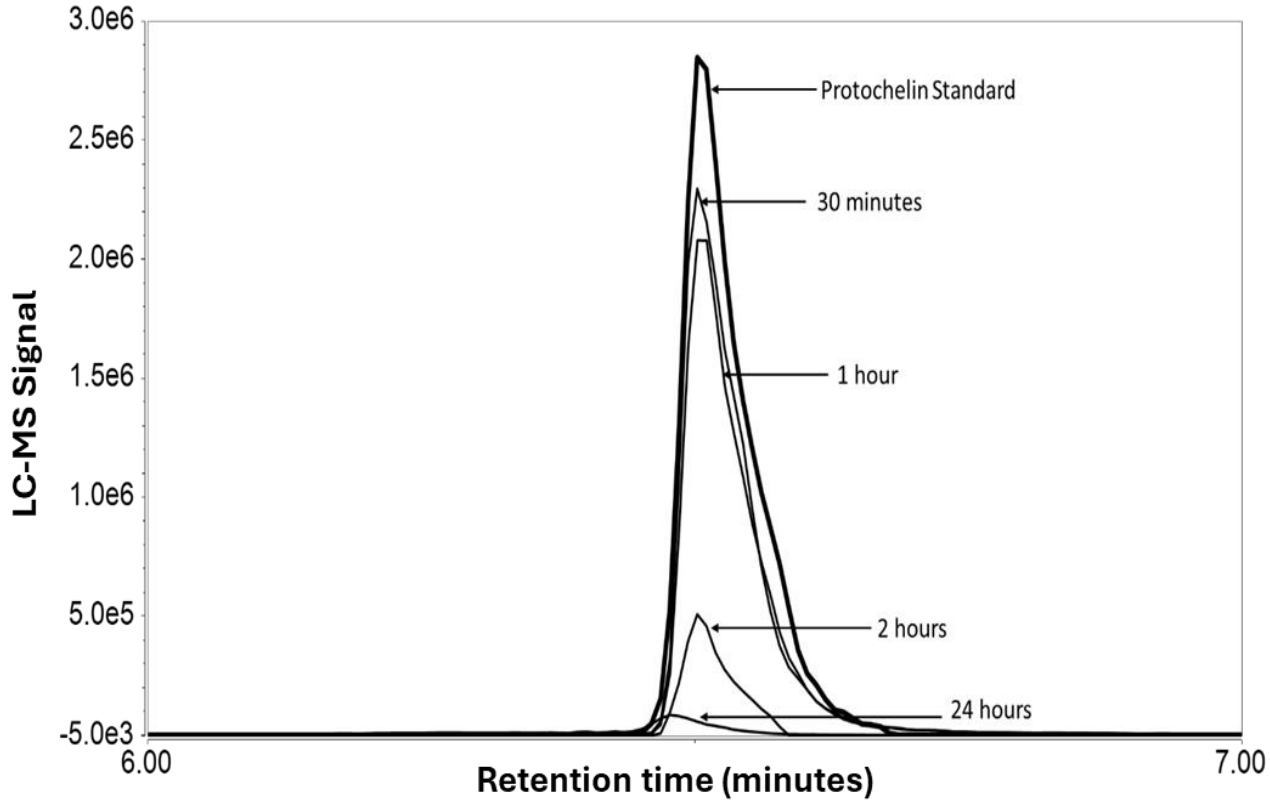

Figure S1. Reduction of protochelin parent peak after reaction with phenol oxidase for 30 minutes, 1,2, and 24 hours from LC-MS analysis.

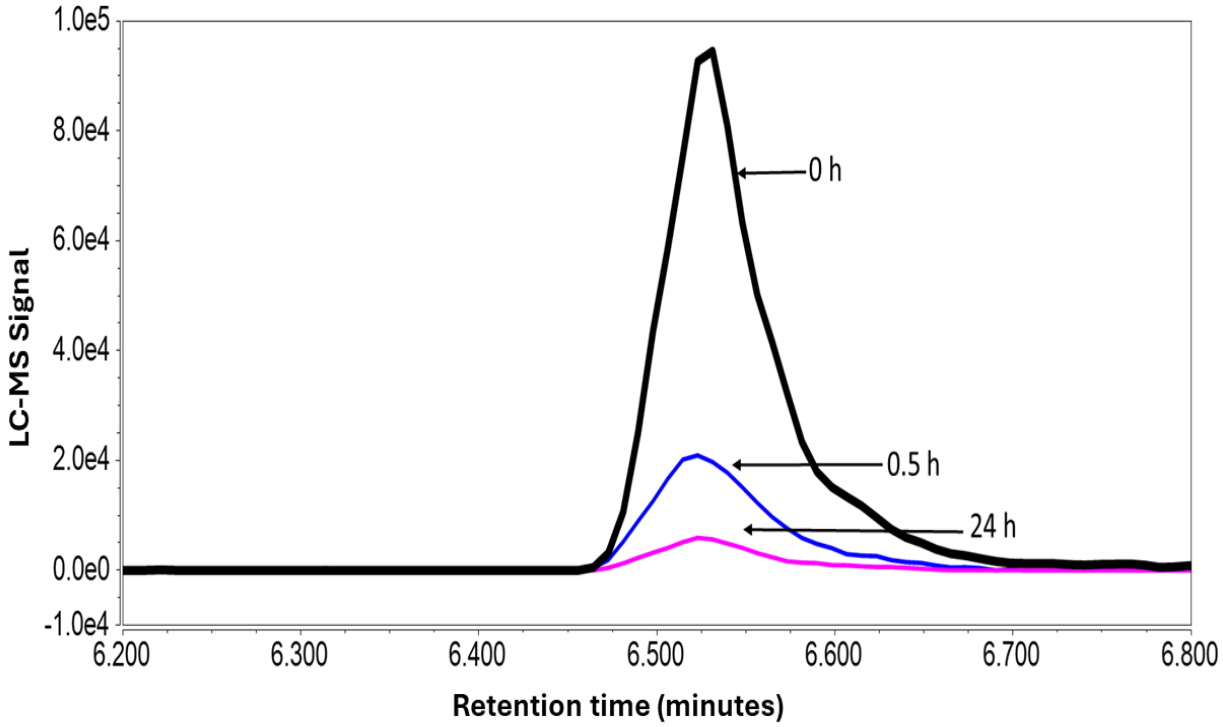

Figure S2. Reduction of protochelin parent peak after reaction with peroxidase immediately after starting the reaction (0 h), 30 minutes (0.5 h), and 24 hours from LC-MS analysis.

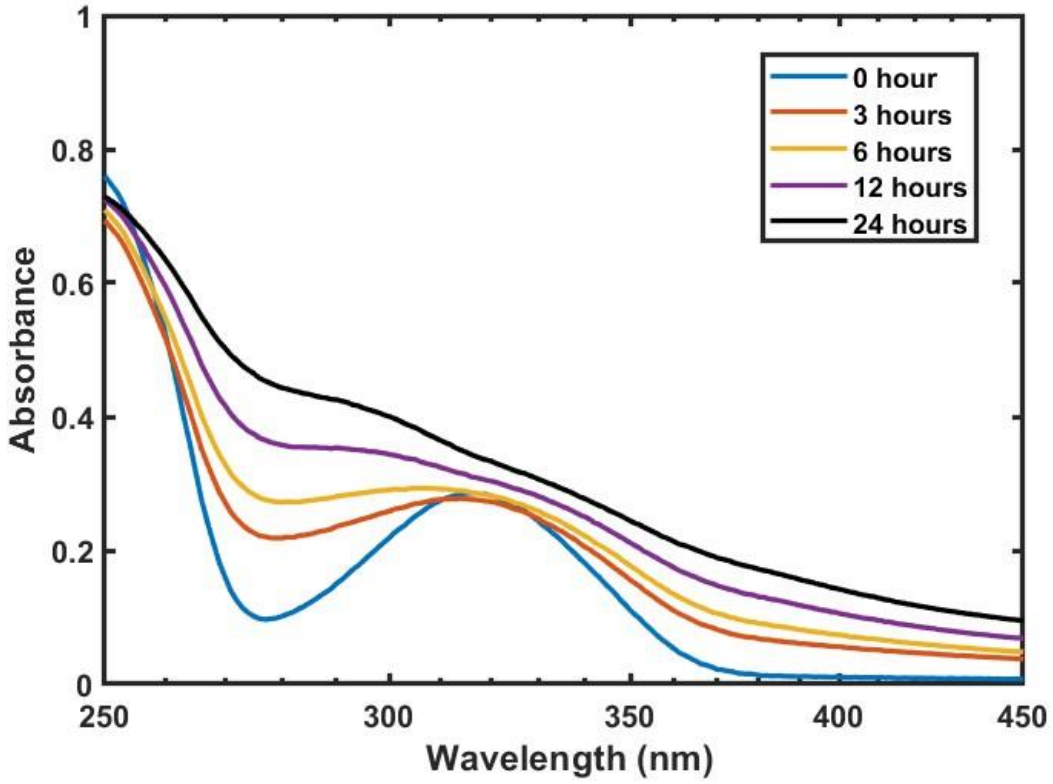

Figure S3. Plot of the change in absorbance spectrum of protochelin in solution over a 24 h period as ligand degradation occurs after reaction with **phenol oxidase enzyme**. Conditions: pH = 7.0, c = 100 μM protochelin siderophore, T = 25˚C.

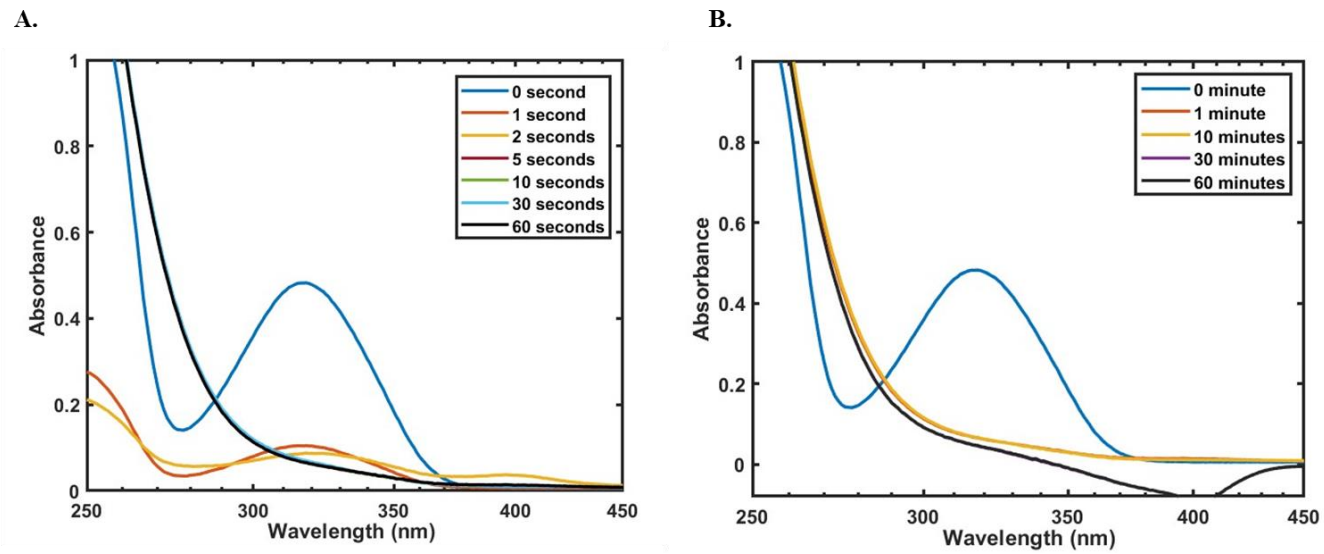

Figure S4. Spectrophotometric changes in the absorbance of protochelin in the solution over (A) 60 seconds and (B) 60 minutes, as ligand degradation occurs after reaction with **peroxidase enzyme** and **H_2O_2** as a cosubstrate. Conditions: pH = 6.79, c = 100 μM protochelin siderophore, T = 25˚C.

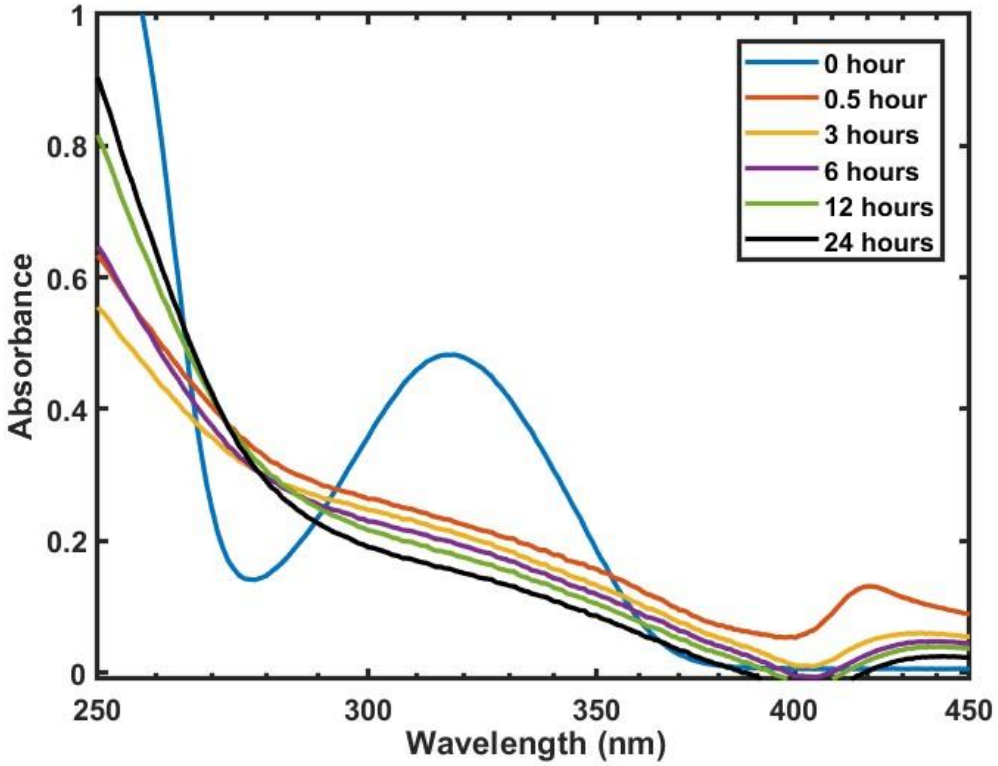

Figure S5. Plot of the change in absorbance spectrum of protochelin in solution over a 24 h period as ligand degradation occurs after reaction with **peroxidase enzyme** and **H_2O_2** as a cosubstrate. Conditions: pH = 6.88, c = 100 μM protochelin siderophore, T = 25˚C.

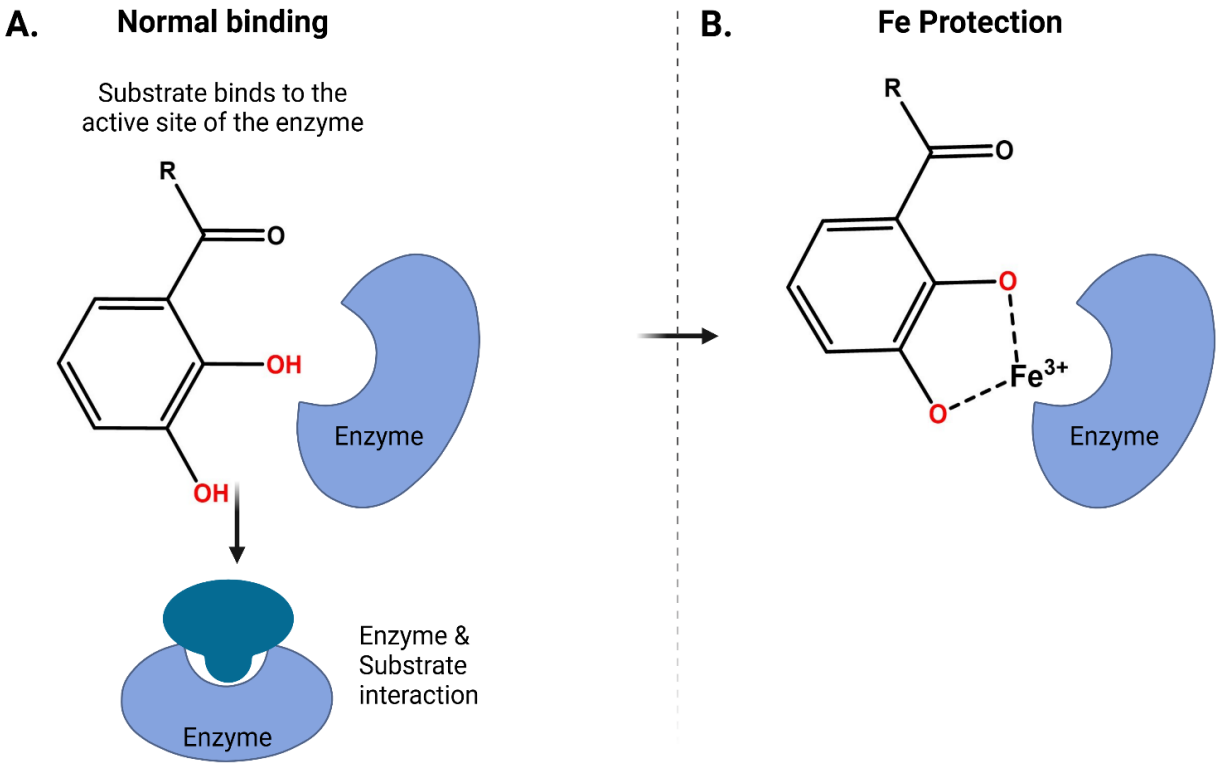

Figure S6. Schematic showing (A) phenol oxidase–Protochelin interaction without Fe, indicating easier binding to enzyme active sites, whereas (B) Fe inhibits direct interaction of phenol oxidase and chelating groups of Protochelin-Fe chelate.

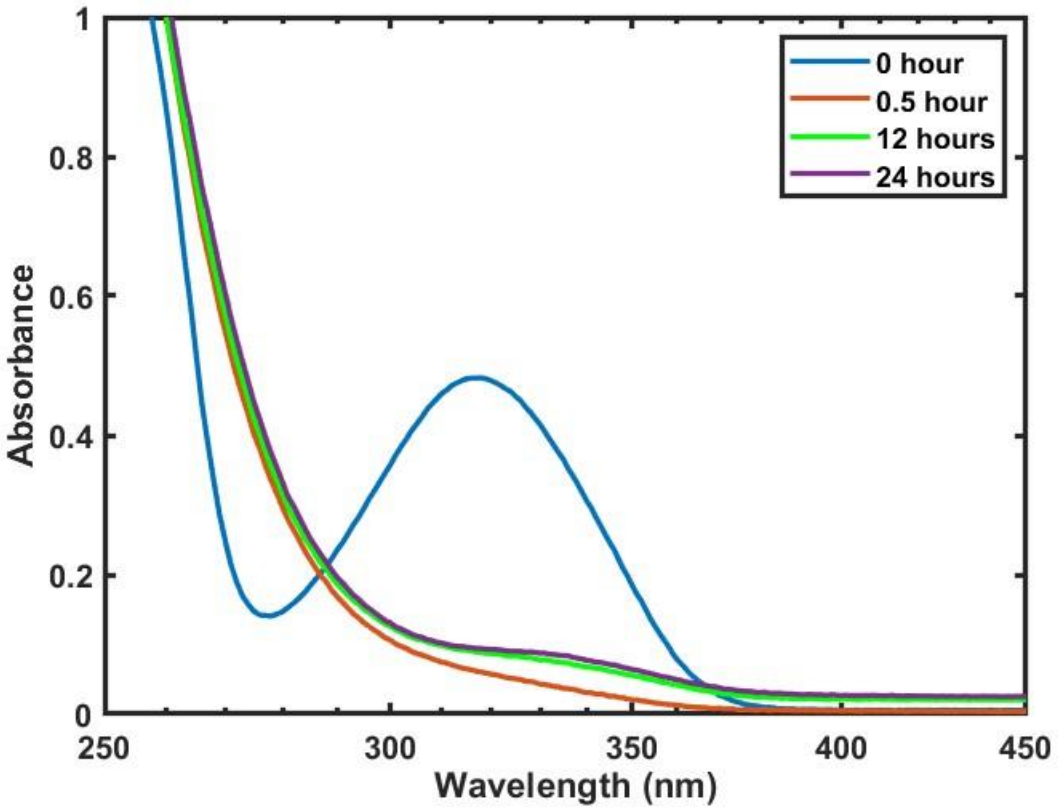

Figure S7. The plot of the change in absorbance spectrum of protochelin in solution over a 24 h period as ligand degradation occurs after reaction with only $\mathbf{H_2O_2}$. Conditions: pH = 7.12, c = 100 μM protochelin siderophore, T = 25˚C.

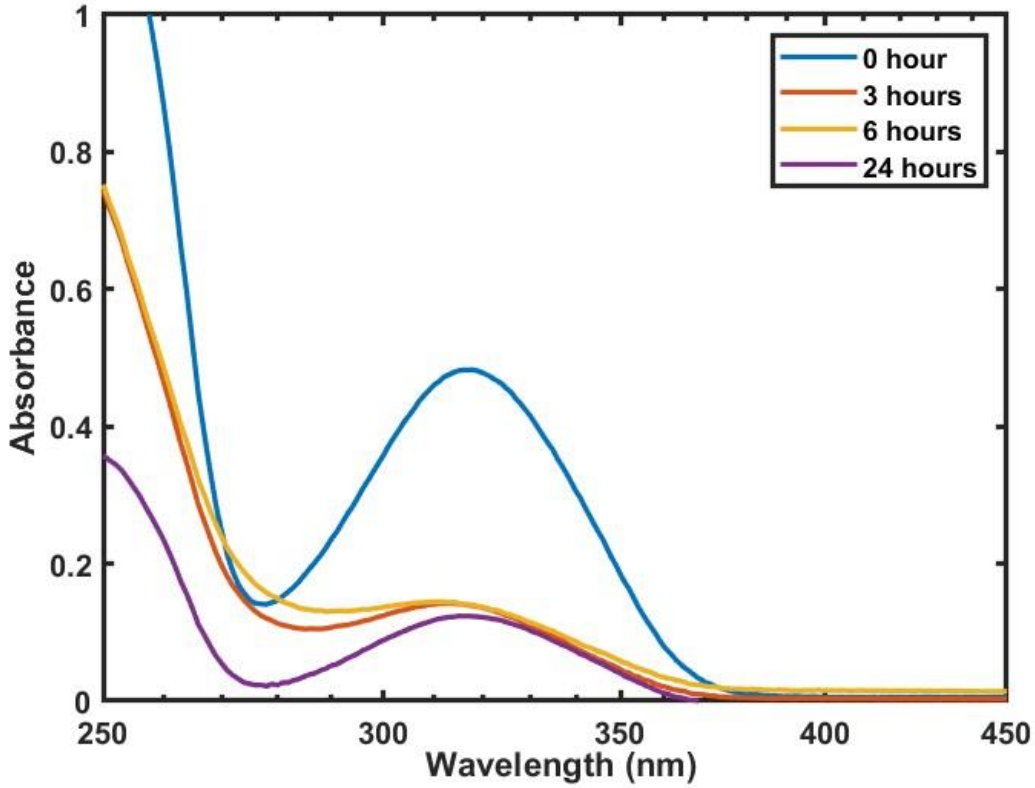

Figure S8. Spectrophotometric changes in the absorbance of protochelin in the solution over a 24 h period, as slow ligand degradation occurred after reaction with just the **peroxidase enzyme**. Conditions: pH = 6.82, c = 100 μM protochelin siderophore, T = 25˚C.

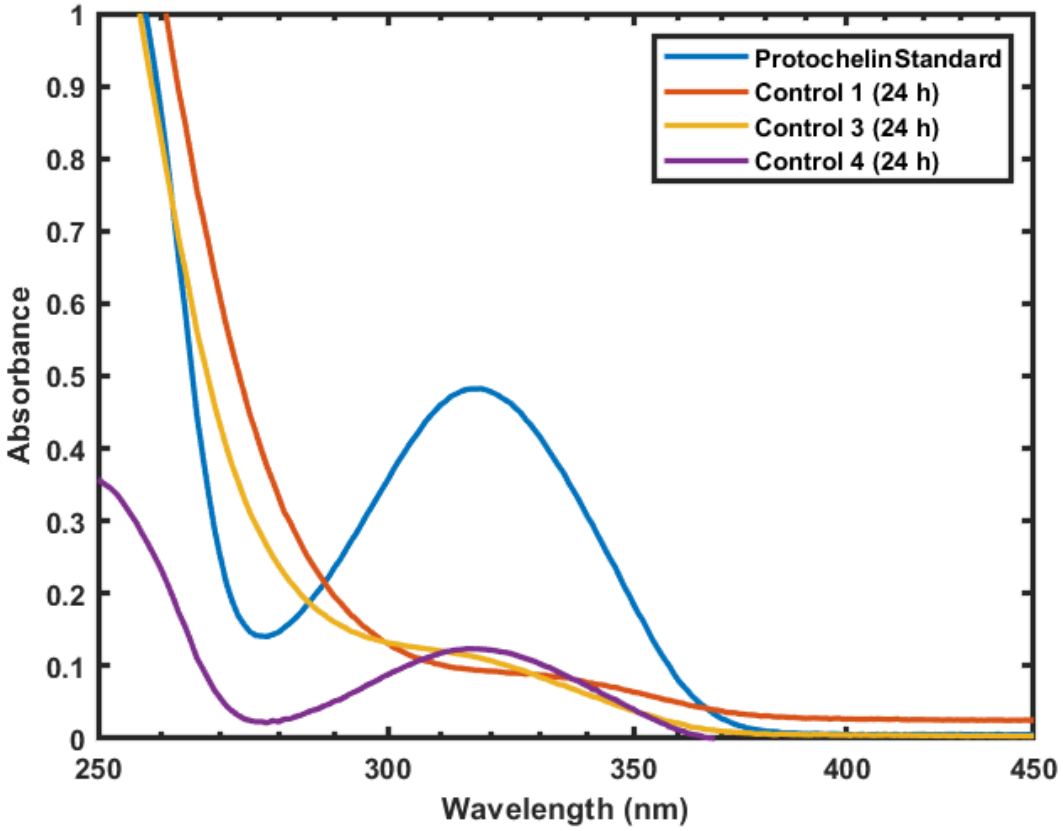

Figure S9. Spectrophotometric changes in the absorbance of protochelin in the solution over a 24 h period, as rapid ligand degradation occurred after reaction with just the **H_2O_2 (Control 1),** with **heat-inactive peroxidase enzyme** and **H_2O_2 (Control 3),** whereas a slower absorbance reduction was observed with only **peroxidase enzyme (Control 4)**. Conditions: pH = 6.81, c = 100 µM protochelin siderophore, T = 25˚C.

Table S1. Siderophore standards, ionization mode, and *m/z* values used in LC-MS analysis with Single-Ion-Monitoring (see methods).

Siderophore	**Ionization**	**Exact mass (M)**	***m/z* (MH^+)**	***m/z* ($M-H)^-$**	***z***
DFOB	Positive	560.3534	561.4		1
DFOB – O	Positive	544.3585	545.4		1
DFOB – 2O	Positive	528.3635	529.4		1
FeDFOB	Positive	613.2648	614.3		1
PDMA	Positive	318.1427	319.1		1
FePDMA	Positive	371.0542	372.1		1
Protochelin	Negative	624.2431		623.2	1
Protochelin – 2H	Negative	622.2256		621.2	1
Protochelin – 4H	Negative	620.2191		619.2	1
FeProtochelin	Negative	677.1546		676.2	1

Table S2. MS/MS fragmentation of protochelin and protochelin reaction products referenced in Figure 3.

Protochelin	
Precursor *m/z*	625.2504
Fragment *m/z*	Intensity (%)
489.2341	1.3
353.2181	7.1
265.1185	3.7
237.2022	0.8
225.1232	53.5
208.0966	31.1
137.0231	9.3
84.0807	100.0

Protochelin-2H	
Precursor *m/z*	623.2348
Fragment *m/z*	Intensity (%)
623.2348	3.1
605.2230	2.4
469.2078	37.4
442.1973	57.9
354.0965	28.5
341.1137	25.9
217.2021	17.5
129.1023	11.3
89.1072	44.7
84.0807	100.0
72.0807	63.6

Protochelin-4H	
Precursor *m/z*	621.2191
Fragment *m/z*	Intensity (%)
621.2191	23.4
533.1181	2.3
487.2117	12.1
468.1761	7.2
485.2029	100.0
440.1808	48.1
371.1128	8.3
369.1069	47.7
343.3286	25.3
260.0550	17.1
155.1542	13.2
89.1072	18.6
84.0807	93.2
72.0807	76.4

Protochelin-6H	
Precursor *m/z*	619.2035
Fragment *m/z*	Intensity (%)
619.2035	4.8
591.2079	37.3
502.1228	4.6
440.1794	31.4
439.1732	100.0
438.1652	32.1
373.1264	45.4
372.1186	23.2
218.0809	18.3
137.1197	7.6
89.1072	41.3
84.0807	62.1
72.0807	38.4

Table S3. Protochelin degradation at different time points of the 24-hour reaction with phenol oxidase. Characteristic MS/MS fragments are shown in Table S2.

m/z	***Sampling time point (h)***	**RT (min)**	**Peak Area**	**Sum formula**
625.2504	0	4.9	1.10E+10	$C_{31}H_{36}N_4O_{10}$
	0.5	4.9	8.40E+09	
	2	4.9	7.50E+09	
	24	4.9	6.20E+08	
623.2348	0	4.4	7.00E+07	$C_{31}H_{34}N_4O_{10}$
	0.5	4.4	6.90E+08	
	2	4.4	1.10E+09	
	24	4.4	3.10E+08	
621.2191	0	4.3	1.60E+07	$C_{31}H_{32}N_4O_{10}$
	0.5	4.4	1.30E+08	
	2	4.3	4.10E+08	
	24	4.3	1.10E+09	

Appendix B
(Supplementary Information for Chapter 3)

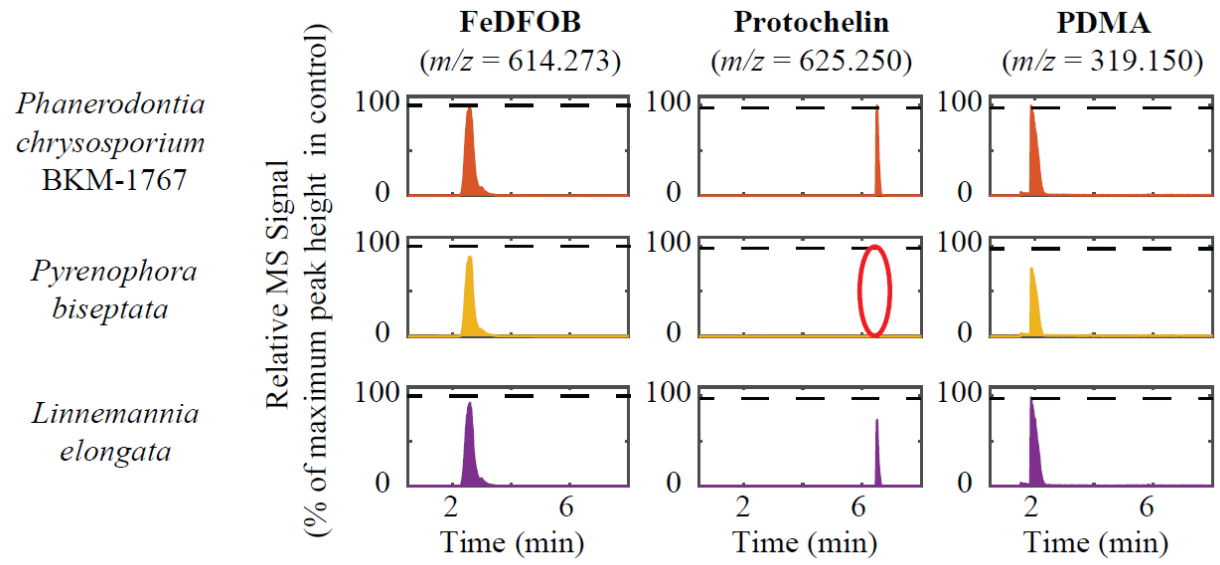

Figure S1. LC-MS peaks showing dissolved siderophores after incubation in iron-replete MSB medium for mycelium of each of the four fungi after 2 d in comparison to initial peak heights (dashed line). To create Fe-replete conditions, 300µM of $FeCl_3$ was added during fungal incubation. This concentration exceeded the combined concentration of Fe chelators ([EDTA] = 100 µM and each of the three siderophores added at 6.7 µM). Shown is the FeDFOB peak because in iron-replete conditions, DFOB was fully bound to iron, and free unbound DFOB was negligible. Protochelin and PDMA were measured as the free siderophore under the LC-MS conditions, which included an acidic mobile phase buffer (0.1% formic acid).

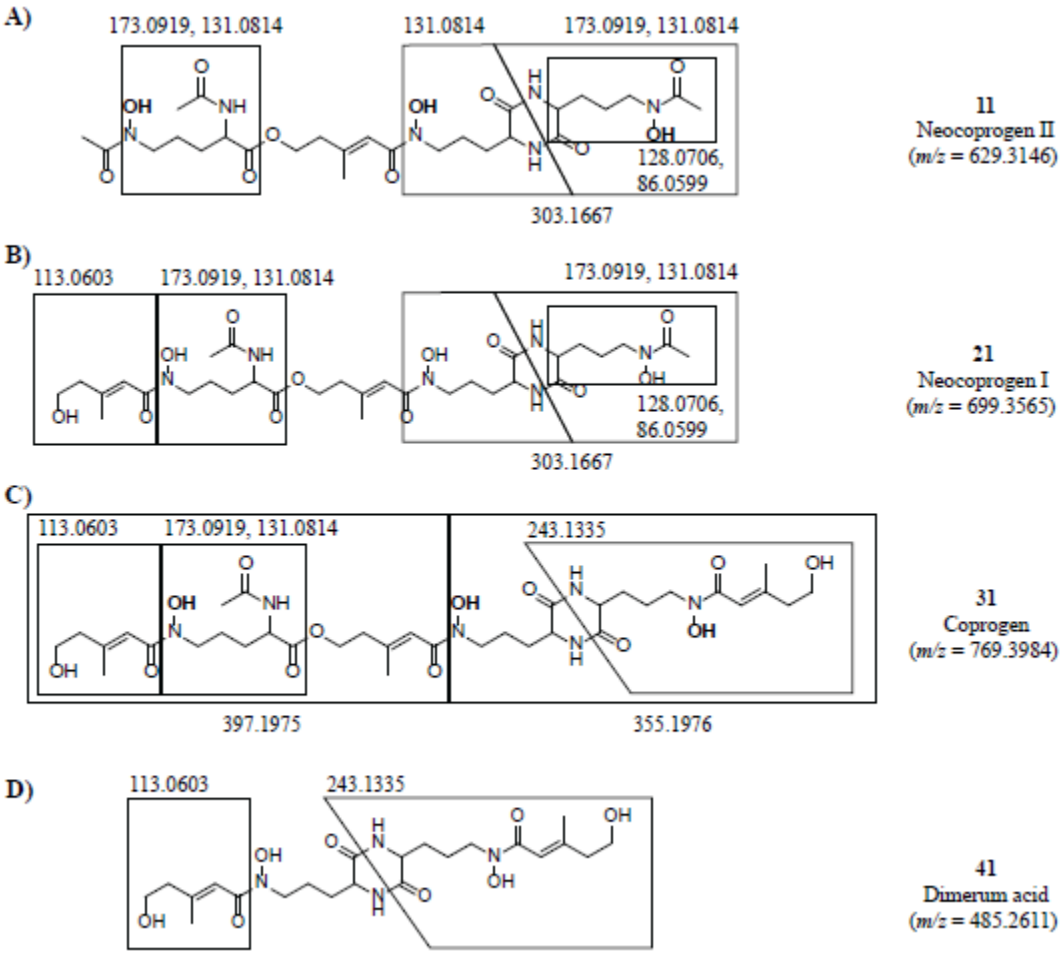

Figure S2. Structures and characteristic MS/MS fragments of the four siderophores with the highest peak area produced by *P. biseptata*: A) Neocoprogen II, B) Neocoprogen I, C) Coprogen, D) Dimerum acid. Shown are the apo forms of each of the siderophores.

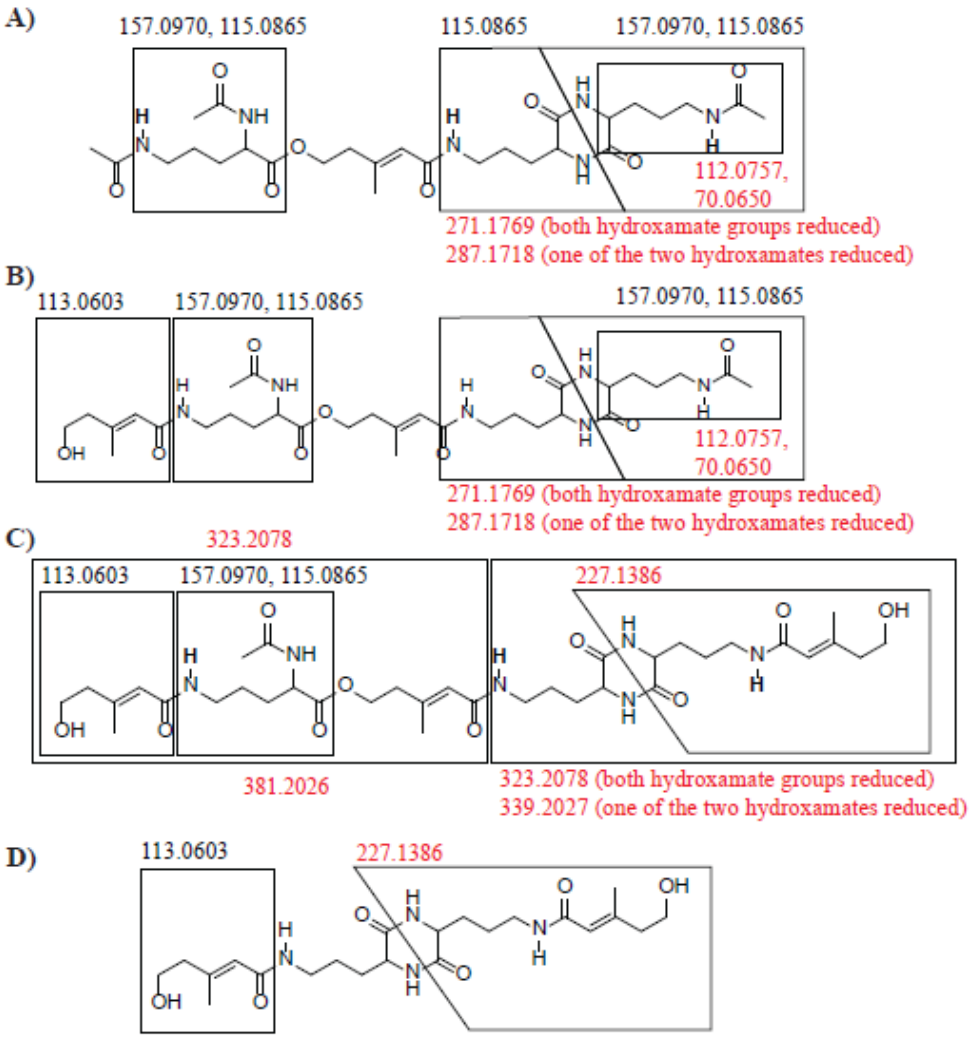

Figure S3. MS/MS fragment *m/z* values in red were used to assign the position of hydroxamate reduction (Figure 5, Table S3) in the four major siderophores produced by *P. biseptata*: A) Neocoprogen II, B) Neocoprogen I, C) Coprogen, D) Dimerum acid.

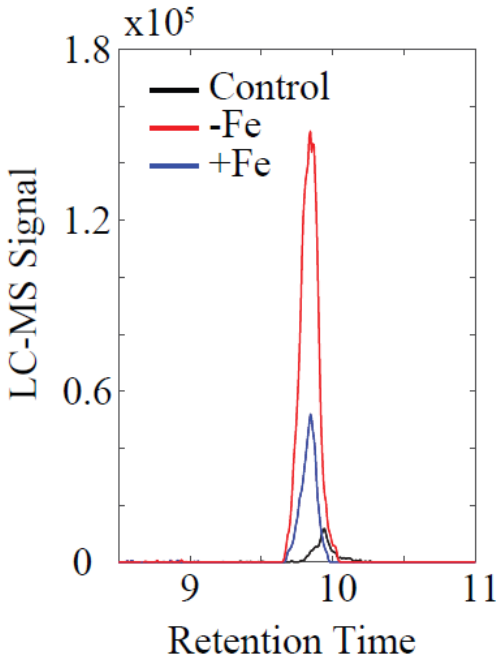

Figure S4. LC-MS chromatograms for the DFOB-O (m/z = 545.4) degradation product after 72h incubation of *S. cerevisiae* mycelium with DFOB in iron-limited media (-Fe) and iron-replete media (+Fe) and comparison to a sterile control.

Table S1. Siderophore standards, ionization mode, and *m/z* values used in LC-MS analysis with Single-Ion-Monitoring (see methods).

Siderophore	**Ionization**	**Exact mass (M)**	***m/z* (MH^+)**	***m/z* ($(M-H)^-$**	***z***
DFOB	Positive	560.3534	561.4		1
DFOB – O	Positive	544.3585	545.4		1
DFOB – 2O	Positive	528.3635	529.4		1
FeDFOB	Positive	613.2648	614.3		1
PDMA	Positive	318.1427	319.1		1
FePDMA	Positive	371.0542	372.1		1
Protochelin	Negative	624.2431		623.2	1
Protochelin – 2H	Negative	622.2256		621.2	1
FeProtochelin	Negative	677.1546		676.2	1

Table S2. MS/MS fragmentation of DFOB and DFOB reaction products referenced in Figure 3

DFOB	
Precursor *m/z*	561.3594
Fragment *m/z*	Intensity (%)
401.2396	3.0
361.2444	2.3
319.2336	10.7
283.1288	2.1
243.1337	51.5
201.1231	100.0
183.1125	5.3
168.1017	1.4
166.086	1.2
165.1021	7.7
154.086	6.6
144.1017	19.1
140.0703	1.7
138.0911	2.2
119.1179	3.5
112.039	1.5
102.0912	17.4
100.0392	5.1
88.0392	1.2

DFOB-O	
Precursor *m/z*	545.3646
Fragment *m/z*	Intensity (%)
545.365	2.7
385.2445	2.0
361.2442	2.1
345.2495	1.9
319.2341	8.5
303.2389	25.9
283.1291	2.5
267.134	1.8
243.1337	18.8
228.1421	1.4
227.1389	100.0
201.1232	63.6
186.1123	5.3
185.1283	47.0
184.0967	1.6
183.1127	4.6
168.1017	12.4
167.118	1.2
165.1021	6.3
154.0862	4.6
144.1018	7.2
138.0913	1.5
128.1069	35.5
119.1182	3.8
103.123	3.4
102.0913	10.8
100.0392	6.4
86.0964	10.8
84.0807	19.3
165.102	10.1
161.1282	16.2
154.086	5.3
144.1018	20.7
140.0708	1.5
138.091	2.8

DFOB-2O	
Precursor *m/z*	529.3697
Fragment *m/z*	Intensity (%)
529.3697	3.2
411.26	1.4
385.2446	2.4
345.2493	6.0
303.2388	45.9
267.1335	5.0
227.1388	100.0
201.1231	17.6
186.1121	5.0
185.1282	72.0
183.1126	2.7
168.1017	21.0
167.1176	2.2
165.1019	2.0
154.0858	1.2
145.1334	1.6
128.1068	43.7
119.1179	1.6
103.1229	6.1
102.0913	2.9
100.0392	5.7
86.0963	21.7
84.0806	12.6
72.0443	3.6

DFOB-3O	
Precursor *m/z*	513.3747
Fragment *m/z*	Intensity (%)
532.9739	1.0
513.3757	12.4
495.3647	4.9
472.8612	1.1
411.26	18.6
393.2501	1.4
369.2492	39.4
351.2387	22.6
329.2544	35.3
329.2289	1.1
312.2276	2.5
311.2442	2.2
287.2438	32.5
285.1446	1.5
270.218	3.2
269.2337	2.9
267.1336	33.3
266.1494	7.0
241.2673	1.1
227.1388	100.0
226.1544	2.0
203.139	1.1
186.1121	6.2
185.1282	86.1
184.1441	4.1
168.1017	61.3
167.1176	27.4
145.1334	28.3
128.1068	33.4
110.745	1.1
103.1228	6.7
100.0392	9.1
86.0963	42.8
84.3068	1.1
81.9933	1.0

131.0812	1.5
128.1069	17.3
119.1179	5.3
113.0599	1.5
112.0391	2.5
103.1229	2.0
102.0913	20.4
100.0392	17.8
98.0965	1.2
86.0963	16.6
84.0807	45.5
72.0442	2.5
69.0698	2.5

72.0443	2.4
69.9539	1.2

Table S3. Siderophores produced by *P. biseptata* in iron-limited culture supernatants (see methods). Characteristic MS/MS fragments shown in Figure S2. MS/MS spectra for Neocoprogen I and Coprogen matched GNPS library reference spectra.

m/z exp	*m/z* calc	Δ ppm	RT (min)	Peak Area	Sum formula	ID	Characteristic MS/MS fragments	GNPS Reference Spectrum
629.3146	629.3130	2.7	3.56	6.3E+09	C27H44N6O11	Neocoprogen II	173.0919, 128.0706, 303.1667	
699.3565	699.3551	2.1	3.66	4.7E+09	C31H50N6O12	Neocoprogen I	113.0603, 173.0919, 128.0706, 303.1667	CCMSLIB00001059086
769.3984	769.3966	2.4	3.74	8.8E+08	C35H56N6O13	Coprogen	113.0603, 173.0919, 397.1975, 355.1976, 243.1335	CCMSLIB00001059084
485.2611	485.2597	3.1	3.39	7.1E+08	C22H36N4O8	Dimerum acid	113.0603, 243.1335	
657.3459	657.3443	2.6	3.33	6.5E+08	C29H48N6O11	Neocoprogen I - H2C2O2	113.0603, 173.0916, 128.0706, 303.1658, 243.1335	
601.3197	601.3182	2.6	3.25	6.2E+08	C26H44N6O10	Neocoprogen I - C5H6O2	113.0603, 128.0706, 303.1658, 141.1022, 205.1182, 159.1127	
587.3041	587.3025	2.8	3.23	4.5E+08	C25H42N6O10	Neocoprogen II - H2C2O2	173.0919, 128.0706	
727.3878	727.3860	2.5	3.41	9.5E+07	C33H54N6O12	Coprogen B	no MS/MS spectrum collected	
715.3514	715.3494	2.9	3.49	4.3E+07	C31H50N6O13	Hydroxy-neocoprogen I	no MS/MS spectrum collected	

Table S4. MS/MS fragments (illustrated in Figure S3) used to assign the coprogen degradation products in Figure 5.

Peak No (see Fig. 5)	Characteristic MS/MS fragments
12	112.0757, 70.0650, 287.1718 (only one of the right two hydroxamate groups is reduced)
13	128.0706, 86.0599, 287.1718
14	112.0757, 128.0706, 70.0650, 86.0599, 271.1769, 287.1718
15	no MS/MS spectrum available
22	112.0757, 70.0650, 287.1718
23	115.0865, 303.1667
24	271.1769
25	287.1718, 115.0865
26	112.0757, 115.0865, 70.0650, 271.1769
32	381.2026
33	381.2026, 227.1386, 339.2027, 323.2079
34	381.2026, 227.1386, 323.2078

Table S5. MS/MS fragmentation spectra used to assign Neocoprogen II and corresponding degradation products in Figure 5.

#11	
Precursor *m/z*	629.3129
Fragment *m/z*	Intensity (%)
472.8634	0.4
411.5243	0.3
303.3865	0.3
303.1662	0.7
288.4533	0.3
285.1565	2.7
284.1575	0.3
270.1439	0.4
266.7634	0.3
257.7534	0.3
241.2520	0.4
233.1131	0.4
226.1184	3.6
215.1028	0.5
210.1224	0.5
208.1079	0.5
195.1122	0.5
193.0969	1.1
191.1027	0.4
187.1074	0.9
184.7034	0.3
183.4151	0.3
174.0952	0.8
173.0918	100.0
162.2937	0.3
155.0813	7.2
146.3174	0.3
145.0970	2.2
140.0734	0.3
131.0814	39.0
128.0705	11.0
127.0865	1.2
114.0548	10.9
113.0707	6.7
113.0596	1.2
112.0758	0.3
97.6973	0.3
95.0526	0.5

#12	
Precursor *m/z*	613.3179
Fragment *m/z*	Intensity (%)
614.2722	1.3
535.7814	0.3
496.1628	1.0
474.3988	0.3
472.8594	0.6
468.1650	0.7
414.1564	1.3
397.1292	0.6
381.2143	0.4
315.0631	0.7
307.4664	0.3
299.0689	0.5
287.1705	1.9
285.1555	1.2
270.1463	0.3
269.1608	3.1
255.0788	0.3
254.1499	1.1
253.0636	0.4
252.1342	0.5
234.8669	0.3
226.1182	2.5
217.1179	0.4
210.1234	0.6
208.1073	0.4
200.0367	0.3
199.1077	9.8
199.0961	0.6
195.1123	0.6
193.0972	2.0
192.1133	0.8
187.1076	0.5
184.7058	0.5
181.0972	0.4
175.1074	0.5
174.0951	0.4
173.0919	49.5
171.1127	4.3

#13	
Precursor *m/z*	613.3182
Fragment *m/z*	Intensity (%)
614.2715	0.6
613.3196	0.5
571.3079	2.2
553.2975	1.8
529.2972	0.4
496.2737	0.3
496.1609	0.6
474.4108	0.3
472.8684	0.4
468.1648	0.7
429.4384	0.3
414.1550	1.0
399.2225	0.6
397.1292	0.5
381.2134	2.6
342.8703	0.3
339.2024	1.2
321.1930	0.8
315.0637	0.7
313.1496	0.5
312.1546	0.3
287.1713	6.7
285.1433	0.5
271.1397	0.6
270.1446	12.7
269.1608	4.1
253.1295	0.6
252.1337	0.4
245.1609	0.4
241.2575	0.3
238.1179	0.8
233.1131	0.7
228.1340	3.2
227.1758	0.3
227.1500	0.4
215.1024	1.0
211.1077	0.5
210.1487	0.8

#14	
Precursor *m/z*	597.3230
Fragment *m/z*	Intensity (%)
555.3135	3.5
537.3024	1.7
525.8546	0.6
478.2647	0.8
477.7274	0.6
472.7739	0.9
365.2179	2.1
297.1554	1.8
287.1709	3.1
271.1765	12.5
271.1400	0.7
270.1448	7.8
269.1608	2.3
261.9319	0.6
254.1499	23.2
253.1661	7.9
241.2070	0.7
238.1180	0.7
236.1397	1.0
228.1343	2.2
217.1183	1.1
212.1394	2.1
210.1234	1.6
203.6904	0.6
199.1079	11.0
195.1127	9.3
194.1288	1.6
192.1133	1.2
189.3848	0.6
187.1079	0.7
184.6788	0.9
173.0920	80.9
171.1129	4.6
163.5618	0.6
157.0970	25.3
155.0816	6.3
145.0972	1.1
140.8370	0.6

95.0490	5.3
90.2185	0.3
86.0599	22.5
85.0759	0.6
82.0943	0.4
70.2552	0.3
70.0650	1.6
68.0495	0.5
67.0541	1.2

158.0812	0.6
157.0970	23.7
155.0814	3.8
149.8852	0.2
149.5689	0.3
145.0971	0.7
139.1606	0.3
139.0865	2.3
138.6906	0.3
131.0814	21.4
129.1023	1.4
128.0706	5.6
127.0866	0.4
118.2161	0.3
115.0865	5.6
114.0548	6.2
113.0789	0.7
113.0709	3.8
113.0596	0.8
112.0756	100.0
106.3973	0.3
102.0547	0.3
95.0490	5.9
94.2744	0.3
89.3210	0.2
86.0600	12.7
84.0809	0.3
82.0988	0.3
70.0651	23.1
69.9486	0.3
67.4167	0.3
67.0542	1.2

210.1234	4.2
195.1127	5.1
194.1288	0.4
193.0968	1.0
192.1126	1.4
191.1025	0.5
187.1073	0.7
185.3105	0.3
184.7046	0.3
183.5429	0.3
174.0958	0.8
173.0918	100.0
169.5284	0.3
167.0813	0.8
159.7301	0.3
156.0896	0.4
155.0813	7.6
145.9406	0.3
145.0970	2.6
140.0901	0.3
132.0848	0.4
131.0813	45.7
128.1139	0.3
128.0705	14.1
127.0865	1.6
125.0706	0.3
124.6813	0.3
115.0865	4.5
114.0548	9.0
113.5952	0.3
113.0708	8.4
113.0596	2.8
112.0756	0.6
98.0599	0.4
97.6969	0.4
96.0443	0.8
95.0490	16.1
94.7586	0.3
90.6315	0.3
86.0599	26.9
85.0759	0.9
84.0804	0.3
83.9547	0.3
72.4551	0.3
70.0650	2.7
69.9493	0.3
69.0572	0.3
68.0495	0.7
67.0542	2.6

139.0866	2.4
137.7252	0.6
131.0815	41.4
129.1022	2.3
129.0899	0.5
128.0705	10.4
115.0866	8.5
114.0549	8.5
113.0789	0.7
113.0710	7.2
113.0595	3.3
112.0757	100.0
95.0491	22.0
95.0452	0.8
86.0600	22.5
85.1724	0.7
85.0759	0.6
70.6444	0.5
70.0651	28.8
69.2583	0.6
67.8381	0.6
67.0542	5.6

Table S6. MS/MS fragmentation spectra used to assign Neocoprogen I and corresponding degradation products in Figure 5.

Precursor *m/z*	699.3545
Fragment *m/z*	Int (%)
587.2983	0.7
474.3994	0.7
473.0003	0.8
397.1993	1.5
380.1930	0.6
303.1660	3.2
285.1572	4.9
281.5170	0.5
281.2018	0.6
270.1456	0.7
243.1462	0.8
243.1326	1.2
228.1350	0.8
226.1182	3.8
225.1224	0.7
210.1231	0.8
208.1083	1.4
208.0963	1.3
207.1246	0.6
199.0990	0.5
198.1123	1.1
195.1124	0.6
193.0970	1.2
192.1141	0.6
191.1024	0.6
184.7629	0.9
180.1017	0.7
179.8684	0.5
173.0918	36.2
155.0813	4.0
154.4425	0.5
145.0969	4.1
131.0813	100.0
128.0703	4.3
127.0865	3.8
119.5985	0.5
114.0548	22.5
114.0497	1.1
113.0705	10.0
113.0596	67.3
112.0756	1.5
110.0598	1.1
103.6100	0.5
97.7251	0.9
96.0482	0.7
96.0443	13.6
95.0490	17.7
86.0599	21.5
85.0759	1.4
85.0646	8.5

Precursor *m/z*	683.3602
Fragment *m/z*	Int (%)
582.2905	1.4
571.3077	1.4
526.8636	1.4
474.3975	1.7
452.2723	1.6
367.0295	4.2
359.0296	1.6
349.0199	12.4
348.0122	1.4
307.9943	1.6
294.3419	1.4
287.1714	10.0
276.5113	1.4
269.1612	8.7
267.9988	1.9
254.1506	2.8
249.9879	3.9
214.1791	1.3
211.1439	1.8
210.1239	3.9
199.1078	1.7
193.0970	3.6
184.6905	1.9
180.1013	1.3
173.0919	27.5
169.8066	1.2
168.1017	14.4
164.1068	4.9
157.0969	14.4
155.0816	3.7
152.1069	1.8
139.0865	2.1
131.0814	100.0
129.1021	6.0
128.0704	1.9
127.0867	2.7
126.0443	1.2
120.9156	1.3
116.0707	1.5
115.0866	9.9
114.0627	1.7
114.0549	24.2
113.0704	8.5
113.0596	84.5
112.0756	43.9
112.0717	1.0
98.0251	1.3
96.0443	14.1
95.0491	22.3
91.8350	1.3

Precursor *m/z*	683.3602
Fragment *m/z*	Int (%)
716.1094	0.5
666.4001	0.5
571.3079	4.9
553.2966	2.6
529.3004	0.9
511.2895	1.1
494.2608	1.0
493.2769	0.7
472.8706	0.6
472.8318	0.5
442.6534	0.5
435.7206	0.5
399.2238	0.9
381.2012	9.6
363.1919	1.6
360.6646	0.5
357.2144	0.6
349.0199	0.6
339.2004	1.5
322.1640	0.6
321.1793	0.5
314.8150	0.5
287.1726	5.4
285.1572	0.9
270.1451	12.8
269.1621	2.5
269.1490	3.3
251.1389	1.7
242.0207	0.5
228.1340	3.8
227.1511	0.7
227.1387	1.7
226.1182	1.7
223.1439	0.5
211.1083	0.5
210.1235	5.6
209.1395	0.8
209.1284	0.6
195.1129	5.1
193.0972	1.7
192.1129	1.4
182.1275	0.7
182.1174	11.9
175.1078	3.4
173.0919	28.6
168.1022	0.6
167.0807	0.5
165.0658	0.6
164.1067	3.3
158.0812	1.5

Precursor *m/z*	667.3651
Fragment *m/z*	Int (%)
555.3129	6.3
537.3016	2.1
495.2937	1.5
478.2677	3.6
463.0604	0.7
409.9456	0.7
383.2282	1.2
381.2021	7.1
365.2186	5.4
363.1910	1.3
297.1554	1.5
271.1766	20.0
269.1634	1.6
269.1462	3.5
254.1499	46.4
253.1658	11.0
252.1348	0.9
251.1385	1.1
236.1387	1.4
227.1398	0.8
223.1446	0.9
212.1390	2.2
210.1244	0.8
209.1282	0.8
199.1073	1.4
195.1129	11.2
194.1288	1.2
193.0973	1.2
182.1172	8.4
175.1075	2.6
173.0921	13.2
164.1070	2.6
158.0807	1.0
157.0971	33.9
155.0817	1.5
146.8862	0.7
145.8965	0.9
139.0867	5.7
131.0815	42.6
129.1020	3.3
127.0868	0.8
115.0865	33.9
114.0550	7.7
113.0706	3.0
113.0597	100.0
112.0757	20.2
111.0917	0.9
110.0601	1.9
107.3057	0.8
100.2857	0.7

Precursor *m/z*	667.3650
Fragment *m/z*	Int (%)
637.4042	0.8
625.3566	2.2
607.3447	2.6
555.3659	1.3
555.3135	17.5
538.2858	1.3
537.3026	6.6
517.0208	0.6
513.3026	1.8
496.2773	1.4
495.2936	1.6
477.2806	0.6
474.1738	0.7
399.2230	1.7
381.2015	13.1
363.1935	0.6
341.2188	1.6
339.2042	1.5
324.1917	3.3
323.2079	2.5
322.1663	1.0
321.1913	1.1
312.7150	0.6
305.1977	0.7
292.4295	0.6
287.1743	6.7
270.1452	25.2
269.1623	3.6
269.1491	5.1
268.1650	1.1
253.1297	1.0
252.1339	0.8
251.1390	2.4
228.1342	5.6
227.1388	2.5
223.1445	1.2
216.2471	0.5
215.1020	0.6
212.1394	4.2
210.1236	6.9
210.1120	0.8
209.1284	1.4
195.1127	17.1
194.6992	0.6
194.1291	1.6
193.0970	1.7
192.1132	2.1
187.9796	0.6
182.1174	17.1
175.1078	4.5

Precursor *m/z*	651.3699
Fragment *m/z*	Int (%)
641.989	0.6
609.360	1.6
591.350	2.3
559.299	0.6
540.322	0.8
539.318	18.7
522.292	0.9
521.308	6.2
480.281	2.4
479.298	1.2
474.159	0.9
472.789	1.1
383.228	1.2
381.202	9.6
367.147	0.9
365.218	9.8
363.192	1.1
339.192	1.4
324.193	0.7
323.209	1.1
322.167	0.7
321.180	1.2
297.156	2.2
287.161	1.2
285.147	0.7
271.176	19.1
270.651	0.6
270.133	1.5
269.150	6.9
255.144	0.9
254.150	54.5
253.166	11.7
251.138	3.9
241.215	0.9
238.119	1.5
236.139	1.0
234.374	0.8
227.139	2.6
223.144	1.5
222.248	0.8
212.139	3.1
209.128	1.6
204.999	0.9
201.087	0.8
199.107	1.1
195.113	12.6
194.129	2.2
192.547	0.6
183.076	1.1
182.117	19.6

82.1172	0.6	89.2612	1.2	157.0970	41.2	96.0443	12.5	173.0920	24.8	175.108	4.4
79.0451	0.5	86.0963	2.3	155.0815	3.6	95.0491	30.6	171.5368	0.6	166.123	0.8
		86.0600	15.5	152.1069	0.6	86.0600	7.3	167.0811	1.4	165.554	0.7
		85.0648	12.5	147.2195	0.4	85.0647	15.5	164.1071	5.1	164.761	0.7
		84.0809	2.1	145.0974	2.6	85.0618	0.4	158.0815	2.9	164.107	5.3
		77.0431	1.3	140.0705	1.1	83.0283	0.7	157.0971	59.1	159.556	0.7
				139.0864	6.3	82.0647	0.7	156.6254	0.6	158.081	2.2
				138.0547	0.5	78.8612	0.7	155.0814	2.0	157.097	59.9
				135.0919	0.5	77.0579	0.6	152.1071	1.9	152.107	1.7
				131.0814	38.4	71.0491	2.2	145.0970	1.7	147.549	0.6

Table S7. MS/MS fragmentation spectra used to assign Coprogen and corresponding degradation products in Figure 5.

#31	
Precursor *m/z*	769.3963
Fragment *m/z*	Intensity (%)
756.4151	0.7
740.8502	0.9
738.7735	1.1
738.7033	1.0
618.4381	0.7
472.8155	0.7
472.7774	0.8
470.9662	0.6
397.1984	1.4
355.1981	4.0
285.1451	1.8
270.1355	0.9
267.1337	0.7
243.1466	3.6
243.1335	1.6
241.2244	0.9
241.1680	0.7
239.1391	1.2
228.1344	1.1
226.1186	3.7
225.1231	1.1
214.5164	0.6
208.1315	0.7
208.1083	2.4
208.0969	1.1
207.1247	1.2
198.1128	1.3
197.1283	1.1
192.1135	1.0
184.6870	0.9
180.1019	2.0
173.0920	28.4
157.0983	0.6
155.0815	4.1
145.9255	0.7
140.0711	0.6
131.0815	100.0
128.0704	0.9
127.0867	1.4
122.2854	0.7

#32	
Precursor *m/z*	753.4017
Fragment *m/z*	Intensity (%)
740.9423	1.0
738.9820	1.2
696.5430	1.2
642.1543	0.9
641.3498	1.8
623.3401	1.2
529.2983	2.9
511.2876	4.0
397.1978	1.4
392.5018	1.2
381.2010	4.4
363.1905	1.4
357.2130	5.6
354.2027	1.0
344.2158	1.0
340.1877	1.0
339.2026	8.4
322.1767	1.8
321.1908	1.1
287.1609	1.6
285.1454	1.5
279.8900	0.9
269.1493	3.1
257.6616	1.1
245.1606	1.5
239.1389	0.9
236.0656	0.9
228.1338	9.3
227.1505	4.3
227.1385	2.2
210.1232	9.0
209.1277	2.2
197.1288	1.4
195.1122	5.4
193.0969	3.5
192.1134	4.5
182.1174	7.6
180.1015	1.5
175.1079	2.2
173.0919	15.8

#33	
Precursor *m/z*	737.4067
Fragment *m/z*	Intensity (%)
738.866	1.2
625.354	6.5
607.347	6.1
513.303	5.3
496.278	2.5
495.293	6.8
478.265	1.0
474.214	0.9
472.875	0.8
472.836	1.0
460.256	0.7
453.271	1.3
436.254	1.4
435.260	1.7
419.229	1.1
418.244	1.7
381.202	9.0
381.128	0.7
377.166	0.7
363.192	1.6
357.213	1.3
354.201	0.7
346.248	0.8
344.071	0.8
341.218	7.4
340.187	0.8
339.202	4.4
324.191	11.9
323.208	8.0
322.177	1.3
314.639	0.7
306.181	1.8
305.197	1.0
287.160	1.4
285.144	0.9
269.150	4.3
251.139	1.7
245.161	0.8
241.249	0.9
238.118	1.1

#34	
Precursor *m/z*	721.4119
Fragment *m/z*	Intensity (%)
738.7526	1.6
721.3346	2.8
703.4001	1.0
609.3603	20.9
592.3346	1.6
591.3498	17.1
573.3394	0.9
550.3229	2.1
549.3411	0.9
498.8751	0.7
497.3072	2.8
480.2807	7.7
479.2968	6.8
472.8552	0.7
462.2706	1.4
453.2699	1.9
437.1891	2.4
435.2605	4.0
403.2437	1.0
400.0091	0.8
381.2018	12.3
367.1470	1.5
363.1930	1.0
341.2183	13.5
339.1920	1.8
324.1917	24.5
323.2079	15.3
319.2365	0.8
306.1803	3.7
305.1980	1.8
287.1600	2.7
284.1886	0.9
270.1338	2.2
269.1496	5.7
260.3320	0.9
255.0370	0.8
251.1393	4.3
241.2253	1.0
238.1185	2.2
229.1663	1.4

118.1990	0.6
116.8224	0.6
114.0629	1.1
114.0549	26.0
113.0705	10.2
113.0597	91.8
112.0757	2.7
110.0600	1.4
100.7364	0.6
96.0444	16.0
95.0491	21.2
86.0600	20.4
85.0760	2.5
85.0647	13.3

167.0815	1.3
164.1069	2.7
158.0809	1.3
157.0970	19.7
155.0814	2.9
139.0864	2.5
132.8399	1.0
132.0844	1.0
131.0814	60.5
127.0865	2.1
115.0865	30.3
114.0549	13.0
113.0707	3.8
113.0596	100.0
112.0757	2.6

229.165	1.0
228.134	5.9
227.139	2.8
212.139	9.7
211.155	2.7
210.124	4.6
209.140	0.9
209.129	3.3
198.197	0.7
195.113	20.5
194.129	5.2
193.097	2.7
192.113	1.3
184.708	1.0
182.117	11.4

227.1391	3.2
223.1439	1.5
212.1393	21.5
211.1549	3.1
209.1283	2.3
202.1264	2.7
201.1232	4.6
199.2635	0.7
195.1127	35.9
194.1289	6.0
184.6911	0.9
184.6802	0.9
182.1173	15.6
181.1333	1.3
175.1077	5.3

Table S8. MS/MS fragmentation spectra used to assign Dimerum acid and corresponding degradation products in Figure 5.

#41	
Precursor *m/z*	485.2598
Fragment *m/z*	Intensity (%)
399.9299	0.3
373.2086	0.5
355.1975	3.0
252.6773	0.3
243.1463	4.5
243.1302	1.4
228.1342	1.3
226.1417	0.4
226.1186	3.1
225.1354	0.6
225.1231	0.8
210.1240	1.6
209.1388	0.5
208.1080	2.2
207.6415	0.3
207.1241	0.4
195.1127	0.5
193.0969	0.7
192.1131	1.3
191.1289	0.4
184.7002	0.5
181.0972	0.4
157.0604	0.3
155.0814	0.3
150.0785	0.4
137.6273	0.3
131.0815	7.2
118.0647	0.4
114.0549	7.7
113.0597	100.0
97.6942	0.4
97.0760	0.4
96.0442	0.5
95.0491	10.7
86.8299	0.3
86.0632	0.6
86.0600	6.3
85.0760	2.4
85.0648	20.8
83.0493	0.3
74.3880	0.4
71.0491	5.3

#42	
Precursor *m/z*	469.2648
Fragment *m/z*	Intensity (%)
357.2134	3.4
340.1882	0.3
339.2027	8.9
324.1918	0.8
322.1999	0.4
321.1922	0.6
309.1917	0.4
273.5017	0.3
259.4561	0.3
245.1611	1.5
243.1339	0.6
241.2530	0.4
236.4974	0.3
228.1342	2.5
227.1504	5.8
227.1385	1.5
212.1393	0.7
210.1236	5.0
209.1399	0.9
209.1283	1.2
199.1441	0.5
197.8588	0.3
195.1128	2.5
194.1282	0.7
193.1208	0.3
193.0972	5.1
192.1130	4.8
191.1289	0.5
184.7101	0.3
182.1175	3.3
165.1019	0.8
164.1179	0.5
132.4349	0.2
131.7037	0.3
131.0815	1.1
115.0866	10.5
114.0550	0.3
113.0597	100.0
107.4073	0.3
106.4298	0.3
97.6979	0.4
96.2303	0.3

#43	
Precursor *m/z*	453.2698
Fragment *m/z*	Intensity (%)
386.2499	3.1
385.2449	2.2
341.2181	50.8
335.1599	20.4
331.0270	1.9
324.1916	40.9
323.2077	73.2
321.2375	1.9
320.2376	10.0
319.2331	14.2
306.1813	5.2
305.1962	3.2
298.4440	1.9
285.1445	3.3
283.1285	3.7
282.1458	1.8
268.1376	12.7
267.1336	21.0
255.1458	2.3
238.1184	11.3
237.1339	4.7
236.1281	44.2
234.6301	4.7
229.1658	8.9
227.1386	10.8
226.1910	2.1
212.1393	34.9
211.1550	28.0
210.1681	4.4
210.1490	3.6
209.1649	5.8
209.1283	6.5
202.1269	13.9
201.1234	47.6
195.1127	57.8
194.1287	25.9
193.1443	1.9
186.1125	2.2
185.1280	7.8
185.1142	3.7
184.7188	2.3
184.6124	5.5

70.4132	0.3
70.0651	6.3
69.9454	0.3
69.0336	0.5
68.0494	3.8
67.0542	18.4
65.0385	0.3
60.3052	0.4
58.9339	0.3
58.3311	0.2
57.0698	2.8
54.4242	0.2

95.0491	11.0
86.0600	1.0
85.0759	0.3
85.0647	19.1
72.0345	0.3
71.0491	5.3
70.0675	0.5
70.0651	9.9
69.0334	0.5
68.0495	0.5
67.1709	0.3
67.0542	16.5

184.0965	4.7
183.1130	9.9
182.1173	15.9
169.1053	20.4
168.1018	100.0
166.1055	2.8
165.1021	8.1
161.0135	2.0
155.0897	2.1
154.0861	7.3
140.2842	1.8

Appendix C
(Supplementary Information for Chapter 4)

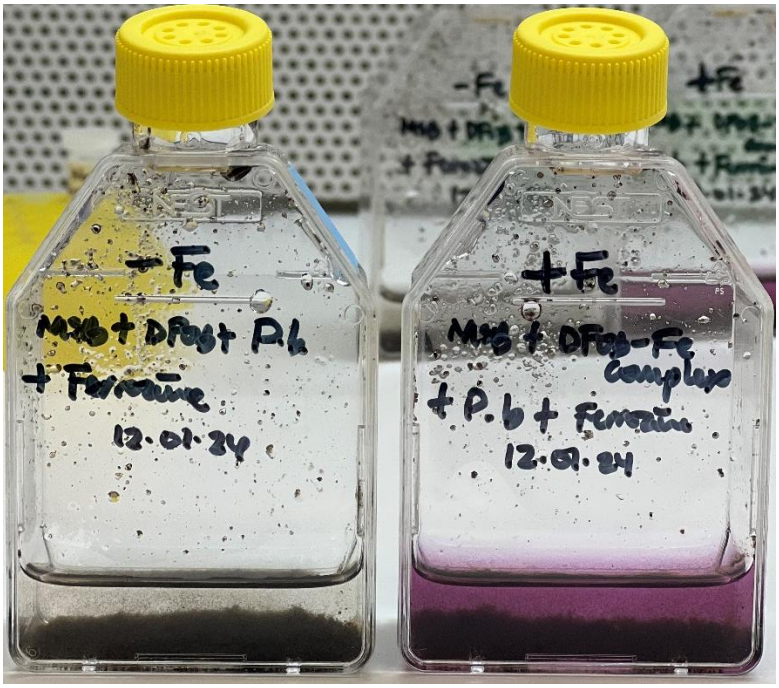

Figure S1. Indication of Fe^{II} formation in samples containing ferrozine in Fe-replete media (right), forming a stable magenta color in contrast to samples in Fe-limited media (left) after 24 h incubation with *P. biseptata*.

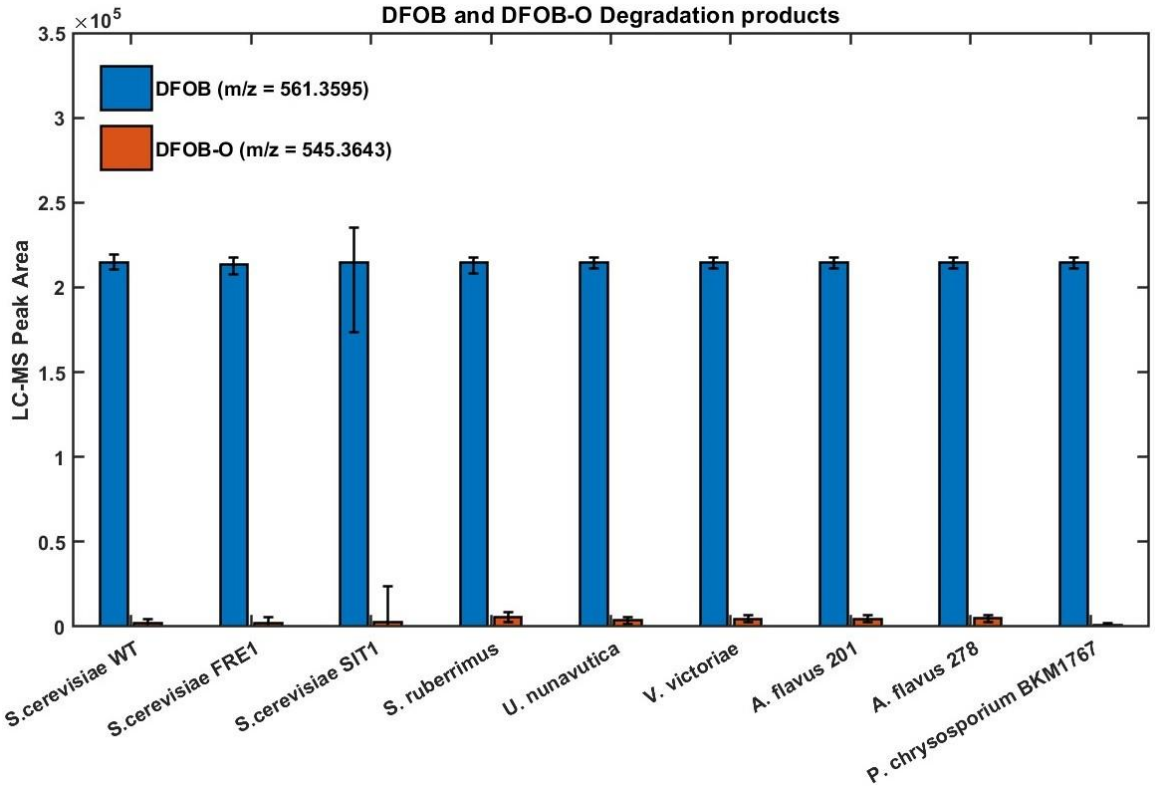

Figure S2. DFOB and ~1-3 % DFOB-O Degradation product peak areas in samples without ferrozine for *Saccharomyces cerevisiae* wild type (WT), *S. cerevisiae* mutants impaired in Fe uptake (FRE1, FRE2, ARN1, ARN2, and SIT1), *Sporobolomyces ruberrimus*, *Ustilago nunavutica*, *Vishniacozyma victoriae*, *Aspergillus flavus* 201 (aflatoxin+), *A. flavus* 278 (aflatoxin-), and *Phanerodontia chrysosporium*. LC-MS peak areas for DFOB (blue) and DFOB degradation product (DFOB-O) (orange) in samples without ferrozine after 72 h incubation, for three biological replicates.

Table S1. MS/MS fragmentation of DFOB and DFOB reaction products referenced in Figure 2

DFOB	
Precursor *m/z*	561.3594
Fragment *m/z*	Intensity (%)
401.2396	3.0
361.2444	2.3
319.2336	10.7
283.1288	2.1
243.1337	51.5
201.1231	100.0
183.1125	5.3
168.1017	1.4
166.086	1.2
165.1021	7.7
154.086	6.6
144.1017	19.1
140.0703	1.7
138.0911	2.2
119.1179	3.5
112.039	1.5
102.0912	17.4
100.0392	5.1
88.0392	1.2

DFOB-O	
Precursor *m/z*	545.3646
Fragment *m/z*	Intensity (%)
545.365	2.7
385.2445	2.0
361.2442	2.1
345.2495	1.9
319.2341	8.5
303.2389	25.9
283.1291	2.5
267.134	1.8
243.1337	18.8
228.1421	1.4
227.1389	100.0
201.1232	63.6
186.1123	5.3
185.1283	47.0
184.0967	1.6
183.1127	4.6
168.1017	12.4
167.118	1.2
165.1021	6.3
154.0862	4.6
144.1018	7.2
138.0913	1.5
128.1069	35.5
119.1182	3.8
103.123	3.4
102.0913	10.8
100.0392	6.4
86.0964	10.8
84.0807	19.3
165.102	10.1
161.1282	16.2
154.086	5.3
144.1018	20.7
140.0708	1.5
138.091	2.8
131.0812	1.5
128.1069	17.3

DFOB-2O	
Precursor *m/z*	529.3697
Fragment *m/z*	Intensity (%)
529.3697	3.2
411.26	1.4
385.2446	2.4
345.2493	6.0
303.2388	45.9
267.1335	5.0
227.1388	100.0
201.1231	17.6
186.1121	5.0
185.1282	72.0
183.1126	2.7
168.1017	21.0
167.1176	2.2
165.1019	2.0
154.0858	1.2
145.1334	1.6
128.1068	43.7
119.1179	1.6
103.1229	6.1
102.0913	2.9
100.0392	5.7
86.0963	21.7
84.0806	12.6
72.0443	3.6

DFOB-3O	
Precursor *m/z*	513.3747
Fragment *m/z*	Intensity (%)
532.9739	1.0
513.3757	12.4
495.3647	4.9
472.8612	1.1
411.26	18.6
393.2501	1.4
369.2492	39.4
351.2387	22.6
329.2544	35.3
329.2289	1.1
312.2276	2.5
311.2442	2.2
287.2438	32.5
285.1446	1.5
270.218	3.2
269.2337	2.9
267.1336	33.3
266.1494	7.0
241.2673	1.1
227.1388	100.0
226.1544	2.0
203.139	1.1
186.1121	6.2
185.1282	86.1
184.1441	4.1
168.1017	61.3
167.1176	27.4
145.1334	28.3
128.1068	33.4
110.745	1.1
103.1228	6.7
100.0392	9.1
86.0963	42.8
84.3068	1.1
81.9933	1.0
72.0443	2.4
69.9539	1.2

119.1179	5.3
113.0599	1.5
112.0391	2.5
103.1229	2.0
102.0913	20.4
100.0392	17.8
98.0965	1.2
86.0963	16.6
84.0807	45.5
72.0442	2.5
69.0698	2.5

Table S2. Siderophores produced by *P. biseptata* in iron-limited culture supernatants (see methods). MS/MS spectra for Neocoprogen I and Coprogen matched GNPS library reference spectra.

m/z exp	*m/z* calc	Δ ppm	RT (min)	Peak Area	Sum formula	ID	Characteristic MS/MS fragments	GNPS Reference Spectrum
629.3146	629.3130	2.7	3.56	6.3E+09	C27H44N6O11	Neocoprogen II	173.0919, 128.0706, 303.1667	
699.3565	699.3551	2.1	3.66	4.7E+09	C31H50N6O12	Neocoprogen I	113.0603, 173.0919, 128.0706, 303.1667	CCMSLIB00001059086
769.3984	769.3966	2.4	3.74	8.8E+08	C35H56N6O13	Coprogen	113.0603, 173.0919, 397.1975, 355.1976, 243.1335	CCMSLIB00001059084
485.2611	485.2597	3.1	3.39	7.1E+08	C22H36N4O8	Dimerum acid	113.0603, 243.1335	
657.3459	657.3443	2.6	3.33	6.5E+08	C29H48N6O11	Neocoprogen I - H2C2O2	113.0603, 173.0916, 128.0706, 303.1658, 243.1335	
601.3197	601.3182	2.6	3.25	6.2E+08	C26H44N6O10	Neocoprogen I - C5H6O2	113.0603, 128.0706, 303.1658, 141.1022, 205.1182, 159.1127	
587.3041	587.3025	2.8	3.23	4.5E+08	C25H42N6O10	Neocoprogen II - H2C2O2	173.0919, 128.0706	
727.3878	727.3860	2.5	3.41	9.5E+07	C33H54N6O12	Coprogen B	no MS/MS spectrum collected	
715.3514	715.3494	2.9	3.49	4.3E+07	C31H50N6O13	Hydroxy-neocoprogen I	no MS/MS spectrum collected	

Table S3. MS/MS fragments used to assign the coprogen degradation products in Figure 3.

Peak No (see Fig. 5)	Characteristic MS/MS fragments
12	112.0757, 70.0650, 287.1718 (only one of the right two hydroxamate groups is reduced)
13	128.0706, 86.0599, 287.1718
14	112.0757, 128.0706, 70.0650, 86.0599, 271.1769, 287.1718
15	no MS/MS spectrum available
22	112.0757, 70.0650, 287.1718
23	115.0865, 303.1667
24	271.1769
25	287.1718, 115.0865
26	112.0757, 115.0865, 70.0650, 271.1769
32	381.2026
33	381.2026, 227.1386, 339.2027, 323.2079
34	381.2026, 227.1386, 323.2078

Table S4. MS/MS fragmentation spectra used to assign Neocoprogen II and corresponding degradation products in Figure 3.

#11	
Precursor *m/z*	629.3129
Fragment *m/z*	Intensity (%)
472.8634	0.4
411.5243	0.3
303.3865	0.3
303.1662	0.7
288.4533	0.3
285.1565	2.7
284.1575	0.3
270.1439	0.4
266.7634	0.3
257.7534	0.3
241.2520	0.4
233.1131	0.4
226.1184	3.6
215.1028	0.5
210.1224	0.5
208.1079	0.5
195.1122	0.5
193.0969	1.1
191.1027	0.4
187.1074	0.9
184.7034	0.3
183.4151	0.3
174.0952	0.8
173.0918	100.0
162.2937	0.3
155.0813	7.2
146.3174	0.3
145.0970	2.2
140.0734	0.3
131.0814	39.0
128.0705	11.0
127.0865	1.2
114.0548	10.9
113.0707	6.7
113.0596	1.2
112.0758	0.3
97.6973	0.3
95.0526	0.5
95.0490	5.3
90.2185	0.3

#12	
Precursor *m/z*	613.3179
Fragment *m/z*	Intensity (%)
614.2722	1.3
535.7814	0.3
496.1628	1.0
474.3988	0.3
472.8594	0.6
468.1650	0.7
414.1564	1.3
397.1292	0.6
381.2143	0.4
315.0631	0.7
307.4664	0.3
299.0689	0.5
287.1705	1.9
285.1555	1.2
270.1463	0.3
269.1608	3.1
255.0788	0.3
254.1499	1.1
253.0636	0.4
252.1342	0.5
234.8669	0.3
226.1182	2.5
217.1179	0.4
210.1234	0.6
208.1073	0.4
200.0367	0.3
199.1077	9.8
199.0961	0.6
195.1123	0.6
193.0972	2.0
192.1133	0.8
187.1076	0.5
184.7058	0.5
181.0972	0.4
175.1074	0.5
174.0951	0.4
173.0919	49.5
171.1127	4.3
158.0812	0.6
157.0970	23.7

#13	
Precursor *m/z*	613.3182
Fragment *m/z*	Intensity (%)
614.2715	0.6
613.3196	0.5
571.3079	2.2
553.2975	1.8
529.2972	0.4
496.2737	0.3
496.1609	0.6
474.4108	0.3
472.8684	0.4
468.1648	0.7
429.4384	0.3
414.1550	1.0
399.2225	0.6
397.1292	0.5
381.2134	2.6
342.8703	0.3
339.2024	1.2
321.1930	0.8
315.0637	0.7
313.1496	0.5
312.1546	0.3
287.1713	6.7
285.1433	0.5
271.1397	0.6
270.1446	12.7
269.1608	4.1
253.1295	0.6
252.1337	0.4
245.1609	0.4
241.2575	0.3
238.1179	0.8
233.1131	0.7
228.1340	3.2
227.1758	0.3
227.1500	0.4
215.1024	1.0
211.1077	0.5
210.1487	0.8
210.1234	4.2
195.1127	5.1

#14	
Precursor *m/z*	597.3230
Fragment *m/z*	Intensity (%)
555.3135	3.5
537.3024	1.7
525.8546	0.6
478.2647	0.8
477.7274	0.6
472.7739	0.9
365.2179	2.1
297.1554	1.8
287.1709	3.1
271.1765	12.5
271.1400	0.7
270.1448	7.8
269.1608	2.3
261.9319	0.6
254.1499	23.2
253.1661	7.9
241.2070	0.7
238.1180	0.7
236.1397	1.0
228.1343	2.2
217.1183	1.1
212.1394	2.1
210.1234	1.6
203.6904	0.6
199.1079	11.0
195.1127	9.3
194.1288	1.6
192.1133	1.2
189.3848	0.6
187.1079	0.7
184.6788	0.9
173.0920	80.9
171.1129	4.6
163.5618	0.6
157.0970	25.3
155.0816	6.3
145.0972	1.1
140.8370	0.6
139.0866	2.4
137.7252	0.6

86.0599	22.5
85.0759	0.6
82.0943	0.4
70.2552	0.3
70.0650	1.6
68.0495	0.5
67.0541	1.2

155.0814	3.8
149.8852	0.2
149.5689	0.3
145.0971	0.7
139.1606	0.3
139.0865	2.3
138.6906	0.3
131.0814	21.4
129.1023	1.4
128.0706	5.6
127.0866	0.4
118.2161	0.3
115.0865	5.6
114.0548	6.2
113.0789	0.7
113.0709	3.8
113.0596	0.8
112.0756	100.0
106.3973	0.3
102.0547	0.3
95.0490	5.9
94.2744	0.3
89.3210	0.2
86.0600	12.7
84.0809	0.3
82.0988	0.3
70.0651	23.1
69.9486	0.3
67.4167	0.3
67.0542	1.2

194.1288	0.4
193.0968	1.0
192.1126	1.4
191.1025	0.5
187.1073	0.7
185.3105	0.3
184.7046	0.3
183.5429	0.3
174.0958	0.8
173.0918	100.0
169.5284	0.3
167.0813	0.8
159.7301	0.3
156.0896	0.4
155.0813	7.6
145.9406	0.3
145.0970	2.6
140.0901	0.3
132.0848	0.4
131.0813	45.7
128.1139	0.3
128.0705	14.1
127.0865	1.6
125.0706	0.3
124.6813	0.3
115.0865	4.5
114.0548	9.0
113.5952	0.3
113.0708	8.4
113.0596	2.8
112.0756	0.6
98.0599	0.4
97.6969	0.4
96.0443	0.8
95.0490	16.1
94.7586	0.3
90.6315	0.3
86.0599	26.9
85.0759	0.9
84.0804	0.3
83.9547	0.3
72.4551	0.3
70.0650	2.7
69.9493	0.3
69.0572	0.3
68.0495	0.7
67.0542	2.6

131.0815	41.4
129.1022	2.3
129.0899	0.5
128.0705	10.4
115.0866	8.5
114.0549	8.5
113.0789	0.7
113.0710	7.2
113.0595	3.3
112.0757	100.0
95.0491	22.0
95.0452	0.8
86.0600	22.5
85.1724	0.7
85.0759	0.6
70.6444	0.5
70.0651	28.8
69.2583	0.6
67.8381	0.6
67.0542	5.6

Table S5. MS/MS fragmentation spectra used to assign Neocoprogen I and corresponding degradation products in Figure 3.

Precursor *m/z*	699.3545
Fragment *m/z*	Int (%)
587.2983	0.7
474.3994	0.7
473.0003	0.8
397.1993	1.5
380.1930	0.6
303.1660	3.2
285.1572	4.9
281.5170	0.5
281.2018	0.6
270.1456	0.7
243.1462	0.8
243.1326	1.2
228.1350	0.8
226.1182	3.8
225.1224	0.7
210.1231	0.8
208.1083	1.4
208.0963	1.3
207.1246	0.6
199.0990	0.5
198.1123	1.1
195.1124	0.6
193.0970	1.2
192.1141	0.6
191.1024	0.6
184.7629	0.9
180.1017	0.7
179.8684	0.5
173.0918	36.2
155.0813	4.0
154.4425	0.5
145.0969	4.1
131.0813	100.0
128.0703	4.3
127.0865	3.8
119.5985	0.5
114.0548	22.5
114.0497	1.1
113.0705	10.0
113.0596	67.3
112.0756	1.5
110.0598	1.1
103.6100	0.5
97.7251	0.9
96.0482	0.7
96.0443	13.6
95.0490	17.7
86.0599	21.5
85.0759	1.4
85.0646	8.5

Precursor *m/z*	683.3602
Fragment *m/z*	Int (%)
582.2905	1.4
571.3077	1.4
526.8636	1.4
474.3975	1.7
452.2723	1.6
367.0295	4.2
359.0296	1.6
349.0199	12.4
348.0122	1.4
307.9943	1.6
294.3419	1.4
287.1714	10.0
276.5113	1.4
269.1612	8.7
267.9988	1.9
254.1506	2.8
249.9879	3.9
214.1791	1.3
211.1439	1.8
210.1239	3.9
199.1078	1.7
193.0970	3.6
184.6905	1.9
180.1013	1.3
173.0919	27.5
169.8066	1.2
168.1017	14.4
164.1068	4.9
157.0969	14.4
155.0816	3.7
152.1069	1.8
139.0865	2.1
131.0814	100.0
129.1021	6.0
128.0704	1.9
127.0867	2.7
126.0443	1.2
120.9156	1.3
116.0707	1.5
115.0866	9.9
114.0627	1.7
114.0549	24.2
113.0704	8.5
113.0596	84.5
112.0756	43.9
112.0717	1.0
98.0251	1.3
96.0443	14.1
95.0491	22.3
91.8350	1.3

Precursor *m/z*	683.3602
Fragment *m/z*	Int (%)
716.1094	0.5
666.4001	0.5
571.3079	4.9
553.2966	2.6
529.3004	0.9
511.2895	1.1
494.2608	1.0
493.2769	0.7
472.8706	0.6
472.8318	0.5
442.6534	0.5
435.7206	0.5
399.2238	0.9
381.2012	9.6
363.1919	1.6
360.6646	0.5
357.2144	0.6
349.0199	0.6
339.2004	1.5
322.1640	0.6
321.1793	0.5
314.8150	0.5
287.1726	5.4
285.1572	0.9
270.1451	12.8
269.1621	2.5
269.1490	3.3
251.1389	1.7
242.0207	0.5
228.1340	3.8
227.1511	0.7
227.1387	1.7
226.1182	1.7
223.1439	0.5
211.1083	0.5
210.1235	5.6
209.1395	0.8
209.1284	0.6
195.1129	5.1
193.0972	1.7
192.1129	1.4
182.1275	0.7
182.1174	11.9
175.1078	3.4
173.0919	28.6
168.1022	0.6
167.0807	0.5
165.0658	0.6
164.1067	3.3
158.0812	1.5

Precursor *m/z*	667.3651
Fragment *m/z*	Int (%)
555.3129	6.3
537.3016	2.1
495.2937	1.5
478.2677	3.6
463.0604	0.7
409.9456	0.7
383.2282	1.2
381.2021	7.1
365.2186	5.4
363.1910	1.3
297.1554	1.5
271.1766	20.0
269.1634	1.6
269.1462	3.5
254.1499	46.4
253.1658	11.0
252.1348	0.9
251.1385	1.1
236.1387	1.4
227.1398	0.8
223.1446	0.9
212.1390	2.2
210.1244	0.8
209.1282	0.8
199.1073	1.4
195.1129	11.2
194.1288	1.2
193.0973	1.2
182.1172	8.4
175.1075	2.6
173.0921	13.2
164.1070	2.6
158.0807	1.0
157.0971	33.9
155.0817	1.5
146.8862	0.7
145.8965	0.9
139.0867	5.7
131.0815	42.6
129.1020	3.3
127.0868	0.8
115.0865	33.9
114.0550	7.7
113.0706	3.0
113.0597	100.0
112.0757	20.2
111.0917	0.9
110.0601	1.9
107.3057	0.8
100.2857	0.7

Precursor *m/z*	667.3650
Fragment *m/z*	Int (%)
637.4042	0.8
625.3566	2.2
607.3447	2.6
555.3659	1.3
555.3135	17.5
538.2858	1.3
537.3026	6.6
517.0208	0.6
513.3026	1.8
496.2773	1.4
495.2936	1.6
477.2806	0.6
474.1738	0.7
399.2230	1.7
381.2015	13.1
363.1935	0.6
341.2188	1.6
339.2042	1.5
324.1917	3.3
323.2079	2.5
322.1663	1.0
321.1913	1.1
312.7150	0.6
305.1977	0.7
292.4295	0.6
287.1743	6.7
270.1452	25.2
269.1623	3.6
269.1491	5.1
268.1650	1.1
253.1297	1.0
252.1339	0.8
251.1390	2.4
228.1342	5.6
227.1388	2.5
223.1445	1.2
216.2471	0.5
215.1020	0.6
212.1394	4.2
210.1236	6.9
210.1120	0.8
209.1284	1.4
195.1127	17.1
194.6992	0.6
194.1291	1.6
193.0970	1.7
192.1132	2.1
187.9796	0.6
182.1174	17.1
175.1078	4.5

Precursor *m/z*	651.3699
Fragment *m/z*	Int (%)
641.989	0.6
609.360	1.6
591.350	2.3
559.299	0.6
540.322	0.8
539.318	18.7
522.292	0.9
521.308	6.2
480.281	2.4
479.298	1.2
474.159	0.9
472.789	1.1
383.228	1.2
381.202	9.6
367.147	0.9
365.218	9.8
363.192	1.1
339.192	1.4
324.193	0.7
323.209	1.1
322.167	0.7
321.180	1.2
297.156	2.2
287.161	1.2
285.147	0.7
271.176	19.1
270.651	0.6
270.133	1.5
269.150	6.9
255.144	0.9
254.150	54.5
253.166	11.7
251.138	3.9
241.215	0.9
238.119	1.5
236.139	1.0
234.374	0.8
227.139	2.6
223.144	1.5
222.248	0.8
212.139	3.1
209.128	1.6
204.999	0.9
201.087	0.8
199.107	1.1
195.113	12.6
194.129	2.2
192.547	0.6
183.076	1.1
182.117	19.6

82.1172	0.6	89.2612	1.2	157.0970	41.2	96.0443	12.5	173.0920	24.8	175.108	4.4
79.0451	0.5	86.0963	2.3	155.0815	3.6	95.0491	30.6	171.5368	0.6	166.123	0.8
		86.0600	15.5	152.1069	0.6	86.0600	7.3	167.0811	1.4	165.554	0.7
		85.0648	12.5	147.2195	0.4	85.0647	15.5	164.1071	5.1	164.761	0.7
		84.0809	2.1	145.0974	2.6	85.0618	0.4	158.0815	2.9	164.107	5.3
		77.0431	1.3	140.0705	1.1	83.0283	0.7	157.0971	59.1	159.556	0.7
				139.0864	6.3	82.0647	0.7	156.6254	0.6	158.081	2.2
				138.0547	0.5	78.8612	0.7	155.0814	2.0	157.097	59.9
				135.0919	0.5	77.0579	0.6	152.1071	1.9	152.107	1.7
				131.0814	38.4	71.0491	2.2	145.0970	1.7	147.549	0.6

Table S6. MS/MS fragmentation spectra used to assign Coprogen and corresponding degradation products in Figure 3.

#31	
Precursor *m/z*	769.3963
Fragment *m/z*	Intensity (%)
756.4151	0.7
740.8502	0.9
738.7735	1.1
738.7033	1.0
618.4381	0.7
472.8155	0.7
472.7774	0.8
470.9662	0.6
397.1984	1.4
355.1981	4.0
285.1451	1.8
270.1355	0.9
267.1337	0.7
243.1466	3.6
243.1335	1.6
241.2244	0.9
241.1680	0.7
239.1391	1.2
228.1344	1.1
226.1186	3.7
225.1231	1.1
214.5164	0.6
208.1315	0.7
208.1083	2.4
208.0969	1.1
207.1247	1.2
198.1128	1.3
197.1283	1.1
192.1135	1.0
184.6870	0.9
180.1019	2.0
173.0920	28.4
157.0983	0.6
155.0815	4.1
145.9255	0.7
140.0711	0.6
131.0815	100.0
128.0704	0.9
127.0867	1.4
122.2854	0.7
118.1990	0.6
116.8224	0.6

#32	
Precursor *m/z*	753.4017
Fragment *m/z*	Intensity (%)
740.9423	1.0
738.9820	1.2
696.5430	1.2
642.1543	0.9
641.3498	1.8
623.3401	1.2
529.2983	2.9
511.2876	4.0
397.1978	1.4
392.5018	1.2
381.2010	4.4
363.1905	1.4
357.2130	5.6
354.2027	1.0
344.2158	1.0
340.1877	1.0
339.2026	8.4
322.1767	1.8
321.1908	1.1
287.1609	1.6
285.1454	1.5
279.8900	0.9
269.1493	3.1
257.6616	1.1
245.1606	1.5
239.1389	0.9
236.0656	0.9
228.1338	9.3
227.1505	4.3
227.1385	2.2
210.1232	9.0
209.1277	2.2
197.1288	1.4
195.1122	5.4
193.0969	3.5
192.1134	4.5
182.1174	7.6
180.1015	1.5
175.1079	2.2
173.0919	15.8
167.0815	1.3
164.1069	2.7

#33	
Precursor *m/z*	737.4067
Fragment *m/z*	Intensity (%)
738.866	1.2
625.354	6.5
607.347	6.1
513.303	5.3
496.278	2.5
495.293	6.8
478.265	1.0
474.214	0.9
472.875	0.8
472.836	1.0
460.256	0.7
453.271	1.3
436.254	1.4
435.260	1.7
419.229	1.1
418.244	1.7
381.202	9.0
381.128	0.7
377.166	0.7
363.192	1.6
357.213	1.3
354.201	0.7
346.248	0.8
344.071	0.8
341.218	7.4
340.187	0.8
339.202	4.4
324.191	11.9
323.208	8.0
322.177	1.3
314.639	0.7
306.181	1.8
305.197	1.0
287.160	1.4
285.144	0.9
269.150	4.3
251.139	1.7
245.161	0.8
241.249	0.9
238.118	1.1
229.165	1.0
228.134	5.9

#34	
Precursor *m/z*	721.4119
Fragment *m/z*	Intensity (%)
738.7526	1.6
721.3346	2.8
703.4001	1.0
609.3603	20.9
592.3346	1.6
591.3498	17.1
573.3394	0.9
550.3229	2.1
549.3411	0.9
498.8751	0.7
497.3072	2.8
480.2807	7.7
479.2968	6.8
472.8552	0.7
462.2706	1.4
453.2699	1.9
437.1891	2.4
435.2605	4.0
403.2437	1.0
400.0091	0.8
381.2018	12.3
367.1470	1.5
363.1930	1.0
341.2183	13.5
339.1920	1.8
324.1917	24.5
323.2079	15.3
319.2365	0.8
306.1803	3.7
305.1980	1.8
287.1600	2.7
284.1886	0.9
270.1338	2.2
269.1496	5.7
260.3320	0.9
255.0370	0.8
251.1393	4.3
241.2253	1.0
238.1185	2.2
229.1663	1.4
227.1391	3.2
223.1439	1.5

114.0629	1.1
114.0549	26.0
113.0705	10.2
113.0597	91.8
112.0757	2.7
110.0600	1.4
100.7364	0.6
96.0444	16.0
95.0491	21.2
86.0600	20.4
85.0760	2.5
85.0647	13.3

158.0809	1.3
157.0970	19.7
155.0814	2.9
139.0864	2.5
132.8399	1.0
132.0844	1.0
131.0814	60.5
127.0865	2.1
115.0865	30.3
114.0549	13.0
113.0707	3.8
113.0596	100.0
112.0757	2.6

227.139	2.8
212.139	9.7
211.155	2.7
210.124	4.6
209.140	0.9
209.129	3.3
198.197	0.7
195.113	20.5
194.129	5.2
193.097	2.7
192.113	1.3
184.708	1.0
182.117	11.4

212.1393	21.5
211.1549	3.1
209.1283	2.3
202.1264	2.7
201.1232	4.6
199.2635	0.7
195.1127	35.9
194.1289	6.0
184.6911	0.9
184.6802	0.9
182.1173	15.6
181.1333	1.3
175.1077	5.3

Table S7. MS/MS fragmentation spectra used to assign Dimerum acid and corresponding degradation products in Figure 3.

#41	
Precursor *m/z*	485.2598
Fragment *m/z*	Intensity (%)
399.9299	0.3
373.2086	0.5
355.1975	3.0
252.6773	0.3
243.1463	4.5
243.1302	1.4
228.1342	1.3
226.1417	0.4
226.1186	3.1
225.1354	0.6
225.1231	0.8
210.1240	1.6
209.1388	0.5
208.1080	2.2
207.6415	0.3
207.1241	0.4
195.1127	0.5
193.0969	0.7
192.1131	1.3
191.1289	0.4
184.7002	0.5
181.0972	0.4
157.0604	0.3
155.0814	0.3
150.0785	0.4
137.6273	0.3
131.0815	7.2
118.0647	0.4
114.0549	7.7
113.0597	100.0
97.6942	0.4
97.0760	0.4
96.0442	0.5
95.0491	10.7
86.8299	0.3
86.0632	0.6
86.0600	6.3
85.0760	2.4
85.0648	20.8
83.0493	0.3
74.3880	0.4
71.0491	5.3

#42	
Precursor *m/z*	469.2648
Fragment *m/z*	Intensity (%)
357.2134	3.4
340.1882	0.3
339.2027	8.9
324.1918	0.8
322.1999	0.4
321.1922	0.6
309.1917	0.4
273.5017	0.3
259.4561	0.3
245.1611	1.5
243.1339	0.6
241.2530	0.4
236.4974	0.3
228.1342	2.5
227.1504	5.8
227.1385	1.5
212.1393	0.7
210.1236	5.0
209.1399	0.9
209.1283	1.2
199.1441	0.5
197.8588	0.3
195.1128	2.5
194.1282	0.7
193.1208	0.3
193.0972	5.1
192.1130	4.8
191.1289	0.5
184.7101	0.3
182.1175	3.3
165.1019	0.8
164.1179	0.5
132.4349	0.2
131.7037	0.3
131.0815	1.1
115.0866	10.5
114.0550	0.3
113.0597	100.0
107.4073	0.3
106.4298	0.3
97.6979	0.4
96.2303	0.3

#43	
Precursor *m/z*	453.2698
Fragment *m/z*	Intensity (%)
386.2499	3.1
385.2449	2.2
341.2181	50.8
335.1599	20.4
331.0270	1.9
324.1916	40.9
323.2077	73.2
321.2375	1.9
320.2376	10.0
319.2331	14.2
306.1813	5.2
305.1962	3.2
298.4440	1.9
285.1445	3.3
283.1285	3.7
282.1458	1.8
268.1376	12.7
267.1336	21.0
255.1458	2.3
238.1184	11.3
237.1339	4.7
236.1281	44.2
234.6301	4.7
229.1658	8.9
227.1386	10.8
226.1910	2.1
212.1393	34.9
211.1550	28.0
210.1681	4.4
210.1490	3.6
209.1649	5.8
209.1283	6.5
202.1269	13.9
201.1234	47.6
195.1127	57.8
194.1287	25.9
193.1443	1.9
186.1125	2.2
185.1280	7.8
185.1142	3.7
184.7188	2.3
184.6124	5.5

70.4132	0.3
70.0651	6.3
69.9454	0.3
69.0336	0.5
68.0494	3.8
67.0542	18.4
65.0385	0.3
60.3052	0.4
58.9339	0.3
58.3311	0.2
57.0698	2.8
54.4242	0.2

95.0491	11.0
86.0600	1.0
85.0759	0.3
85.0647	19.1
72.0345	0.3
71.0491	5.3
70.0675	0.5
70.0651	9.9
69.0334	0.5
68.0495	0.5
67.1709	0.3
67.0542	16.5

184.0965	4.7
183.1130	9.9
182.1173	15.9
169.1053	20.4
168.1018	100.0
166.1055	2.8
165.1021	8.1
161.0135	2.0
155.0897	2.1
154.0861	7.3
140.2842	1.8